ESD-TR-67-358 MTR-424

THE ARPA CALIBRATION SATELLITE - THEORETICAL AND EXPERIMENTAL ELECTROMAGNETIC SCATTERING CONSIDERATIONS

MARCH 1968

L. J. Kaplan

Work Performed for

ADVANCED RESEARCH PROJECTS AGENCY

Contract Administered by

DEVELOPMENT ENGINEERING DIVISION
DIRECTORATE OF PLANNING AND TECHNOLOGY
ELECTRONIC SYSTEMS DIVISION
AIR FORCE SYSTEMS COMMAND
UNITED STATES AIR FORCE
L. G. Hanscom Field, Bedford, Massachusetts

Sponsored by
Advanced Reseorch Projects Agency
Project Defender
ARPA Order No. 596

Project 8051
Prepared by
THE MITRE CORPORATION
Bedford, Massachusetts
Contract AF19(628)-5165

FOREWORD

The work reported in this document was performed by The MITRE Corporation, Bedford, Massachusetts, for Advanced Research Projects Agency; the contract was monitored by the Directorate of Planning and Technology, Electronic Systems Division, of the Air Force Systems Command under Contract AF 19(628)-5165.

REVIEW AND APPROVAL

Publication of this technical report does not constitute Air Force approval of the report's findings or conclusions. It is published only for the exchange and stimulation of ideas.

RAYMOND L. McCONNELL
ESD Project Officer
ARPA Order 596

ABSTRACT

This report contains a theoretical and experimental determination of the shape of the ARPA calibration satellite from the viewpoint of electromagnetic scattering. Theoretical and experimental scattering computations and measurements are discussed and presented in detail.

ACKNOWLEDGEMENT

The author is especially indebted to E. N. Fowle, P. C. Waterman and J. F. A. Ormsby for their many helpful suggestions in the course of this work. Many of the ideas contained herein are those of the aforementioned. The aid of Mary Derderian and Pat Grassler with the machine computations and J. E. Doucette with graph plotting is gratefully acknowledged. M. R. Weiss pointed out some of the discrepancies of the RCA data.

TABLE OF CONTENTS

SECTION I

INTRODUCTION

This report is intended to document a systematic theoretical and experimental determination of the shape of the test satellite. The determination herein is based only on electromagnetic scattering. Modification may be made for reasons of mechanical design, space environment, or increasing the probability of obtaining booster space. A prolegomenon is contained in the ARPA report, but this discussion will attempt to be complete and self-contained.

The electromagnetic scattering requirements for the test satellite are formulated in Section II. The theoretical data is discussed in Section III, while the experimental data is discussed in Section IV. The discussion of the "calibration" or accuracy of the range is given in the next section. The final section discusses the determination of the optimum shape and the possible differences caused by considering full-sized bodies. This discussion also includes bodies made of wire mesh.

SECTION II

THE TEST SATELLITE

The primary electromagnetic requirement is that it have a known large radar cross section. The simplest shape is a sphere. Its physical optics* cross section is πa^2, where a is the radius of the sphere. One of the radars to be calibrated is the MITRE L-band scattering matrix radar. This radar will transmit a right (left) circularly polarized signal and measure the return in the two orthogonal circular polarizations. Therefore, it measures the complete polarization scattering matrix, in a circular basis,

$$S_C = \begin{pmatrix} s_{RR} & s_{RL} \\ s_{LR} & s_{LL} \end{pmatrix} . \qquad (1)$$

The subscript C distinguishes S_C from S_L, the matrix defined in a linear basis**, while the double subscripts denote transmitted and received polarizations. The perfect metallic sphere has no depolarized return, so that $s_{RR} = s_{LL} = 0$. One also has $s_{RL} = s_{LR}$, which is always true for reciprocal scatterers in a reciprocal propagation medium. Therefore the polarization scattering matrix may be written,

---

*For the frequencies of the radars considered and the size of the required sphere this approximation is valid here.

**The interrelation between S_L and S_C is given in Appendix A and the difference between σ and s is given in Appendix B.

$$S_C = \begin{pmatrix} 0 & \alpha \\ \alpha & 0 \end{pmatrix} \tag{2}$$

Because of antenna errors and system error among others, the measured polarization scattering matrix will not have the simple form of Equation 2. Under the assumptions that the errors are small and deterministic* one can derive the following relation between the actual scattering matrix, S, and the measured scattering matrix, W,

$$W = A' SA \tag{3}$$

The prime denotes matrix transposition and the matrix A is given by

$$A = \begin{pmatrix} 1 + \mu & \varepsilon \\ \eta & 1 + \nu \end{pmatrix} \tag{4}$$

where the magnitudes of all the Greek symbols are small. The method of solving Equation 3 for the elements of the matrix A is given elsewhere [1]. The solution of (3) is especially easy in the case of the sphere because of the zeros that are present in S_C. The only problem is that the depolarized signal components, i.e. w_{LL} and w_{RR}, are much smaller than the polarized components. Therefore to measure the depolarized signal components accurately the test target must have a large radar cross section. A minimum cross section of 100 m^2 at L-band was selected. For a sphere this leads to a sphere with diameter greater than 10 meters. It does not appear possible

* That is, they are time invariant.

to build a precision sphere of this size. Therefore it was decided that another shape would be required. A cylinder at broadside produces a large cross section and it was chosen as the basic shape for the test satellite. The cylinder introduces aerodynamic problems such as requiring a motion so that the radar will see the target broadside several times during a pass. However, these complications do give the cylinder the advantage of having a function for which a sphere can not be used. That is it can be used to exercise the body motion capability of the radars. Ideally the cylinder's polarization scattering matrix at broadside should be as near to that of a sphere as possible. Therefore its depolarization should be small and ideally be zero. This cannot be obtained by resonance phenomena because this device should be a useful target over the wide range of radar frequencies. Technical Research Group, West, Menlo Park, California calculated the scattering matrix for nine infinite cylinders of radius varying between 0.5λ and 3.0λ. The depolarization, D, which is the ratio of the depolarized signal to the polarized signal in a circular basis, is given in Figure 1. This led to the selection of a radius 3λ at L-band (about 4 feet). This was felt would insure at least a thirty to one ratio of polarized to depolarized returns for almost all radars of interest. The physical optics cross section of a finite cylinder at broadside is

$$\sigma = \frac{2\pi a L^2}{\lambda} \tag{5}$$

Again using the criteria of $100m^2$ at L-band one obtains a length of about 8 feet. These considerations do not include the effect of depolarization because of edge diffraction by the ends of the cylinder. It was decided to minimize this effect by terminating the cylinder in a smooth manner by using hemispherical ends. Later practical considerations of the available space aboard boosters forced the considerations of other capping shapes. The various cappings and their effectiveness will be discussed in other sections of this report.

SECTION III

THEORETICAL DATA

Theoretical calculations of the exact scattering from three-dimensional bodies were performed at TRG and at MITRE. The TRG calculations were for a right circular cylinder with hemispheric ends. The diameter was 2.25λ and the length of the cylindrical section was 5.4λ which produces an overall length of 7.65λ. These dimensions were chosen to be about one half of the full size body at L-band. The limitation on size was caused by the capability of the TRG program*. Figure 2 shows the normalized cross section as a function of the angle of incidence. The normalization in this case is σ/λ^2. Figure 3 shows the scattering in a circular basis and has plots of the element s_{LR}** and the quantity $D = \left| \frac{s_{LL}}{s_{LR}} \right|$*** . These elements indicate for bodies of interest, i.e. bodies that do not depolarize strongly the main returned signal and how far down the depolarized component is. All plots of circular data, herein, will show these quantities. The program was to have model range measurements at RCA on both a TRG sized body and a full sized body. It was expected

---

*It was the largest body that TRG has ever calculated.

**See Appendix A

***These curves are not normalized, λ = 3.02cm (At RCA).

that the comparison of the theoretical and experimental results for the "same" body would help in determining reliability of models for which no theoretical results are available.

In order to obtain further checks on the range MITRE calculated the exact scattering from two two-to-one prolate spheroids, of semi-major axes a where ka = 8.9 and ka = 20, and a two-to-one oblate spheroid with semi-minor axis a, where ka = 8.175. These results are presented in Figures 4, 5 and 6 where the cross sections normalized to πa^2 are plotted as a function of aspect angle. Figures 7, 8 and 9 present the circular polarization data.

From the theoretical data we can see the close resemblance of s_{LR} with the cross section data for the linear polarizations. We also see the wide fluctuations of D for theoretical data which is a harbinger of the erratic fluctuations that occur when experimental data is considered. The rapid fluctuation in D occurs because σ_{LL} is the difference of two nearly equal quantities. When measured results are considered, the effect of errors tend to become magnified since the errors are of the order of magnitude of the quantity to be determined.

SECTION IV

EXPERIMENTAL RESULTS

RCA measured the backscattered scattering matrix of 16 bodies in its X-band anechoic chamber. These bodies are identified in the following listing and are assigned a number that they may be used to identify the body:

(1) TRG body, but slightly off (1%) in scaling*

(2) The "exact" TRG body

(3) The full sized cylinder with hemispheric ends

(4) The full sized cylinder section, as body 3, with a two-to-one oblate spheroid end

(5) Two-to-one prolate spheroid ka = 20

(6) Two-to-one oblate spheroid ka = 8.175

(7) A cylinder whose length and radius are the same as body (1) with flat ends.

(8) Same as body 7 except hollow ends i.e. stovepipe

(9) Same as body 7 except the cylindrical section has ends that are zones of a sphere of twice the radius of the cylinder.

(10) Same as body 7 except cylindrical section has an end section that is two-to-one oblate spheroid.

---

* the length of the cylindrical section, L, in the TRG body should be 6.41 inches, but in body 1 it is 6.48 inches.

(11) Cylinder with hemispheric ends where the length of the cylindrical section is the same as body (1) but the diameter is one half

(12) Two-to-one prolate spheroid with ka = 8.9

(13) Square mesh version of body (7) 6 per inch

(14) Square mesh version of body (7) 12 per inch

(15) Square mesh version of body (1) 6 per inch

(16) Square mesh version of body (1) 12 per inch

Pictures of these targets are given in Figure 10. The RCA data in linear polarization for the 16 bodies is given in Figures 11 through 26. These show the linear basis cross sections as a function of aspect. The cross sections are given in dbsm. For all the bodies except 13 and 15 the depolarized term σ_{HV} was set arbitrarily at -90 dbsm because it was not measureable. However for bodies 13 and 15, the coarse mesh bodies, values are obtained and plotted in Figure 27. For the fine mesh bodies 14 and 16 these quantities were significantly more noticeable than the solid bodies, although still not measureable. Figures 28 through 43 present this data in a circular basis*.

Bodies 2, 5, 6 and 11 were intended to check on the accuracy of the range. Bodies 1, 7, 8, 9 and 10 form a set for comparing the

*In bodies 13 and 15 the quantity σ_{HV} has not been used which would increase D, see Appendix A.

effect of various end shapes for the cylinder, while bodies 3 and 4 form another such set. Bodies 1 and 11 compare the results of different diameters, to check on the results of Figure 1. The mesh bodies were measured to check the effect of a mesh structure on electromagnetic scattering, because at one time such a structure was being considered. The difference between body 1 and 2 arose from a misunderstanding of the RCA frequency. It should also be noted that the measurements of body 1 were made at 9930 Mc., compared with all other runs at 9924.2 Mc. The basic comparisons were done using models about the size of the TRG body to allow comparison with theoretical data. This also enabled easier construction* of the test models and more accurate measurements because of the reduction of coupling to the back wall. The full sized bodies 3 and 4 had an equivalent length at L-band of cylindrical section of 8 feet with a diameter of 4 feet. These dimensions, which were obtained earlier in this report, are not related to the TRG body. The length of the test satellite was reduced because of practical considerations in obtaining a launch while the TRG body was scaled from tentative dimensions before this reappraisal was made**.

---

*The full sized models had to be hollowed out to obtain models within the weight limitations of the range.

**In fact the calculations were already complete.

SECTION V

ACCURACY OF MEASUREMENTS

The measured results for bodies 2, 5, 6, and 12 can be compared with the theoretical computer results. In addition, for bodies of revolution the nose-on cross sections and phase angles should be the same for both polarizations. Table I lists $\sigma_{HH} - \sigma_{VV}$ and $\phi_{HH} - \phi_{VV}$ for the 16 measured bodies. Theoretically these should be zero. With the exception of bodies 11 and 12 the cross sections were within 1db of each other. The two bodies where this was not the case are the bodies with the smallest nose-on geometrical optics cross section. It is thought that this accounts for the differences. Since body 11 is a computed shape, its scattering will be examined more carefully later in this section. The differences in phases show the inherent difficulties in measuring phase in a radar range and suggest great difficulty in obtaining s_{LL} or D which depends critically on the phase*. This will be considered later in this section.

It is also expected that the broadside cross sections (in either polarization) of cylinders of same lengths but different ends should be approximately the same. Table II lists the broadside cross section for bodies 1, 2, 7, 8, 9, and 10 which should be approximately the same, and 3 and 4 which should also be similar.

---

*See Equation A7 and remember that the magnitudes of A and B are nearly equal.

Table I

Body Number	$\sigma_{HH} - \sigma_{VV}$	$\phi_{HH} - \phi_{VV}$
1	-0.1db	1.6 ^{o}
2	-0.3	-19.0
3	-0.8	13.1
4	0.3	4.4
5	0	-0.1
6	0.6	-1.2
7	-0.7	-26.8
8	-0.1	-18.2
9	0	-21.5
10	-0.4	-6.2
11	-2.4	-27.6
12	-1.2	-6.6
13	0	-5.0
14	-0.4	-8.6
15	-0.1	5.0
16	-0.5	-5.6

Table II

Body Number	σ_{HH}	σ_{VV}
1	-4.8 dbsm	-5.5 dbsm
2	-6.9	-7.1
7	-6.0	-5.5
8	-6.3	-7.3
9	-8.5	-8.6
10	-7.5	-8.4
3	1.3	0.5
4	-7.5 (0.7)	-7.6 (0.6)

Two values are entered for body 4 because it was discovered that RCA had made an error in the data for body 4. They had used a three inch sphere in calibrating the range, but the computer program used the cross section of a one inch sphere. The result is that 8.2 db should be added to all the cross sections for body 4. Therefore Figure 14 should be shifted up 8.2 db. In the conversion to circular data, this would also increase σ_{LL} and σ_{LR} by 8.2 db, but since the depolarization D involves only ratios, it is unchanged. Comparing the smaller bodies, one sees no glaring discrepancies. However, bodies 1 and 9 appear to be in error. Body 1, whose cross section should be almost the same as body 2, is about 2db higher throughout the entire range of aspect angles. As was mentioned previously there should be slight differences between the two measured results for

the two bodies because of the small differences in size and in the frequency of measurement. It is also to be noted that body 1 was measured before RCA closed down the range for vacation while the remaining bodies were measured after the vacation period. It must be concluded that there is an error in the measurements of body 1. The cross section for body 9 seems to be slightly lower than the other bodies in the group consisting of bodies 1, 2, 7, 8, 9 and 10 and perhaps may be in error. An inverse scattering program was run at MITRE using both the theoretical and experimental data to determine the shape and dimensions of the scatterer. The results were excellent for the theoretical calculations and produced good results for most of the experimental data. These results also indicate some error in the measurements for bodies 1 and 9.

The comparison of the cross sections of the TRG calculations and body 2 show agreement within 1 db except for the first two nulls off broadside and one isolated point (σ_{VV} at an aspect angle of 6^{o} which is 1.2 db off). For these values, as expected, the theoretical results show sharper nulls than the experimental results, with a maximum difference of about 3.6 db. These results indicate the reliability for the experimental cross section measurements. This conclusion is supported by comparison for the two prolate and one oblate spheroid. For the large prolate spheroid only one experimental value differs more than 1 db from the theoretical value (1.3 db in this case). For the oblate spheroid six points differ more than 1 db,

but none more than 1.2 db. Five of these points occur at angles of incidence nearly orthogonal to the axis of revolution. At these angles, cross section is the smallest and the effect of different polarizations is most pronounced. For the small prolate spheroid five points have differences that exceed 1 db (up to 1.5 db). The previously noted experimental discrepancy of 1.2 db at nose-on between the two polarizations is not counted here because the theoretical value splits the differences and both experimental values are within 1 db of the theoretical value. Some of these values occurred at angles of incidence where the cross section is most polarization sensitive, but other errors occur when this is not the case. It is thought that the small size of this target may make it slightly more sensitive to positioning and other such errors.

The comparison of the phase accuracy is more difficult than cross section accuracy. Eschewing the question of absolute phase, there are two meaningful phase comparisons. The first is within each channel (HH or VV) and the second is the phase difference between the two channels. For comparison in these two cases it is convenient to label the phase value as $\phi_i(u)$ where i denotes HH or VV and u is the aspect angle. In each channel $\phi_i(u) - \phi_i(0)$, where nose-on is arbitrarily chosen as reference, can be compared for bodies for which both theoretical and experimental results occur. For the TRG shape the comparison of $\phi_i(90^\circ) - \phi_i(0)$ for the theoretical and experimental results produces a difference of -6° and $+13^\circ$ for the two polarizations.

It should be noted that there are values of u, $0<u<90^{o}$ for which this difference is about 20^{o}. For the large prolate spheroid the difference in values of $\phi_i(90^{o}) - \phi_i(0)$ are 14^{o} and 20^{o} while the small prolate spheroid has differences of 10^{o} and 12^{o}. In the case of the oblate spheroid in the region 0^{o} to 90^{o} the errors tend to cancel and the differences in $\phi_i(90^{o}) - \phi_i(0)$ are 0^{o} and 1^{o}. There appears to be no angle for any body where the difference in $\phi_i(u) - \phi_i(0)$ between theoretical and experimental is more than 20^{o}. The phase accuracy within each channel appears to be adequate. The main error in these measurements is in the relative phase in the scattering matrix, $\phi_{HH}(u) - \phi_{VV}(u)$. This quantity, which should be zero in the case of nose-on incidence, was detailed in Table I. It might be thought that this error is a uniform quantity that could be subtracted out. To examine this more carefully Figures 44 and 45 show $\phi_{HH}(u)-\phi_{VV}(u)$ from both the theoretical and experimental results for the large prolate spheroid and the TRG shapes. For the spheroid one notes that the two curves agree at nose-on but from then on there is little correlation between the curves. This is supported by the curves for the TRG body. This leads to the conclusion that there are random errors in the relative phase of the experimental data. These errors are significant in the determination of D as pointed out previously. Comparisons of the magnitude of the main term s_{LR} in the scattering matrix show agreement comparable to the accuracy of radar cross section measurements. The conversion of the linear basis scattering matrix to the

circular basis was rerun with the phase on element, s_{VV}, shifted by a constant phase angle so that the phases in the two channels agree at nose-on. The results s_{LR} and D are plotted in Figures 46-61. The curves of D do not show any global improvement, but there are some sharper nulls where the phases agree at and near nose-on. The curves of s_{LR} do not change significantly and seem to be as accurate as prior to the shift. An error analysis would be called for to see if there is any real improvement in both quantities by this shift. The author feels that there should be an optimum phase shift that will improve the data, but that its determination would be arithmetical and that its improvement would not be clear except by an error analysis. That is to say the graphs of this optimum value would not differ significantly from the curves plotted herein. This is further substantiated in Figures 62-68 where the shift of 19^{o} appropriate to body 2^{*} is applied to bodies 1, 3, 4, 5 and 6. The curves of D change in no apparent pattern. There is a slight deterioration for some of the bodies in s_{LR}. Therefore the conclusion is made that except for s_{LL} and D the experimental results are satisfactory. It is to be noted that satisfactory is not applied to the results from body 1 and particularly to body 9. Even in these cases there is reason to believe that a consistent error was made that if removed would enable reasonably accurate determination of σ. The errors in D and s_{LR} which do not, to a large order, depend on the cross section are about the same for these bodies as those for which the cross section measurements are thought to be accurate.

*In the sense that it would provide agreement in nose-on phases for body 2.

SECTION VI

CONCLUSION

This section will present the conclusions drawn from these experiments. They can be divided into three portions; the usefulness of wire grid models, the accuracy of the full scale measurement and the "best" capping for the test satellite.

The differences in the wire grid measurements as compared with the same solid body are not completely fair, since the solid body was made to much stricter tolerances. The wire grid models were made quickly because of time requirements, and in addition to the larger tolerances than the solid model, they were easily deformed. The coarse screen models showed measurable depolarization in a linear basis, and it is clear that they are completely unacceptable. The finer meshed bodies also had more depolarization than a solid body but the value was in the noise level. Both screen models had comparable broadside cross sections with the solid models. The shape of the cross section versus aspect angle curves for the fine mesh was close to the solid body. However, the depolarization D, was an order of magnitude greater than the solid body. Since the pressures to use a wire mesh model* abated, no effect was expended to see how closely

---

* Low altitude orbit for test satellite if a NASA launch was used.

the finer wire mesh could satisfy the test satellite requirements. A furth_r study would have then found an upper bound to the mesh size*.

As has been pointed out the values and curves for D are unreliable. It is felt that gross, order of magnitude, differences in D are meaningful. It is also thought the bodies depolarize where D shifts exceedingly rapidly more than a body that has about the same variation but changes more smoothly. This leads to the conclusion that the measurements on the full size body are less accurate than those for the TRG sized bodies. Physical explanations supporting the greater accuracy of the smaller body measurements were given earlier.

The choice for capping becomes a choice between the oblate spheroid and the hemisphere. The other considered shapes show greater depolarization. It appears, quick glance look, that the sphere is slightly better than the oblate spheroid. To choose between the two terminations on the basis of the full size measurement is almost impossible. Practical considerations e.g. smaller overall length, may result in the final selection of the oblate spheroid over the hemisphere.

* Assuming a mesh structure would work.

APPENDIX A

INTERRELATION BETWEEN THE TWO SCATTERING MATRICES

Polarized electromagnetic waves are usually described in either of two orthogonal bases* which are linear and circular. In the linear choice the bases are horizontal and vertical and if carats denote the scattered field a polarization scattering matrix may be defined.

$$\begin{pmatrix} \hat{H} \\ \hat{V} \end{pmatrix} = \begin{pmatrix} S_{HH} & S_{HV} \\ S_{VH} & S_{VV} \end{pmatrix} \begin{pmatrix} H \\ V \end{pmatrix} = S_L \begin{pmatrix} H \\ V \end{pmatrix} \tag{A1}$$

Similarly if a circular basis is chosen with right and left handed circular waves as basis vector, a polarization scattering matrix can be defined,

$$\begin{pmatrix} \hat{R} \\ \hat{L} \end{pmatrix} = \begin{pmatrix} S_{RR} & S_{RL} \\ S_{LR} & S_{LL} \end{pmatrix} \begin{pmatrix} R \\ L \end{pmatrix} = S_C \begin{pmatrix} R \\ L \end{pmatrix} \tag{A2}$$

The basis vectors are interrelated by

$$\begin{aligned} R &= H + jV \\ L &= H - jV \end{aligned} \tag{A3}$$

*There are infinitely many bases (orthogonal and non-orthogonal) but other bases rarely find application.

Other definitions can be chosen which are equivalent. These include replacing j by -i, which reverses the time dependence i.e. $e^{-i\omega t}$ versus $e^{j\omega t}$, and multiplying the right sides of A3 by $\frac{1}{2}$ or $1/\sqrt{2}$. This is a matter of whether the $\frac{1}{2}$ appears in the transformation (as in A3) going from circular to linear or vise versa, while the $1/\sqrt{2}$ symmetrizes the equations. The problem in this section is to find the relation between S_L and S_C and in particular S_C as a function of S_L since the available data is in terms of the linear basis yet is based on a circular basis. It is obvious that many other formulations are also possible. The method chosen here is simple and direct.*

Rewriting (A1) in more convenient notation

$$\begin{pmatrix} \hat{H} \\ \hat{V} \end{pmatrix} = \begin{pmatrix} A & C \\ C & B \end{pmatrix} \begin{pmatrix} H \\ V \end{pmatrix} \tag{A4}$$

where $s_{HV} = s_{VH}$ by reciprocity and since the test satellite is a body of revolution C = 0. Solving (A3) one has

$$\begin{aligned} 2H &= R + L \\ 2jV &= R - L \end{aligned} \tag{A5}$$

*Alternate derivations of the results of this Appendix may be found in Reference 2.

For the reflected wave the direction of incidence is the opposite of that for the incident wave. This interchanges left and right handedness for a fixed observer at the radar* and instead of (A5) one has

$$2\hat{H} = -\hat{R} - \hat{L}$$
$$2j\hat{V} = -\hat{R} + \hat{L} \qquad \text{(A6)}$$

Substituting (A5) and (A6) in (A4) one derives the main result herein,

$$\begin{pmatrix} \hat{R} \\ \hat{L} \end{pmatrix} = \tfrac{1}{2} \begin{pmatrix} A - B & A + B \\ A + B & A - B \end{pmatrix} \qquad \text{(A7)}$$

If C is not zero then the magnitude of s_{RR} and s_{LL} becomes $|\tfrac{1}{2}(A - B) + j\,C|$ while $s_{LR} = s_{RL}$ remain invariant. Therefore the resultant effect of deviations from a perfect body of revolution is to increase the depolarized signal.

*A right handed screw will appear left handed if viewed from the bottom.

APPENDIX B

RADAR CROSS AND POLARIZATION SCATTERING MATRICES

A careful distinction has to be made between the elements of the polarization scattering matrix and the quantity called radar cross section. Radar cross section is a power quantity while the elements of the polarization scattering matrix are essentially the square root of power. Using σ_{ij} for cross section and s_{ij} for the matrix element we have

$$\sigma_{ij} = |s_{ij}|^2$$

Measurements usually present the four values of σ and the phase information for s. The transformation theory in Appendix A requires the use of the polarization scattering matrix elements. In this report a constant distinction between σ and s will be maintained, but since knowledge of one implies the other only one quantity will be shown in graphs and in tabulated results.

APPENDIX C (ILLUSTRATIONS)

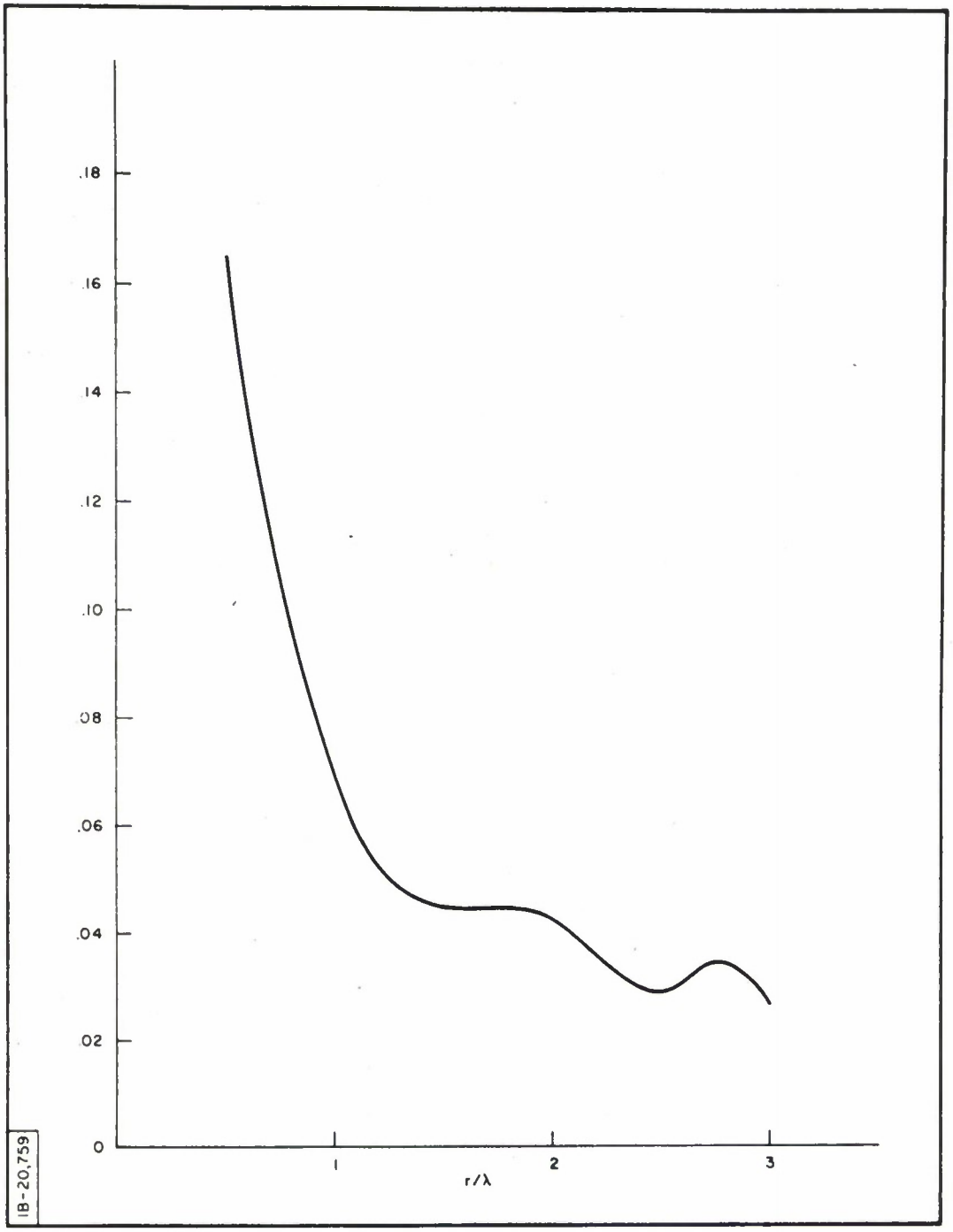

Figure I. D, THE RATIO OF s_{LL} TO s_{LR} FOR INFINITE CYLINDERS OF DIFFERENT RADII

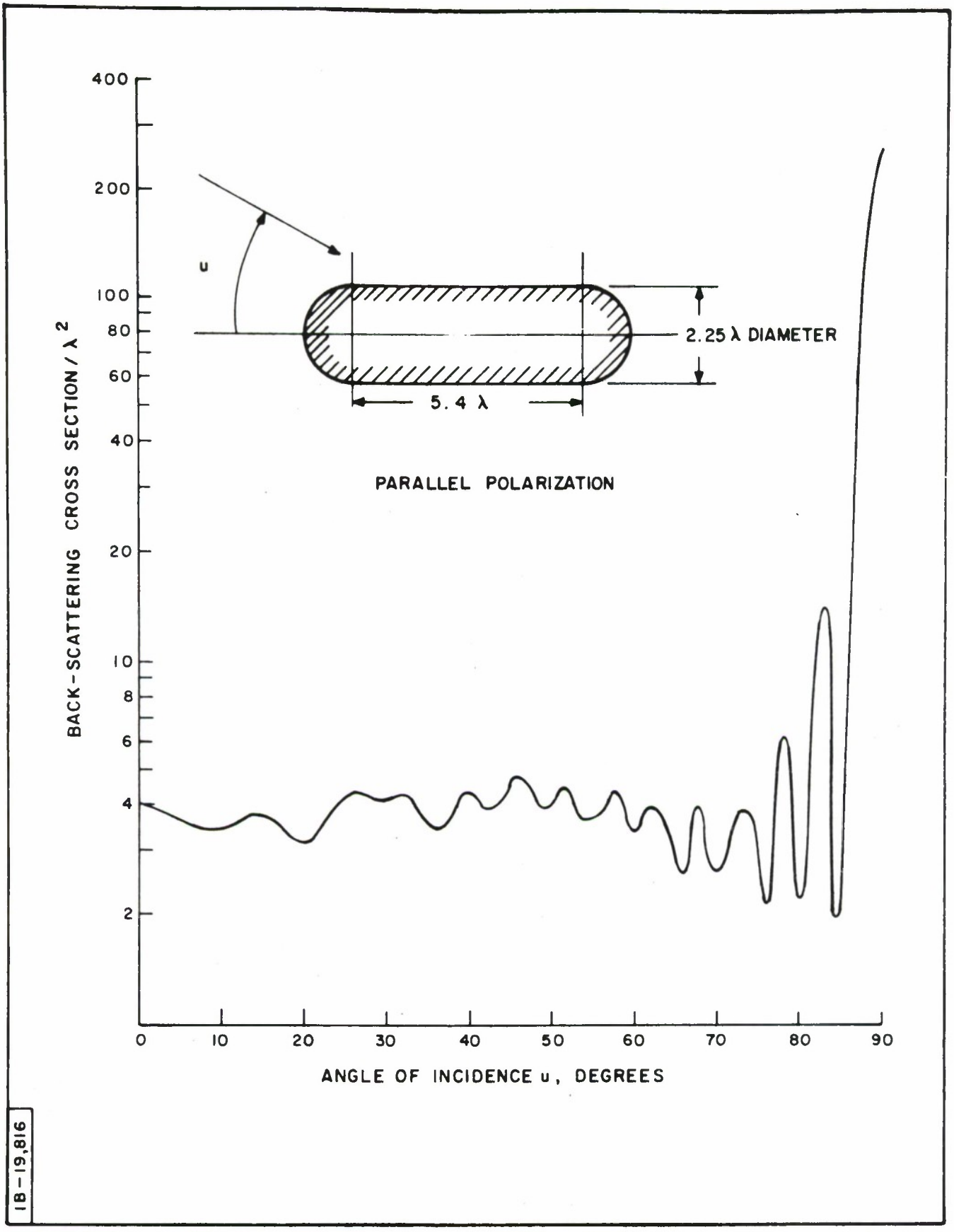

Figure 2a RADAR CROSS-SECTION OF A CIRCULAR CYLINDER WITH HEMISPHERICAL ENDCAPS, HORIZONTAL POLARIZATION

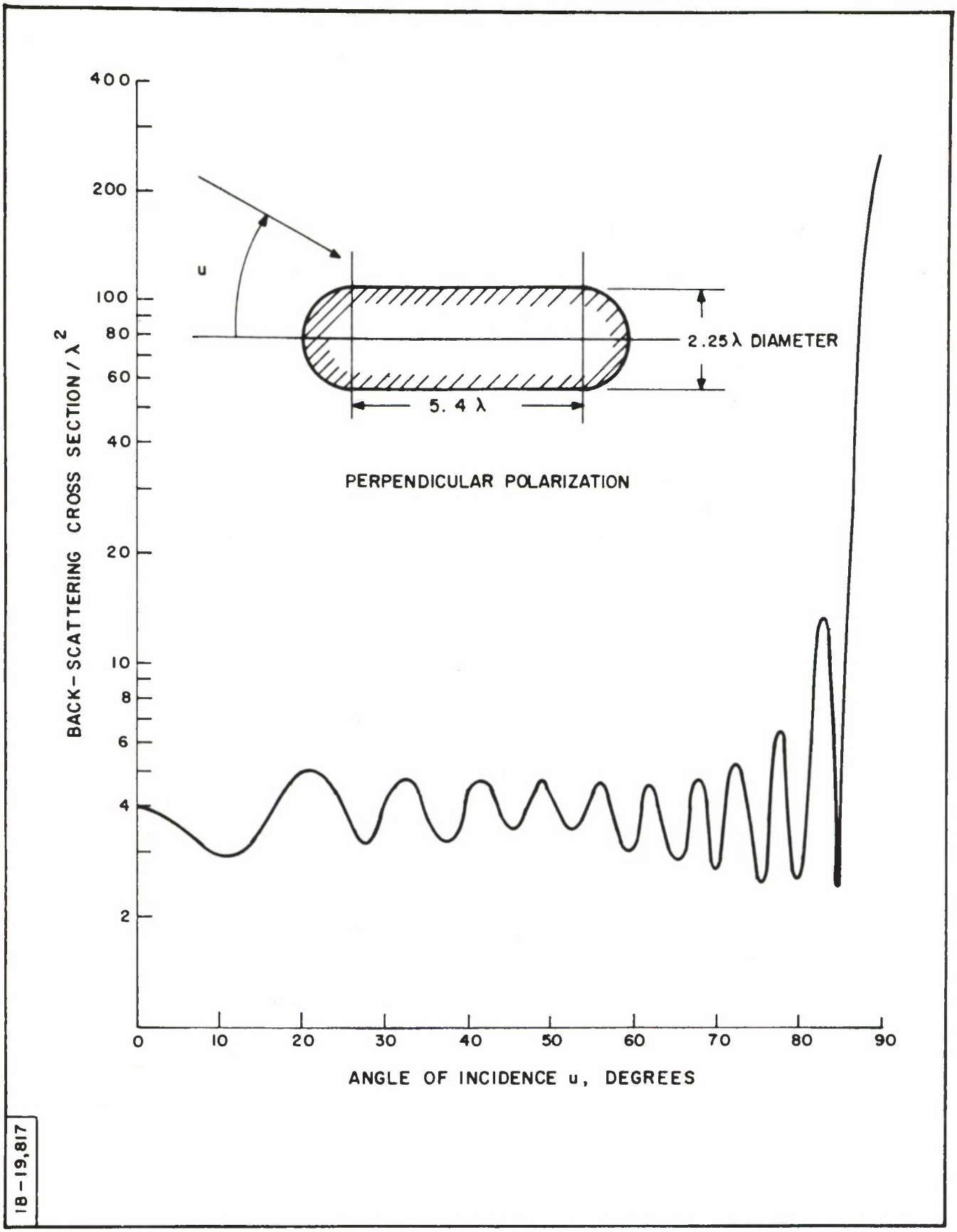

Figure 2b RADAR CROSS-SECTION OF A CIRCULAR CYLINDER WITH HEMISPHERICAL ENDCAPS, HORIZONTAL POLARIZATION

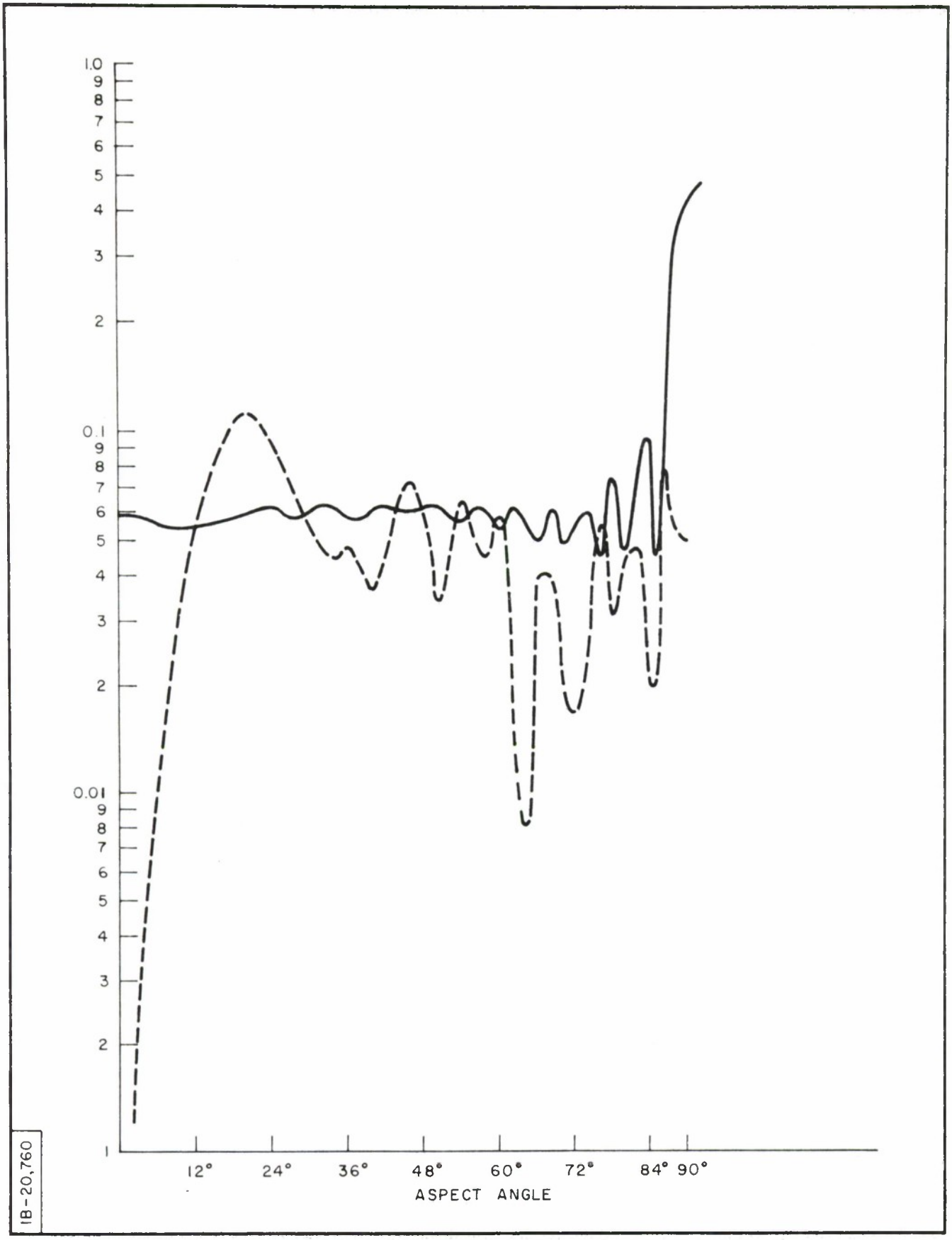

Figure 3. THE S-MATRIX ELEMENT s_{LR} (SOLID) AND $D = s_{LL}/s_{LR}$ (DOTTED) VERSUS ASPECT ANGLE FOR "TRG BODY"

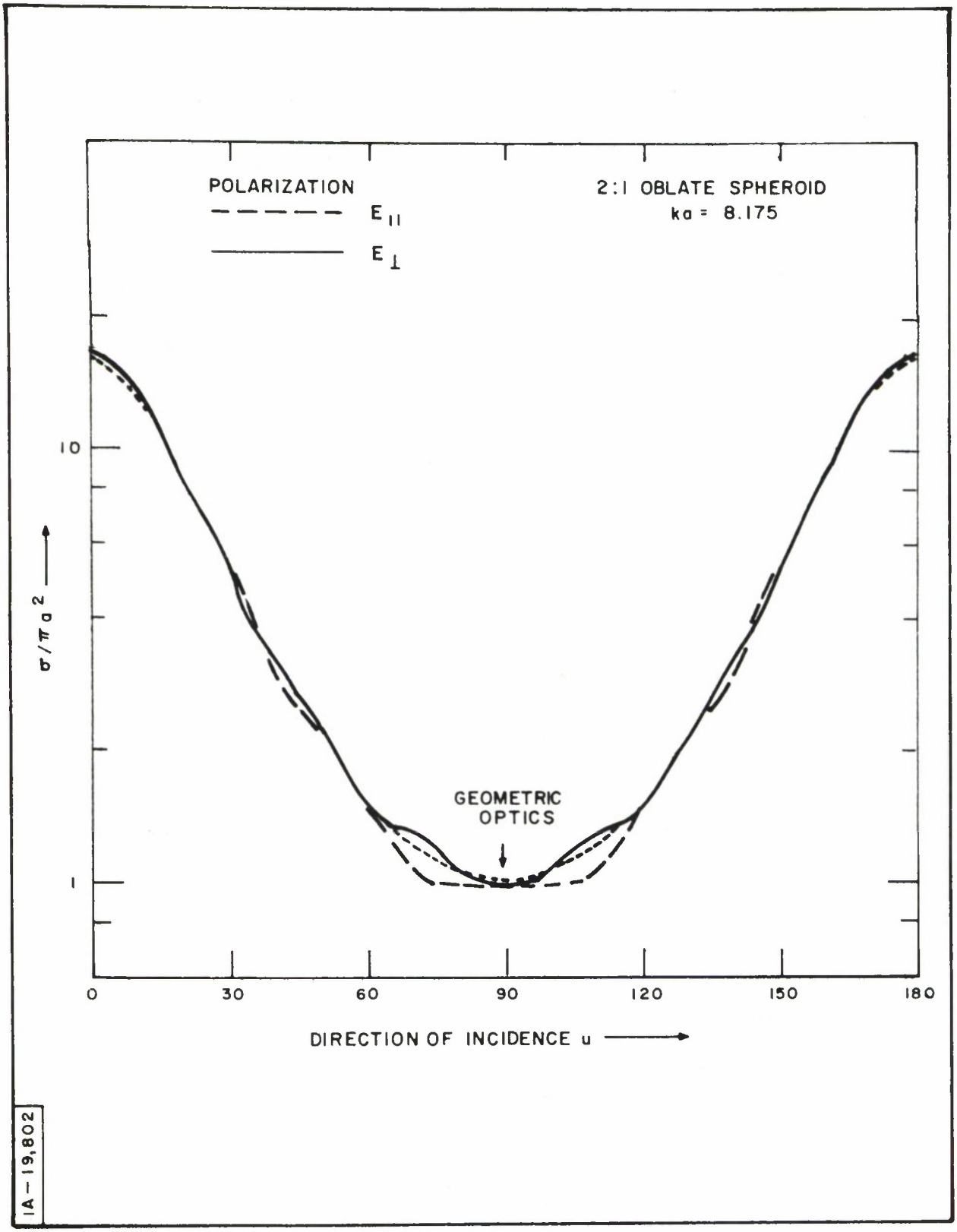

Figure 4. RADAR CROSS SECTION OF OBLATE SPHEROID VERSUS ASPECT ANGLE WITH ka = 8.175

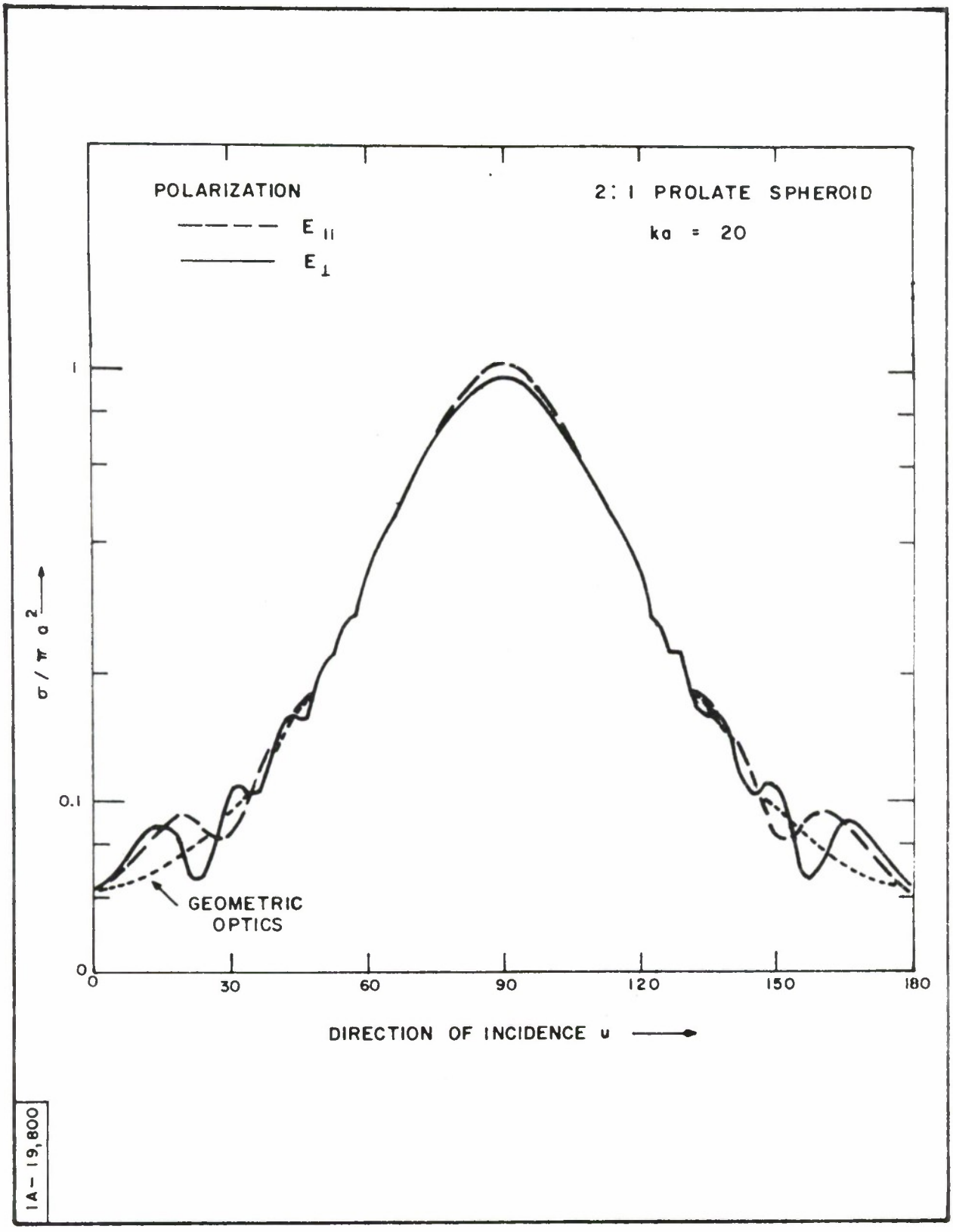

Figure 5. RADAR CROSS SECTION OF PROLATE SPHEROID VERSUS ASPECT ANGLE WITH ka = 20

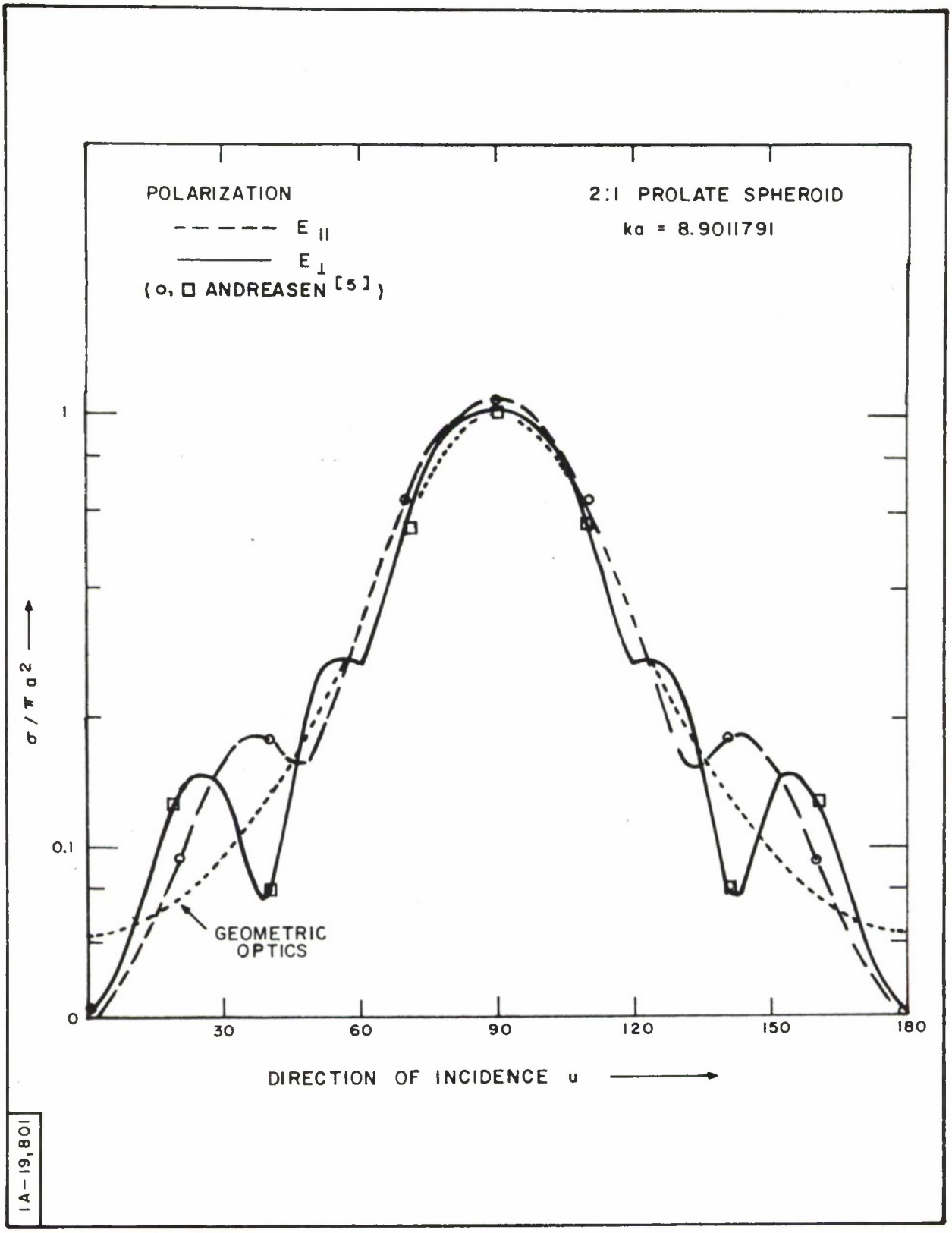

Figure 6. RADAR CROSS SECTION OF PROLATE SPHEROID VERSUS ASPECT ANGLE WITH ka = 8.9

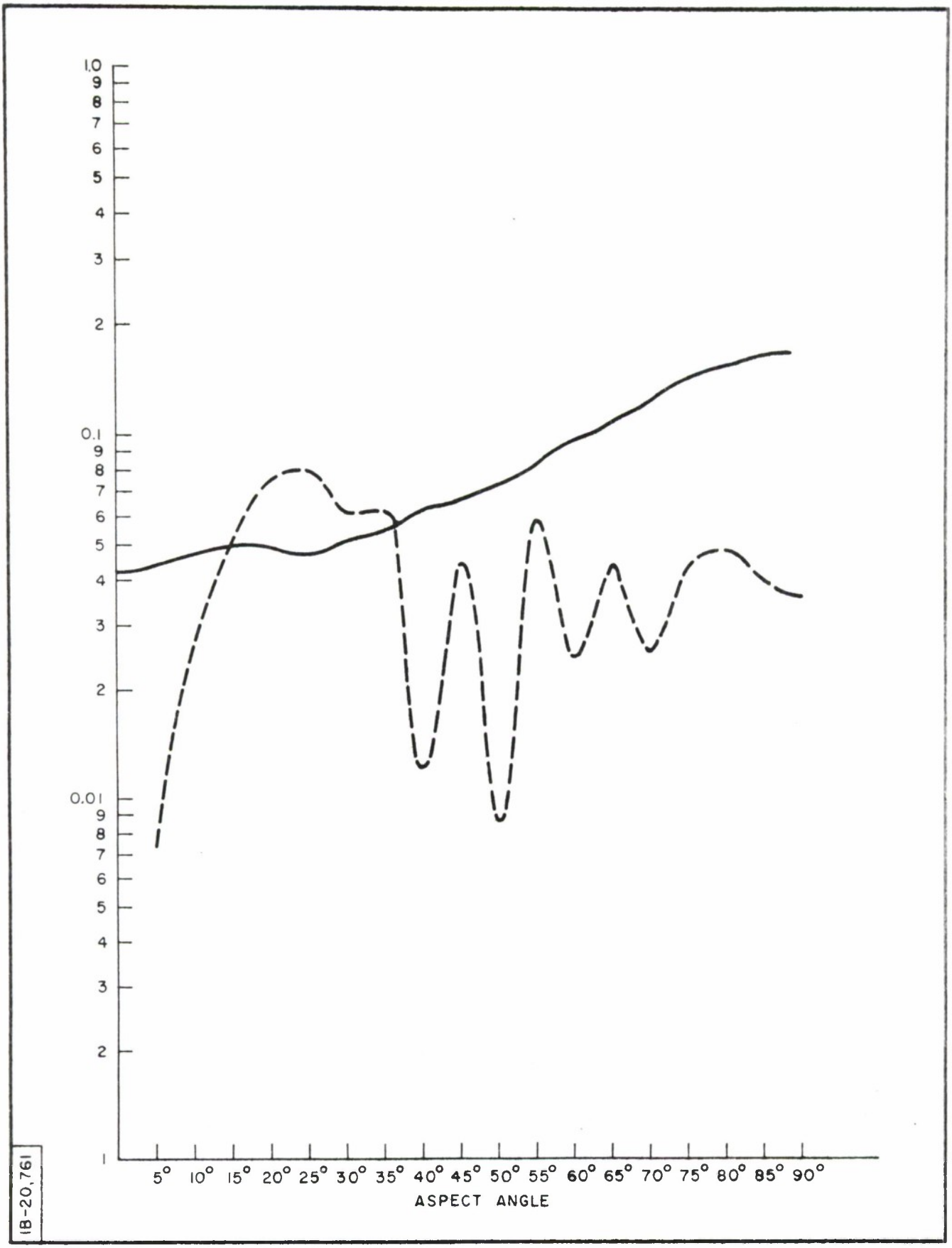

Figure 7. THE S-MATRIX ELEMENT s_{LR} (SOLID) AND $D = s_{LL}/s_{LR}$ (DOTTED) VERSUS ASPECT ANGLE FOR PROLATE SPHEROID $ka = 20$

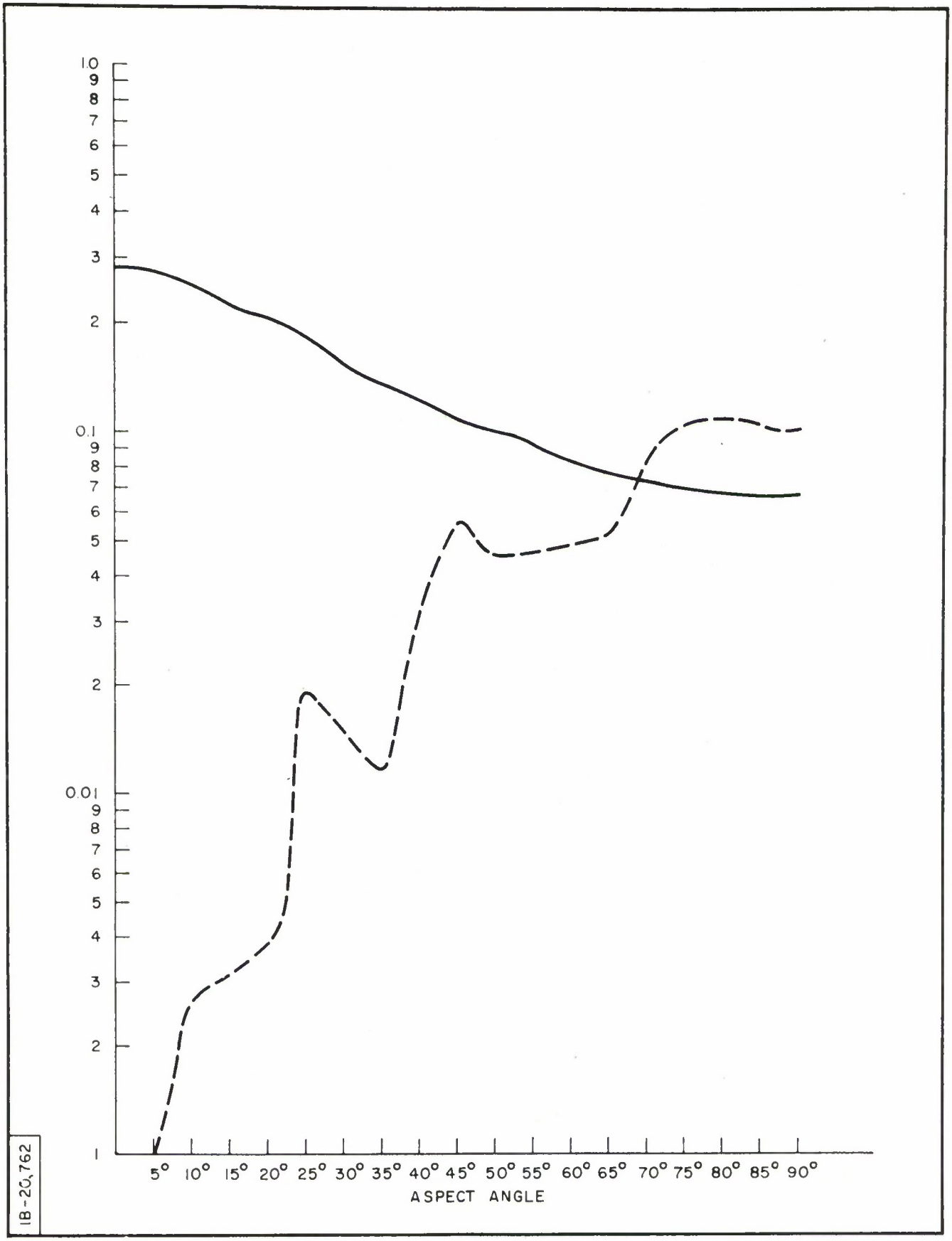

Figure 8. THE S-MATRIX ELEMENT s_{LR} (SOLID) AND $D = s_{LL}/s_{LR}$ (DOTTED) VERSUS ASPECT ANGLE FOR OBLATE SPHEROID ka = 8.175

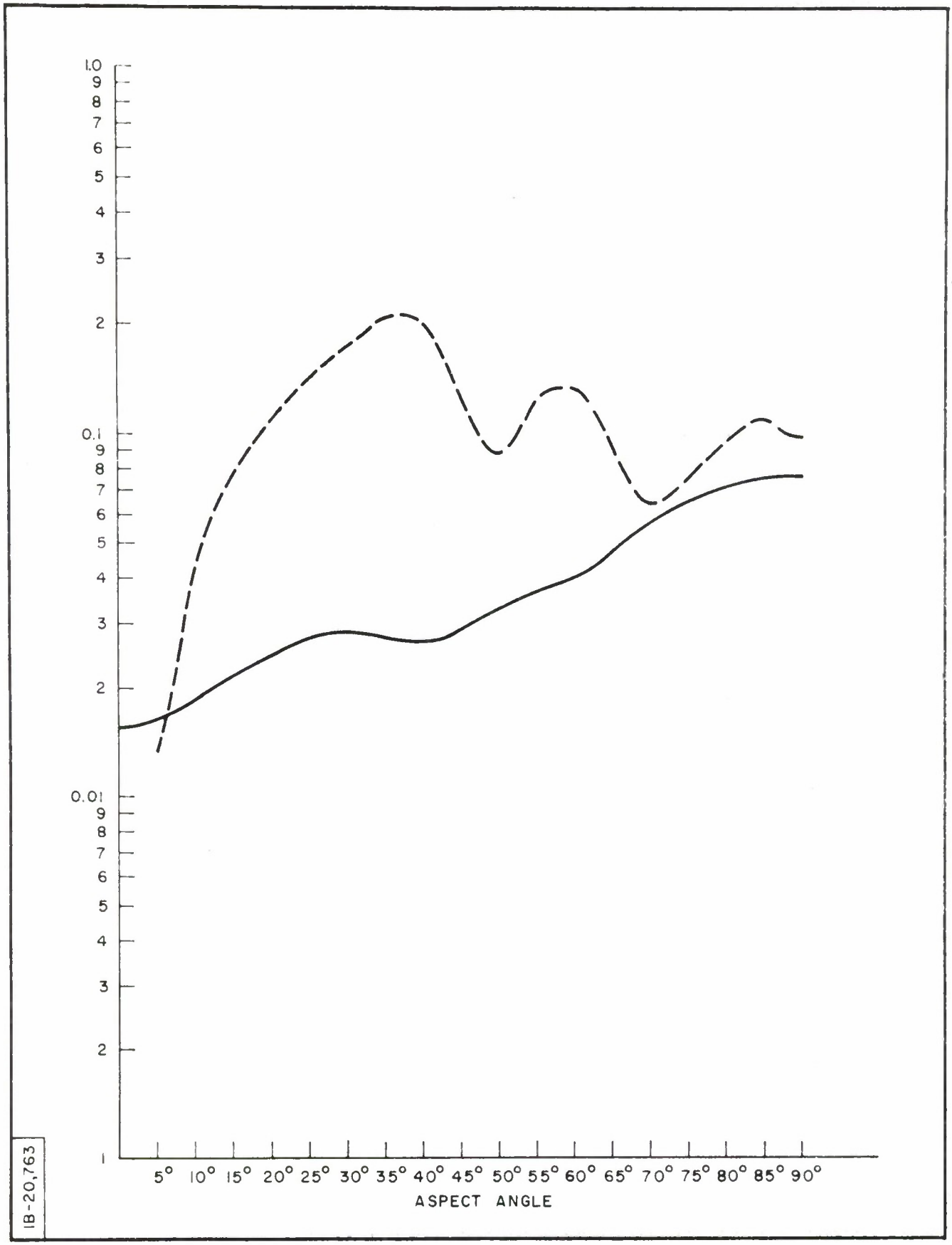

Figure 9. THE S-MATRIX ELEMENT s_{LR} (SOLID) AND $D = s_{LL}/s_{LR}$ (DOTTED) VERSUS ASPECT ANGLE FOR PROLATE SPHEROID $ka = 8.9$

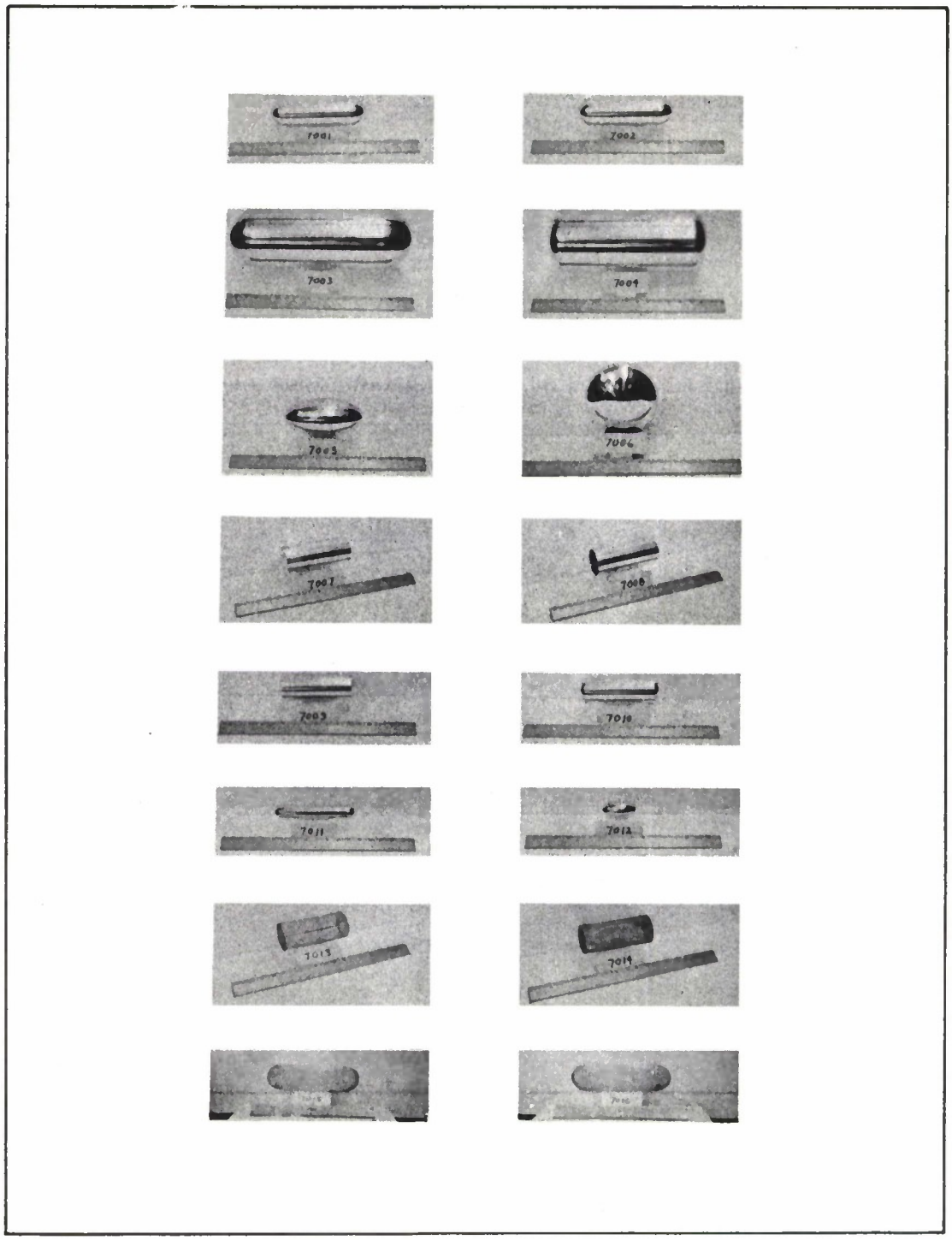

Figure 10. PHOTOGRAPHS OF THE 16 MEASURED BODIES

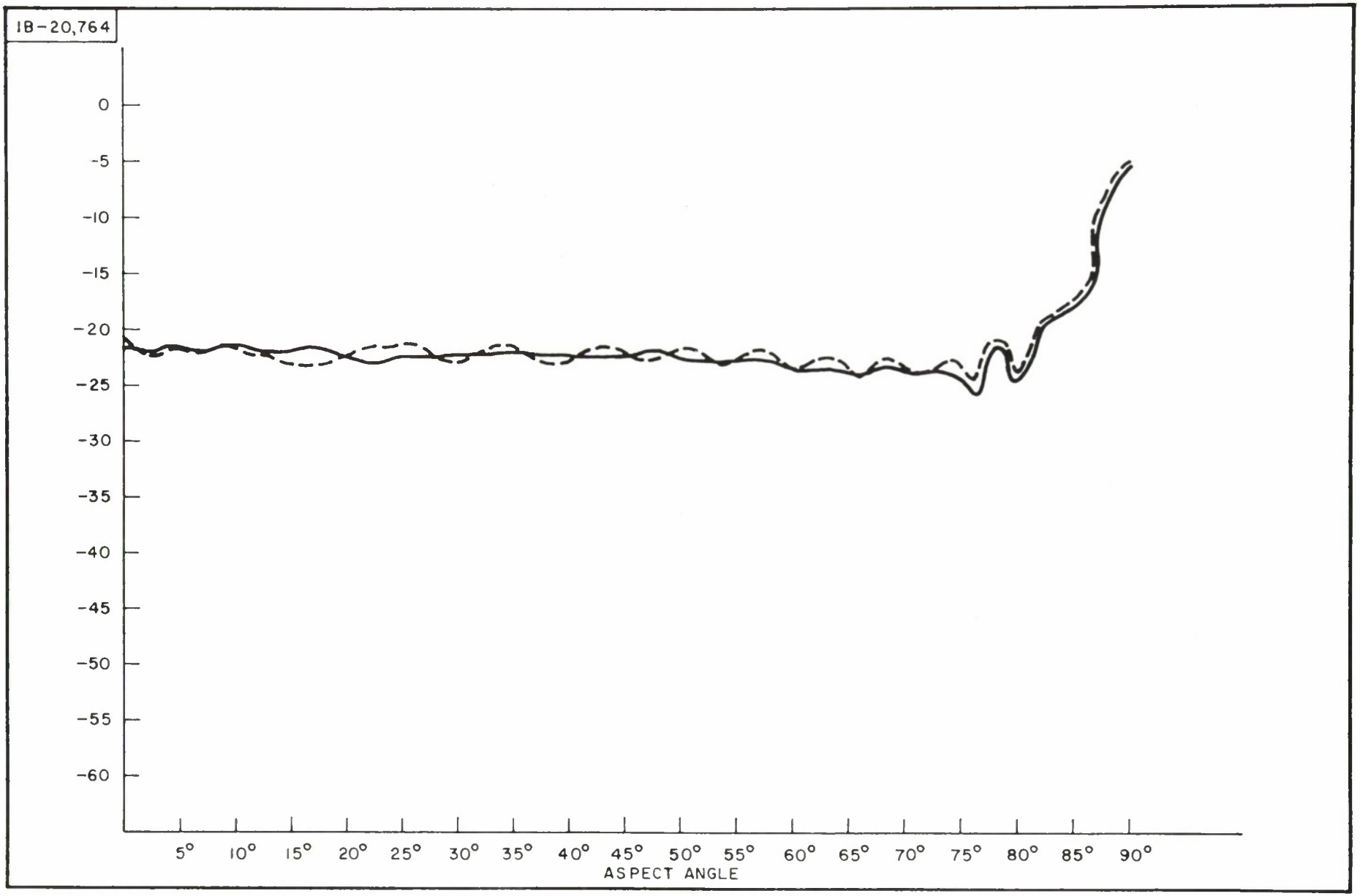

Figure 11. RADAR CROSS SECTION (DBSM) VERSUS ASPECT ANGLE FOR BODY NO. 1. HORIZONTAL POLARIZATION (SOLID) AND VERTICAL POLARIZATION (DOTTED)

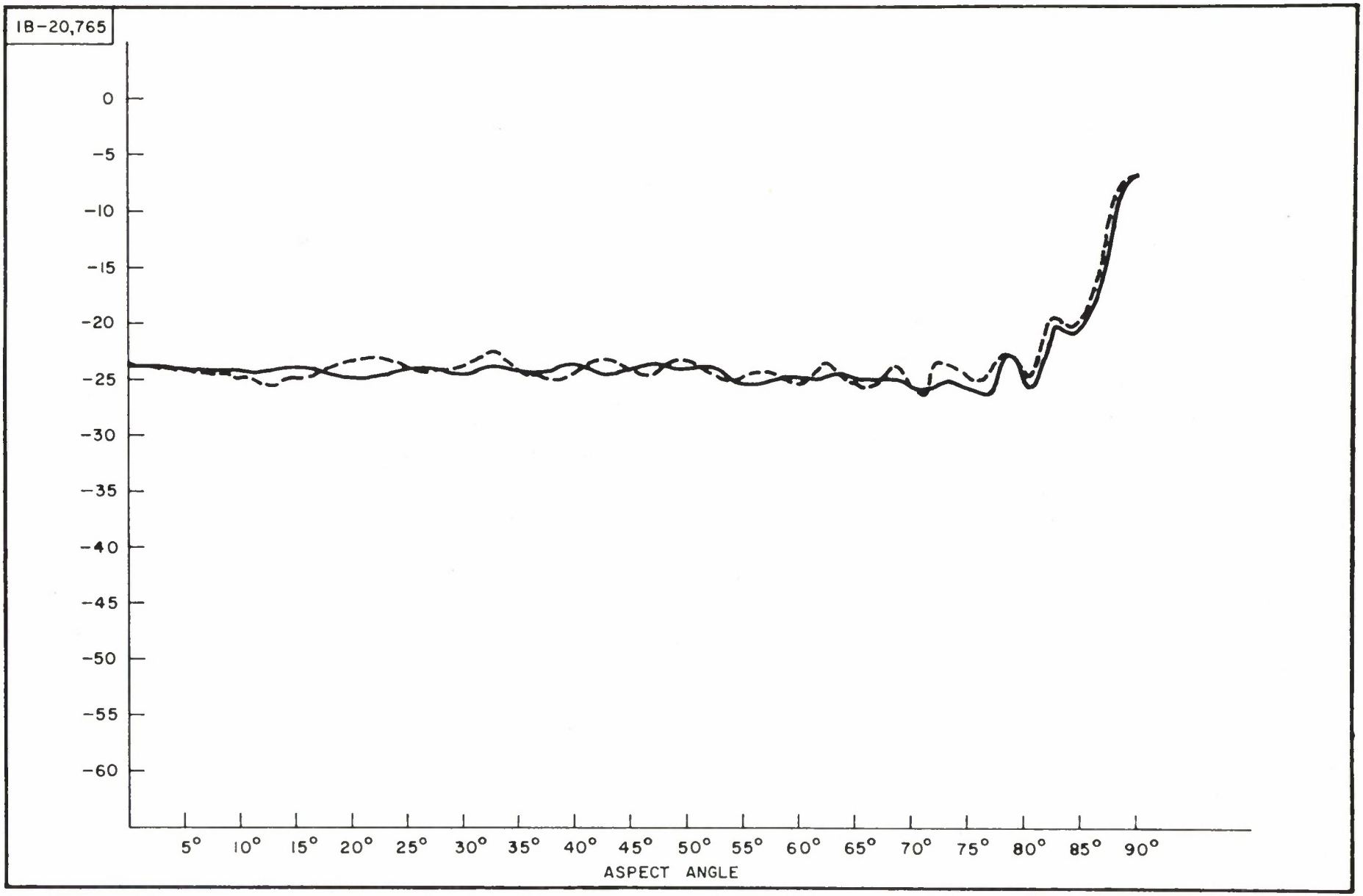

Figure 12. RADAR CROSS SECTION (DBSM) VERSUS ASPECT ANGLE FOR BODY NO. 2. HORIZONTAL POLARIZATION (SOLID) AND VERTICAL POLARIZATION (DOTTED)

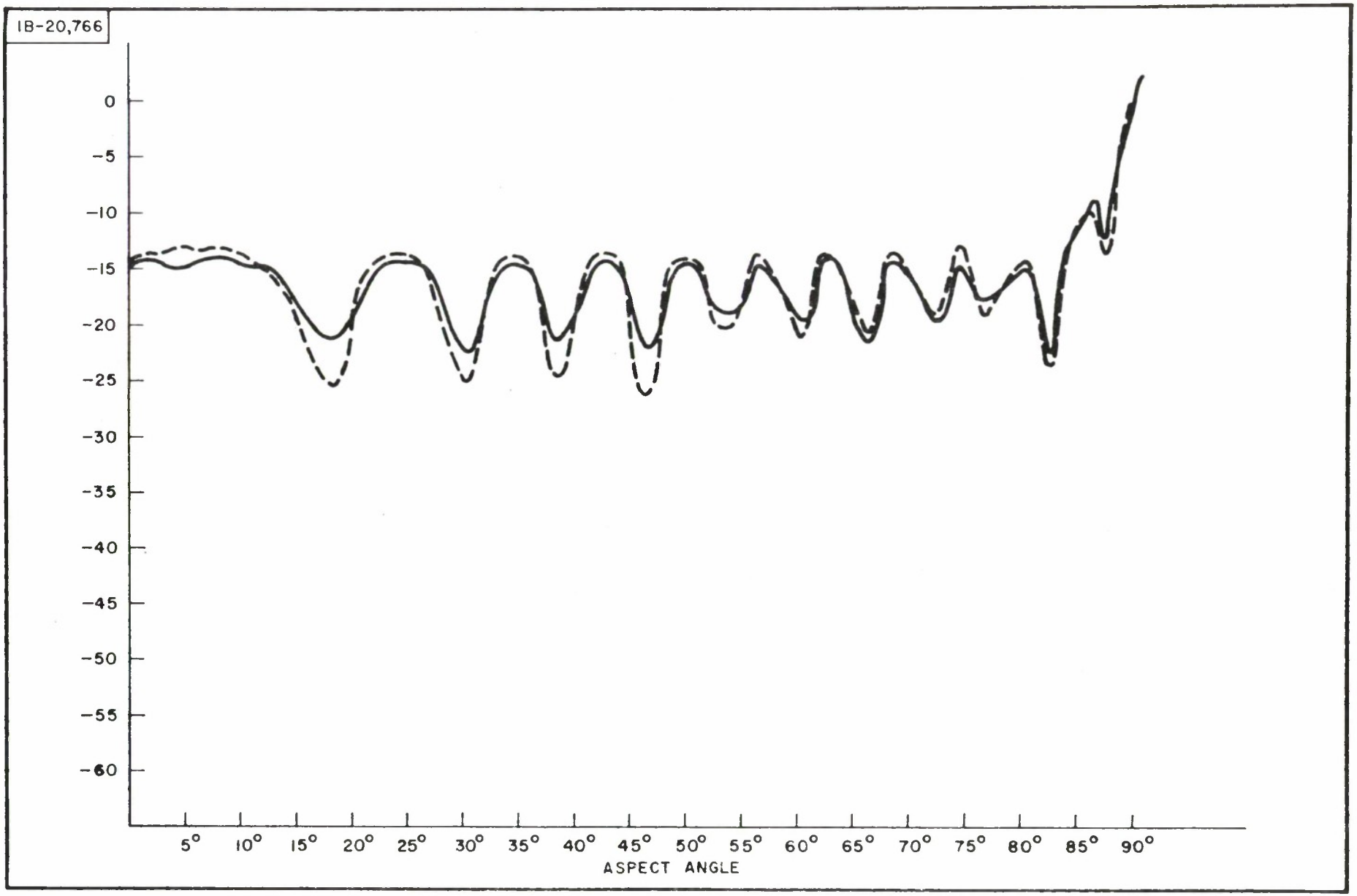

Figure 13. RADAR CROSS SECTION (DBSM) VERSUS ASPECT ANGLE FOR BODY NO. 3. HORIZONTAL POLARIZATION (SOLID) AND VERTICAL POLARIZATION (DOTTED)

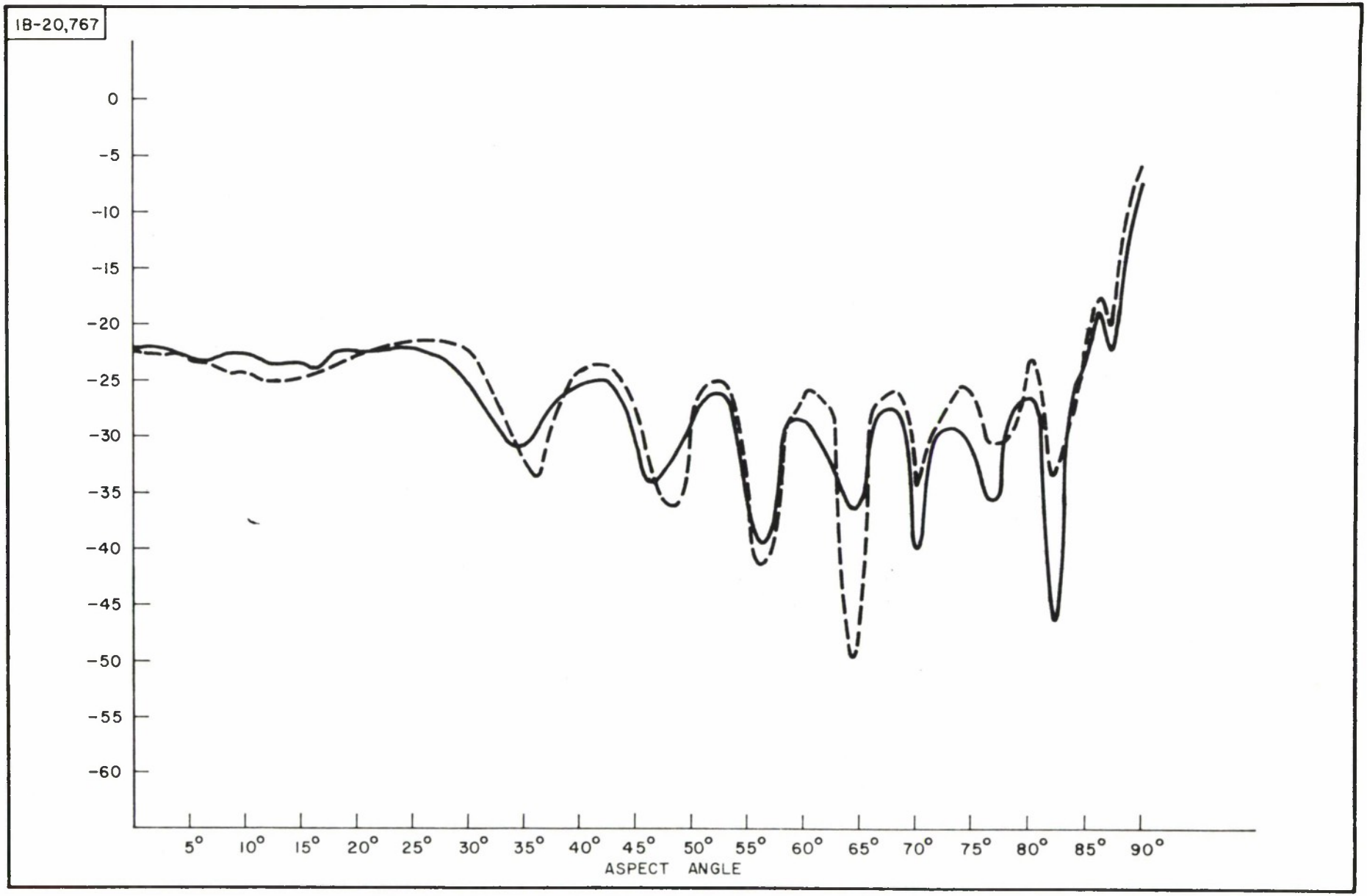

Figure 14. RADAR CROSS SECTION (DBSM) VERSUS ASPECT ANGLE FOR BODY NO. 4. HORIZONTAL POLARIZATION (SOLID) AND VERTICAL POLARIZATION (DOTTED)

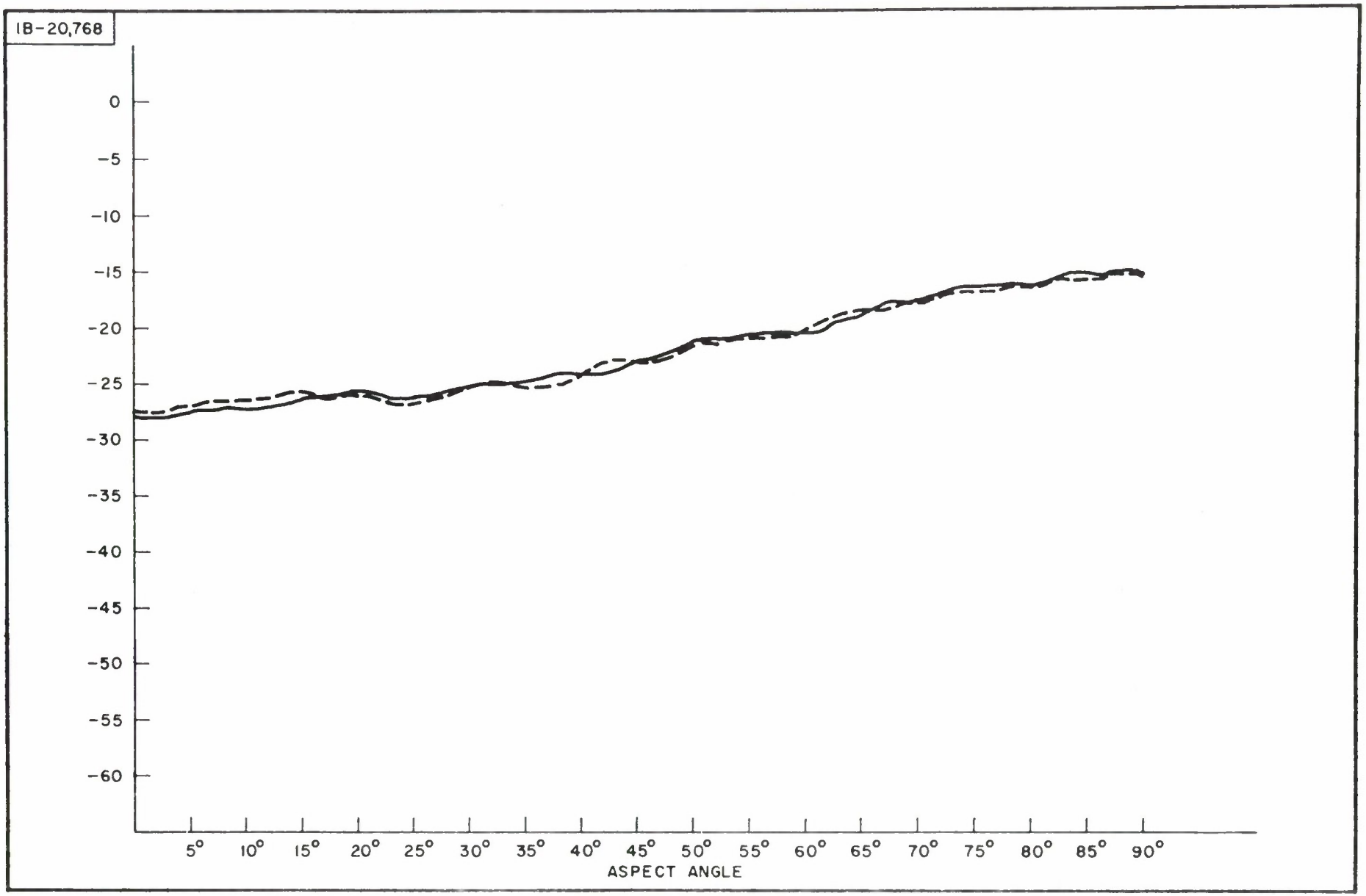

Figure 15. RADAR CROSS SECTION (DBSM) VERSUS ASPECT ANGLE FOR BODY NO. 5. HORIZONTAL POLARIZATION (SOLID) AND VERTICAL POLARIZATION (DOTTED)

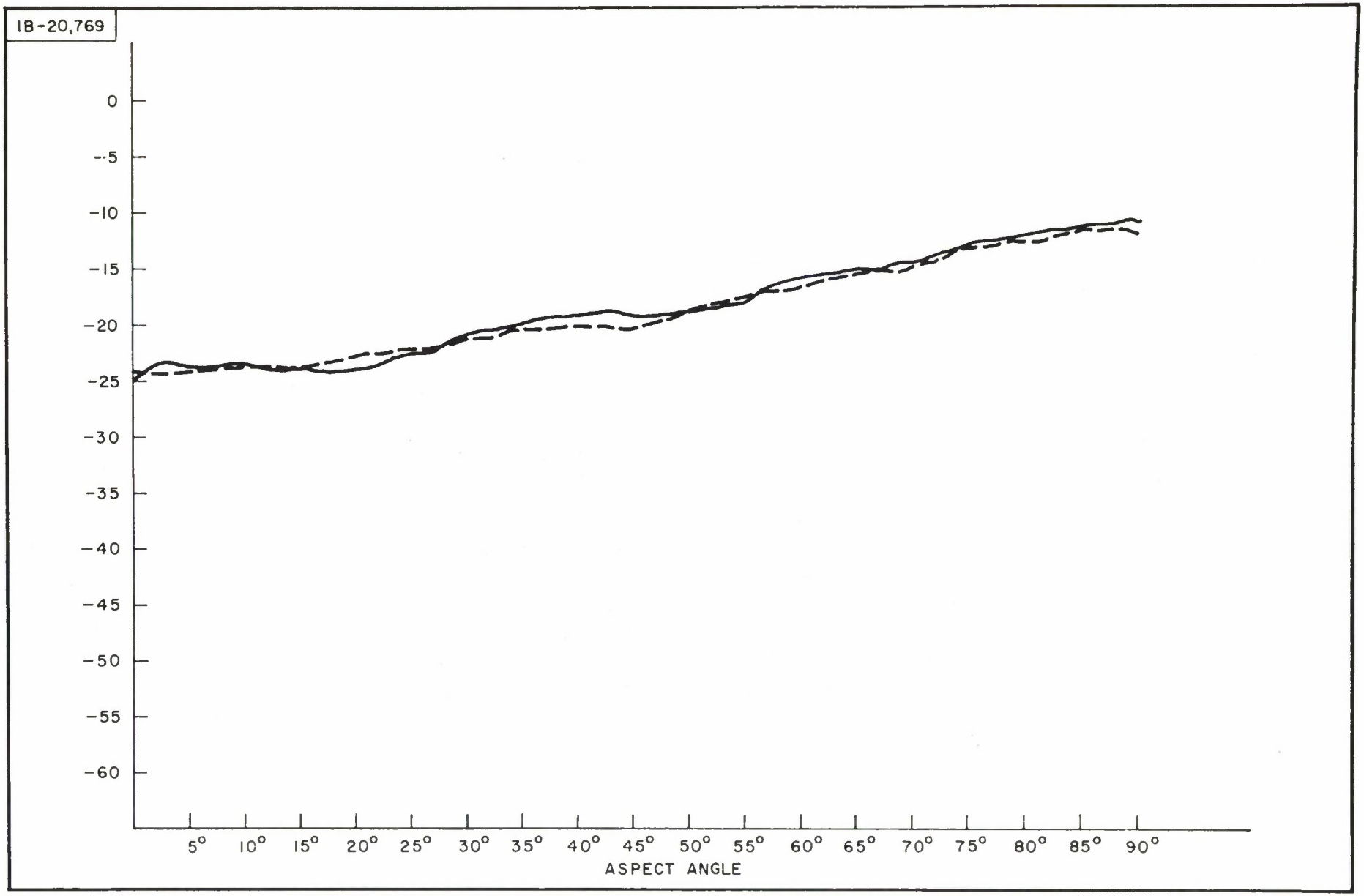

Figure 16. RADAR CROSS SECTION (DBSM) VERSUS ASPECT ANGLE FOR BODY NO. 6. HORIZONTAL POLARIZATION (SOLID) AND VERTICAL POLARIZATION (DOTTED)

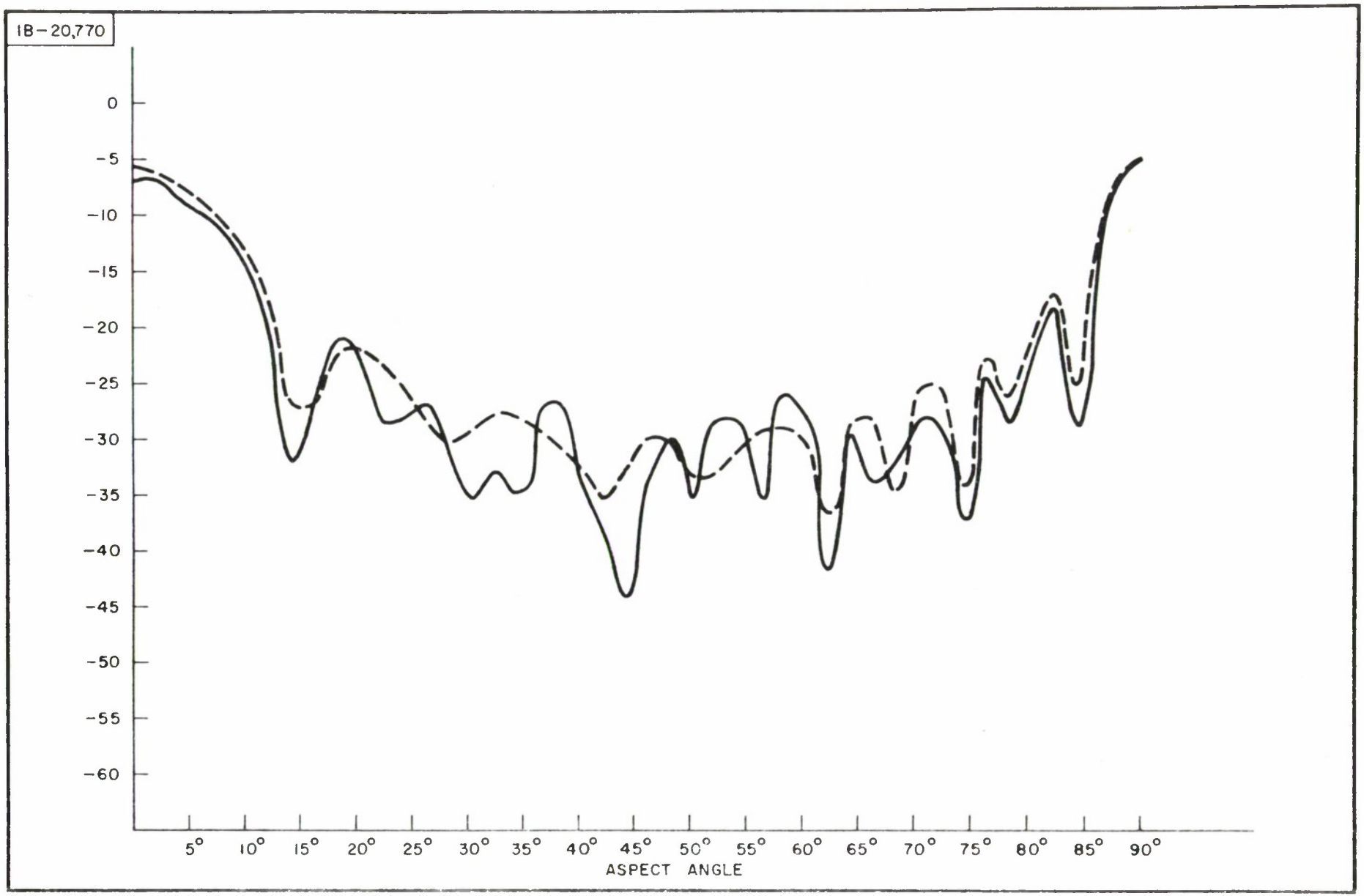

Figure 17. RADAR CROSS SECTION (DBSM) VERSUS ASPECT ANGLE FOR BODY NO. 7. HORIZONTAL POLARIZATION (SOLID) AND VERTICAL POLARIZATION (DOTTED)

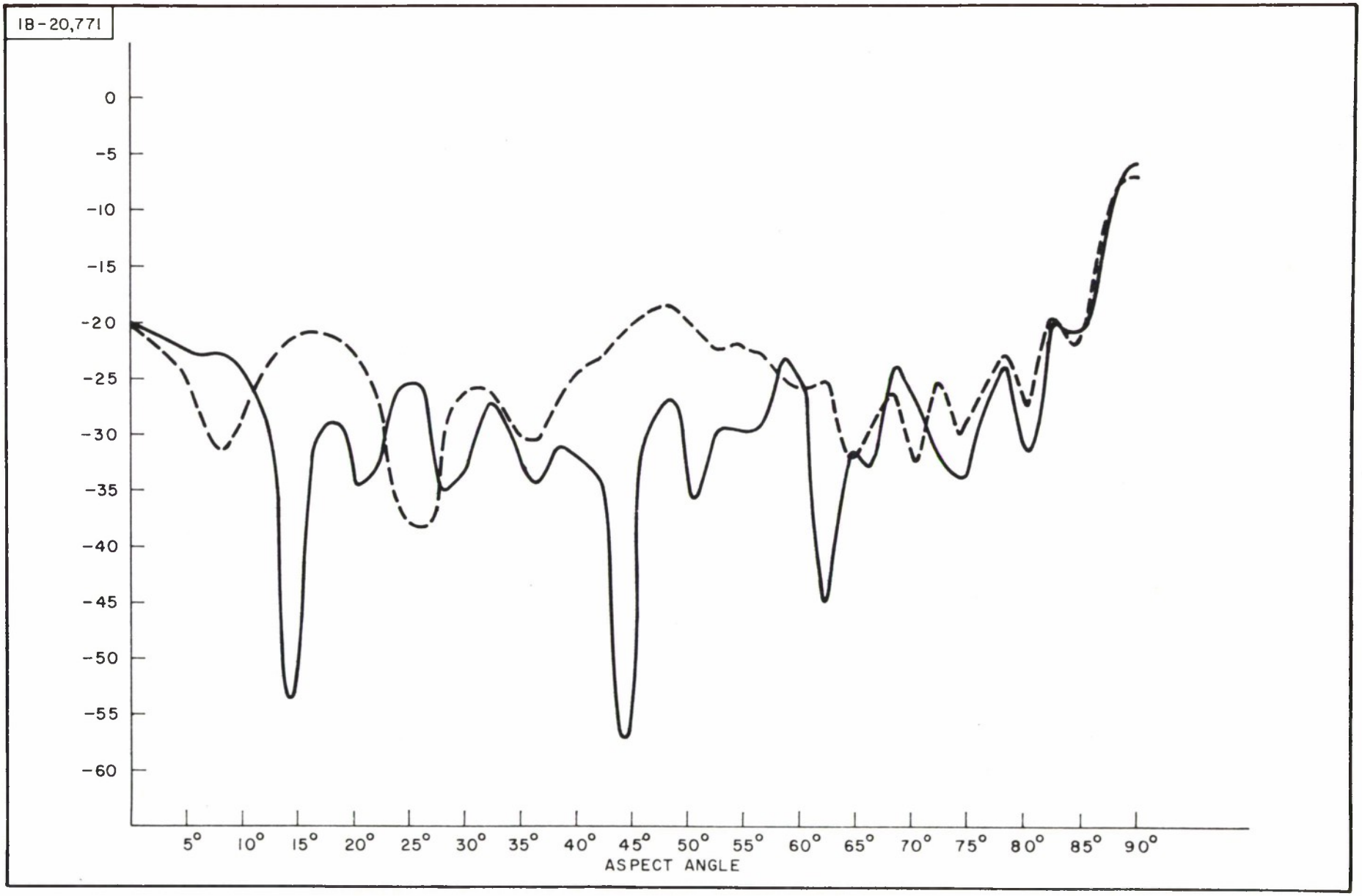

Figure 18. RADAR CROSS SECTION (DBSM) VERSUS ASPECT ANGLE FOR BODY NO. 8. HORIZONTAL POLARIZATION (SOLID) AND VERTICAL POLARIZATION (DOTTED)

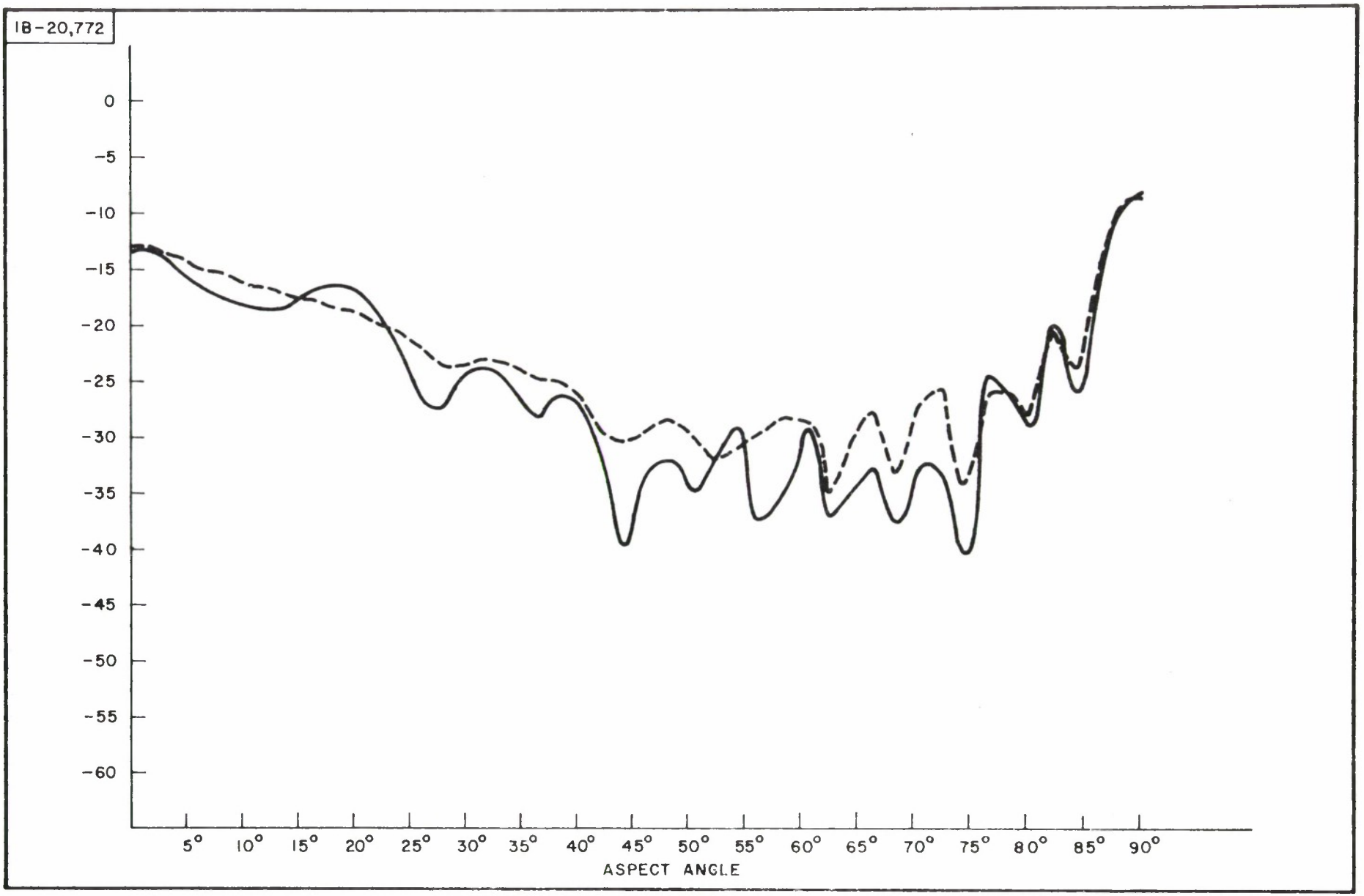

Figure 19. RADAR CROSS SECTION (DBSM) VERSUS ASPECT ANGLE FOR BODY NO. 9. HORIZONTAL POLARIZATION (SOLID) AND VERTICAL POLARIZATION (DOTTED)

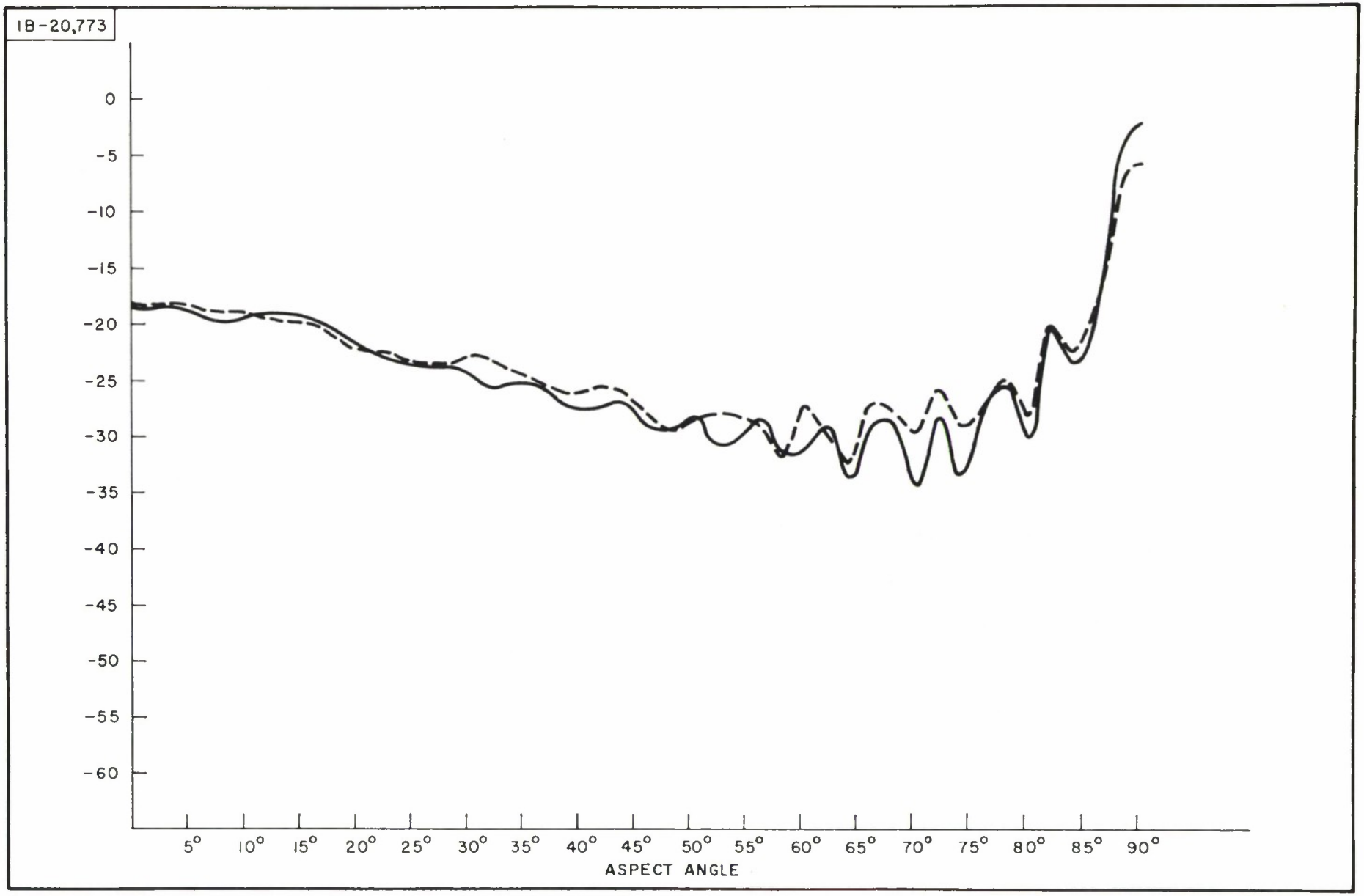

Figure 20. RADAR CROSS SECTION (DBSM) VERSUS ASPECT ANGLE FOR BODY NO. 10. HORIZONTAL POLARIZATION (SOLID) AND VERTICAL POLARIZATION (DOTTED)

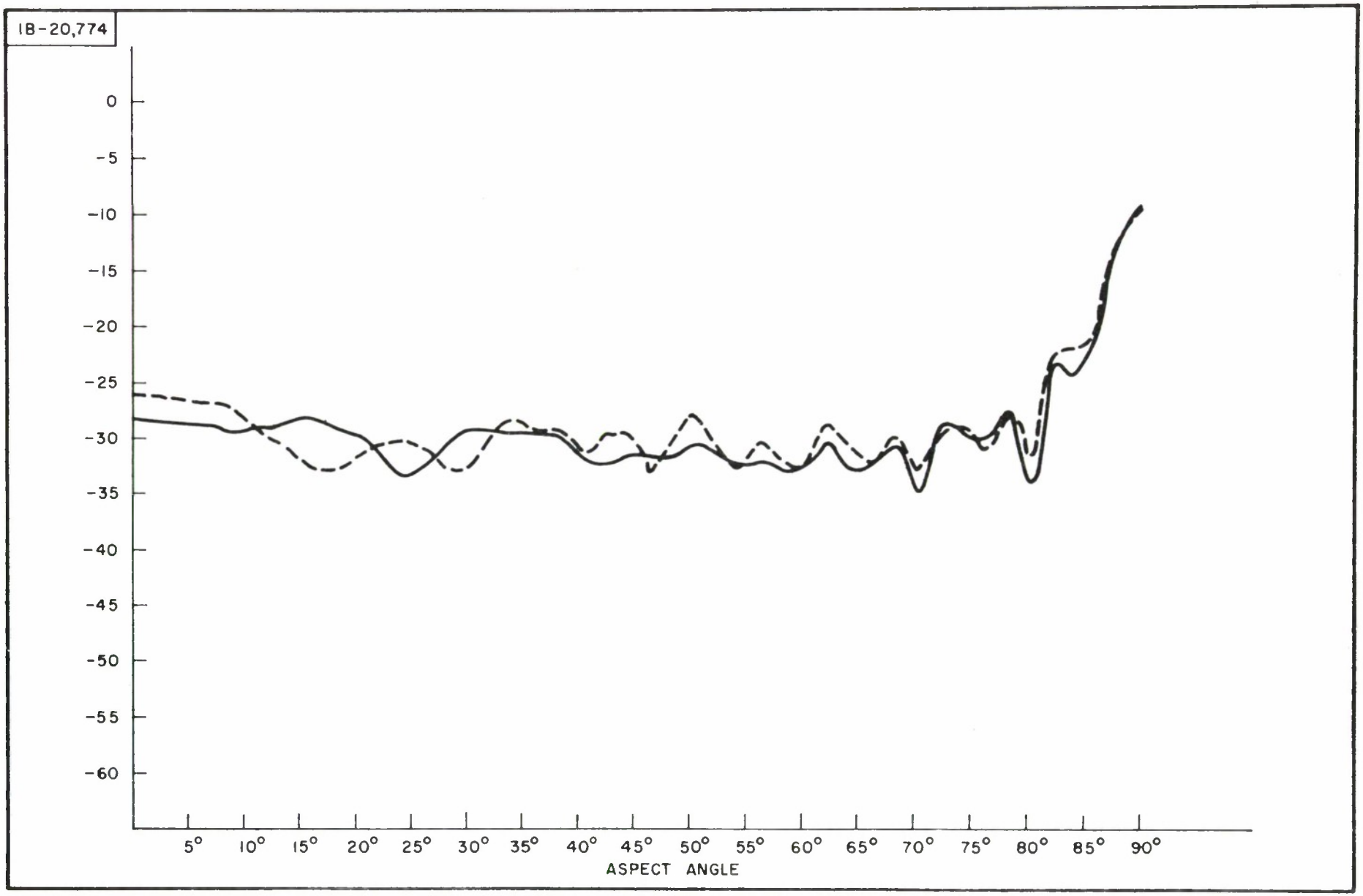

Figure 21. RADAR CROSS SECTION (DBSM) VERSUS ASPECT ANGLE FOR BODY NO. II. HORIZONTAL POLARIZATION (SOLID) AND VERTICAL POLARIZATION (DOTTED)

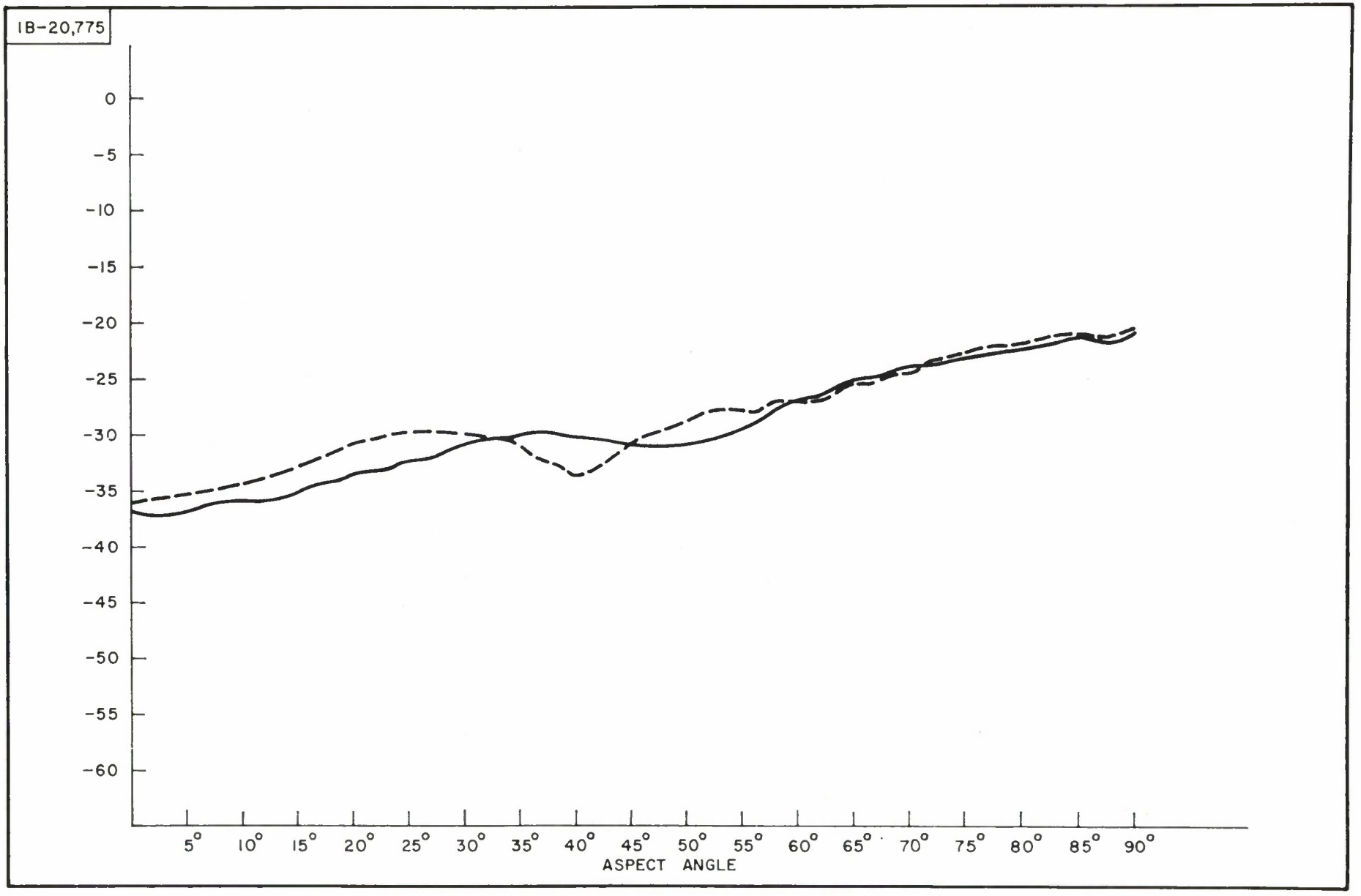

Figure 22. RADAR CROSS SECTION (DBSM) VERSUS ASPECT ANGLE FOR BODY NO.12. HORIZONTAL POLARIZATION (SOLID) AND VERTICAL POLARIZATION (DOTTED)

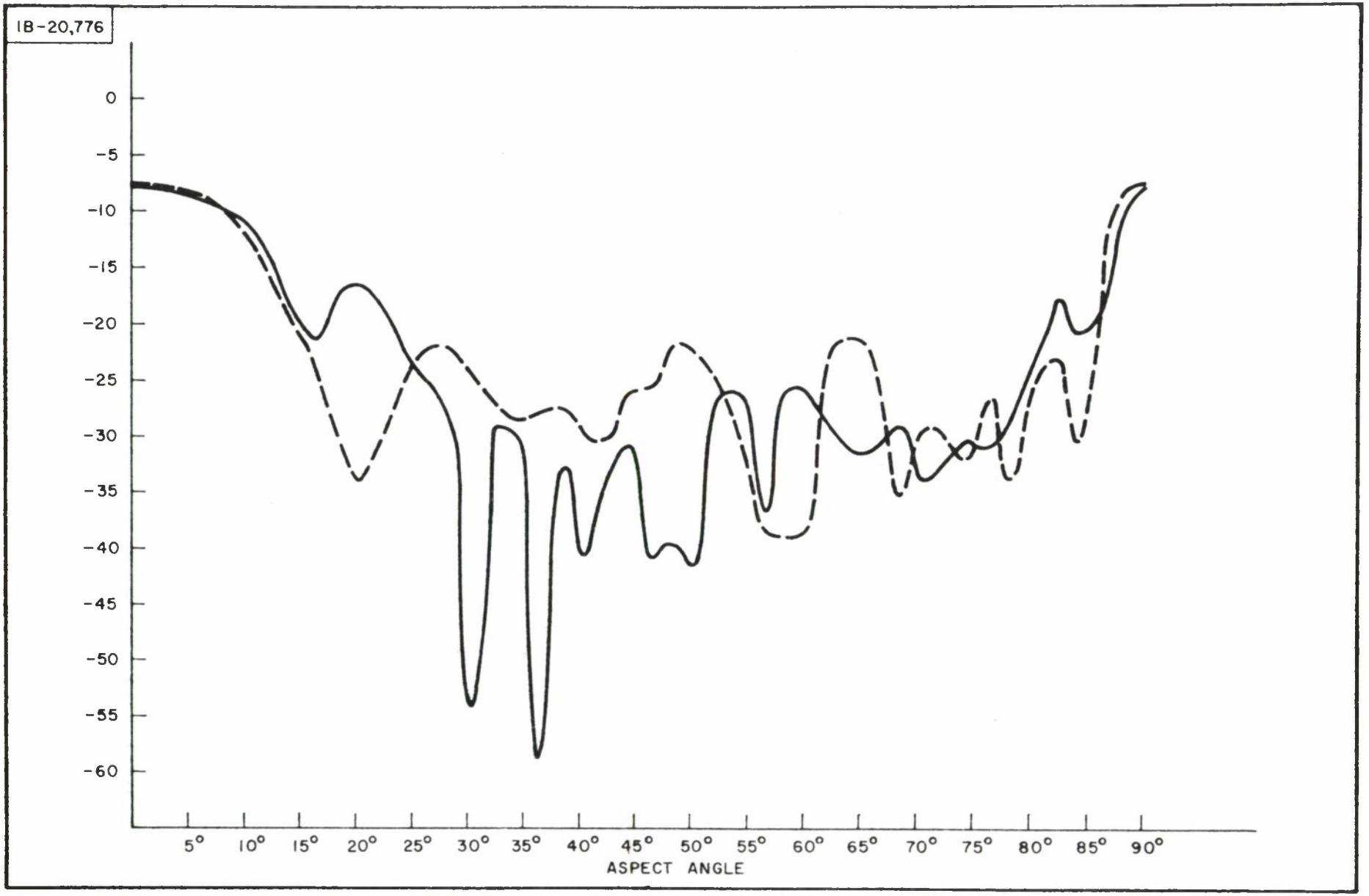

Figure 23. RADAR CROSS SECTION (DBSM) VERSUS ASPECT ANGLE FOR BODY NO. 13. HORZONTAL POLARIZATION (SOLID) AND VERTICAL POLARIZATION (DOTTED)

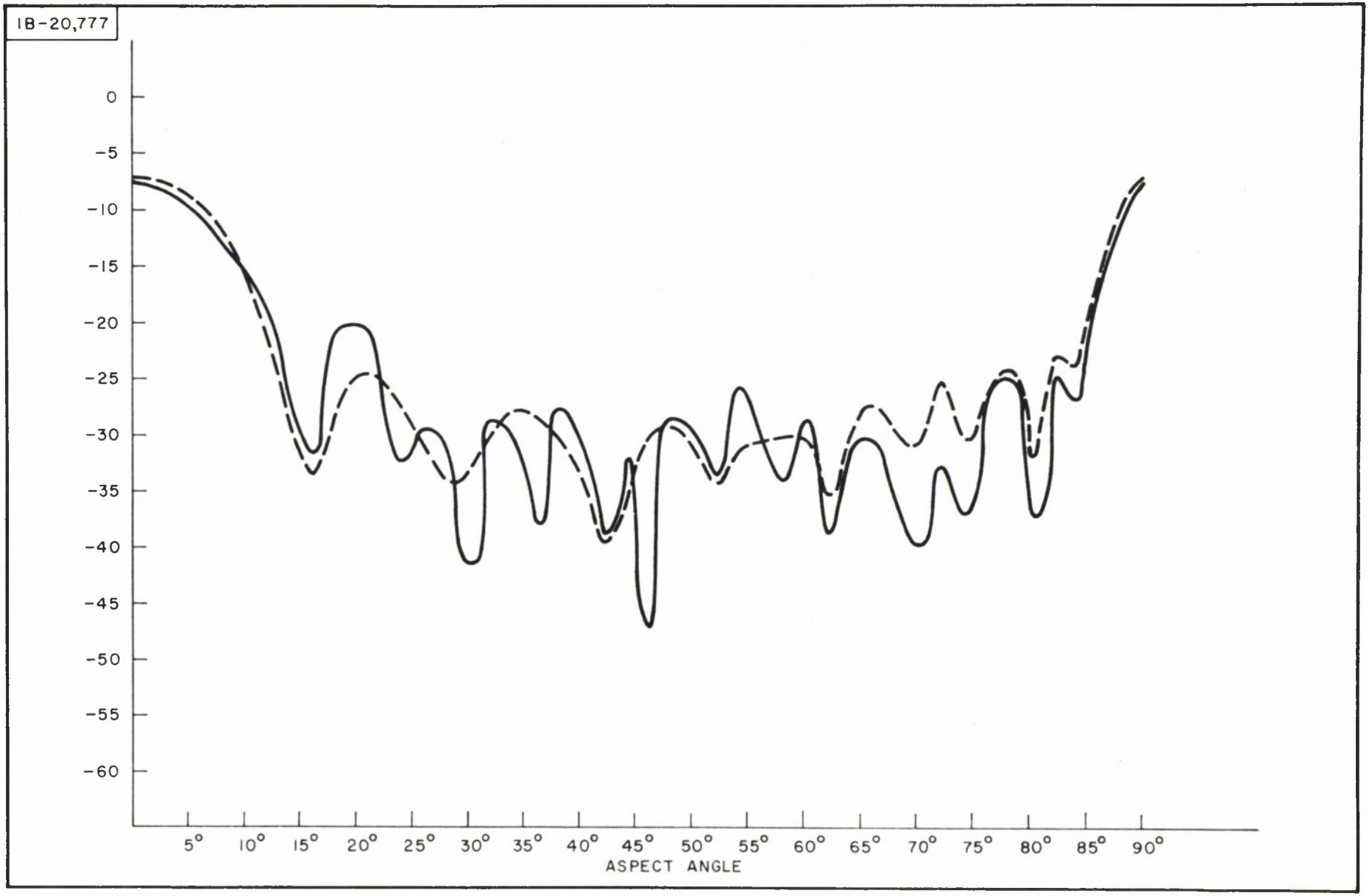

Figure 24. RADAR CROSS SECTION (DBSM) VERSUS ASPECT ANGLE FOR BODY NO. 14. HORIZONTAL POLARIZATION (SOLID) AND VERTICAL POLARIZATION (DOTTED)

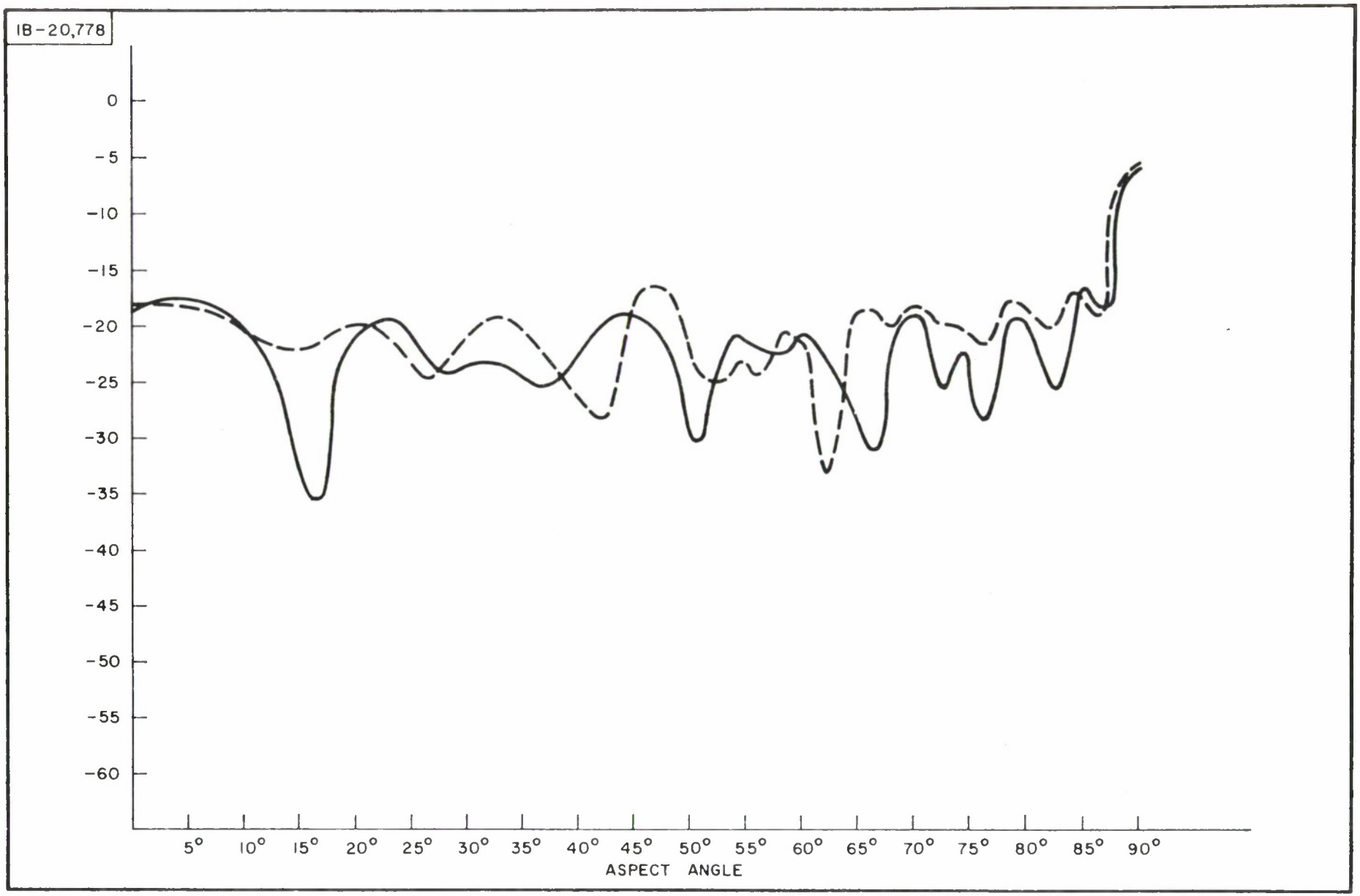

Figure 25. RADAR CROSS SECTION (DBSM) VERSUS ASPECT ANGLE FOR BODY NO. 15. HORIZONTAL POLARIZATION (SOLID) AND VERTICAL POLARIZATION (DOTTED)

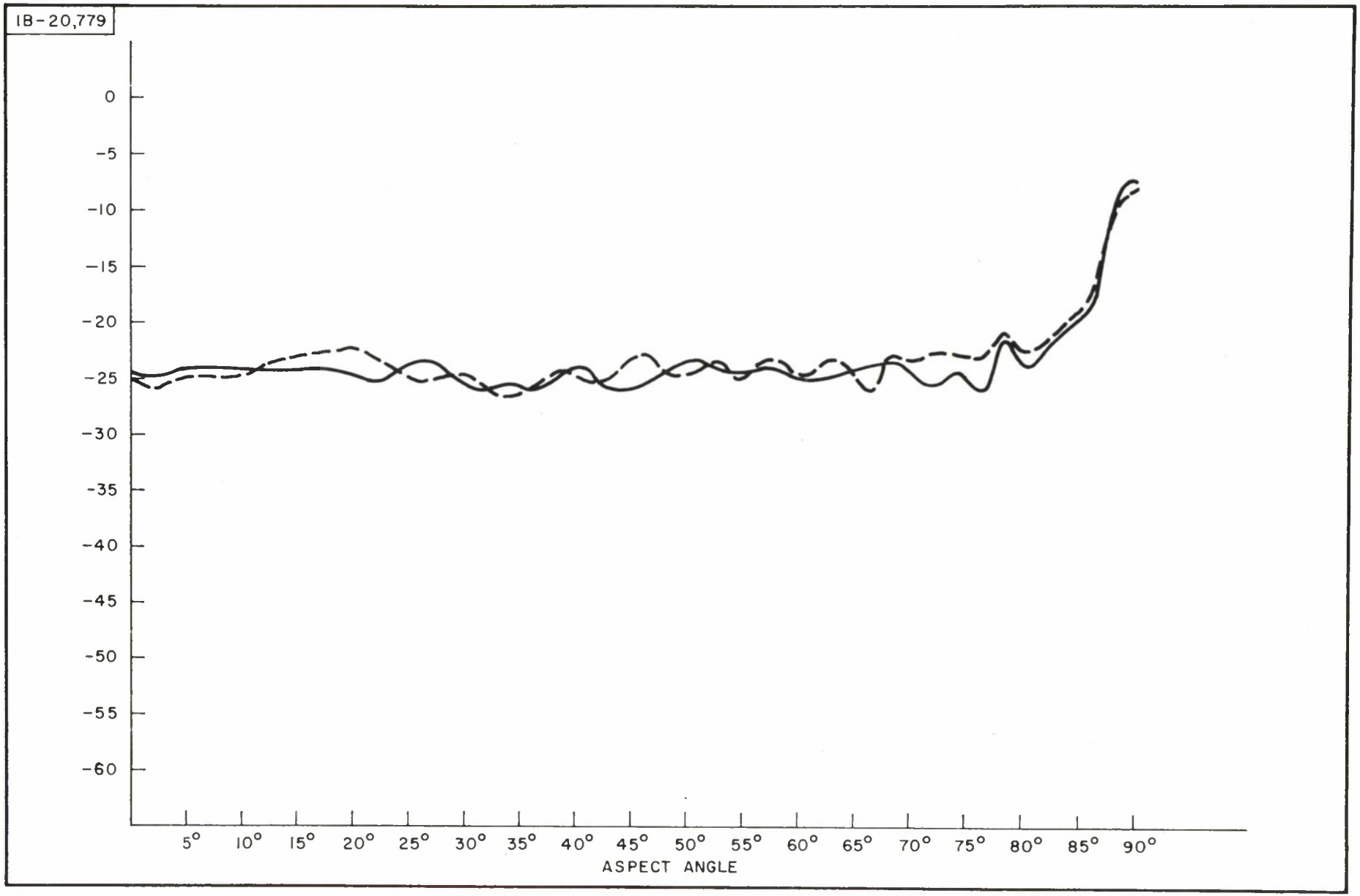

Figure 26. RADAR CROSS SECTION (DBSM) VERSUS ASPECT ANGLE FOR BODY NO. 16. HORIZONTAL POLARIZATION (SOLID) AND VERTICAL POLARIZATION (DOTTED)

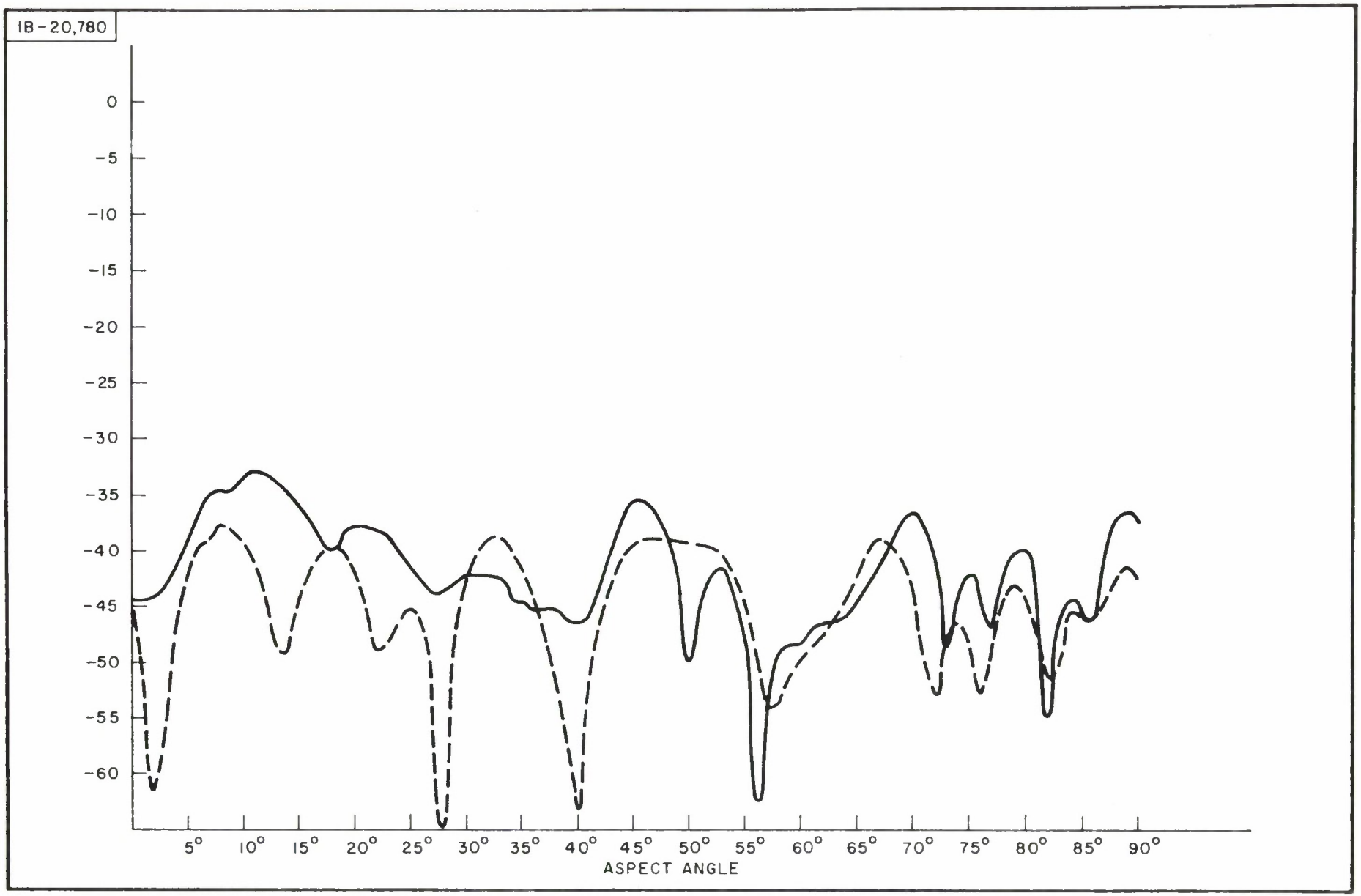

Figure 27. RADAR CROSS SECTIONS σ_{HV} FOR BODY NO. 13 (DOTTED) AND BODY NO. 15 (SOLID) VERSUS ASPECT ANGLE

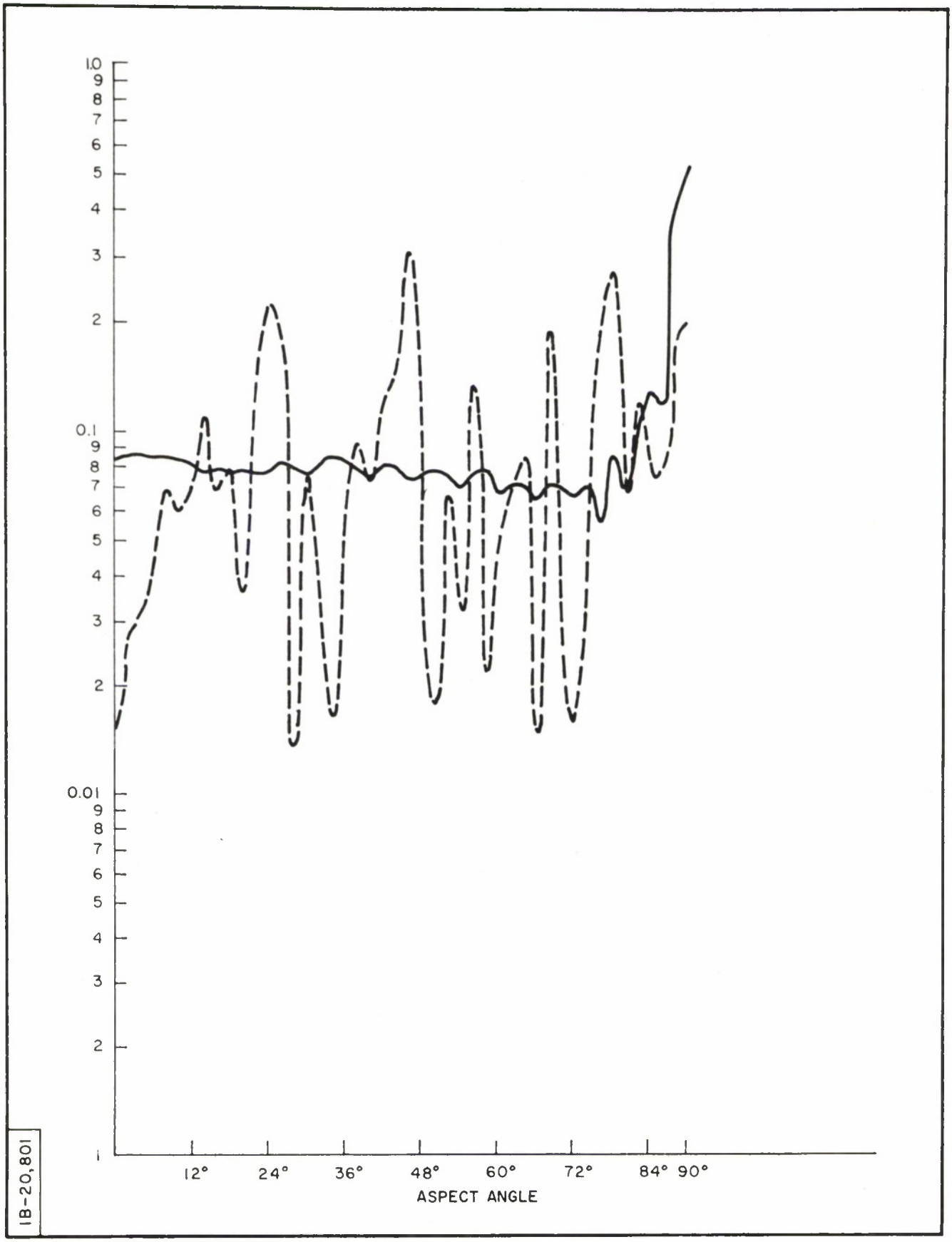

Figure 28. THE S-MATRIX ELEMENT s_{LR} (SOLID) AND $D=s_{LL}/s_{LR}$ (DOTTED) VERSUS ASPECT ANGLE FOR BODY NO. 1

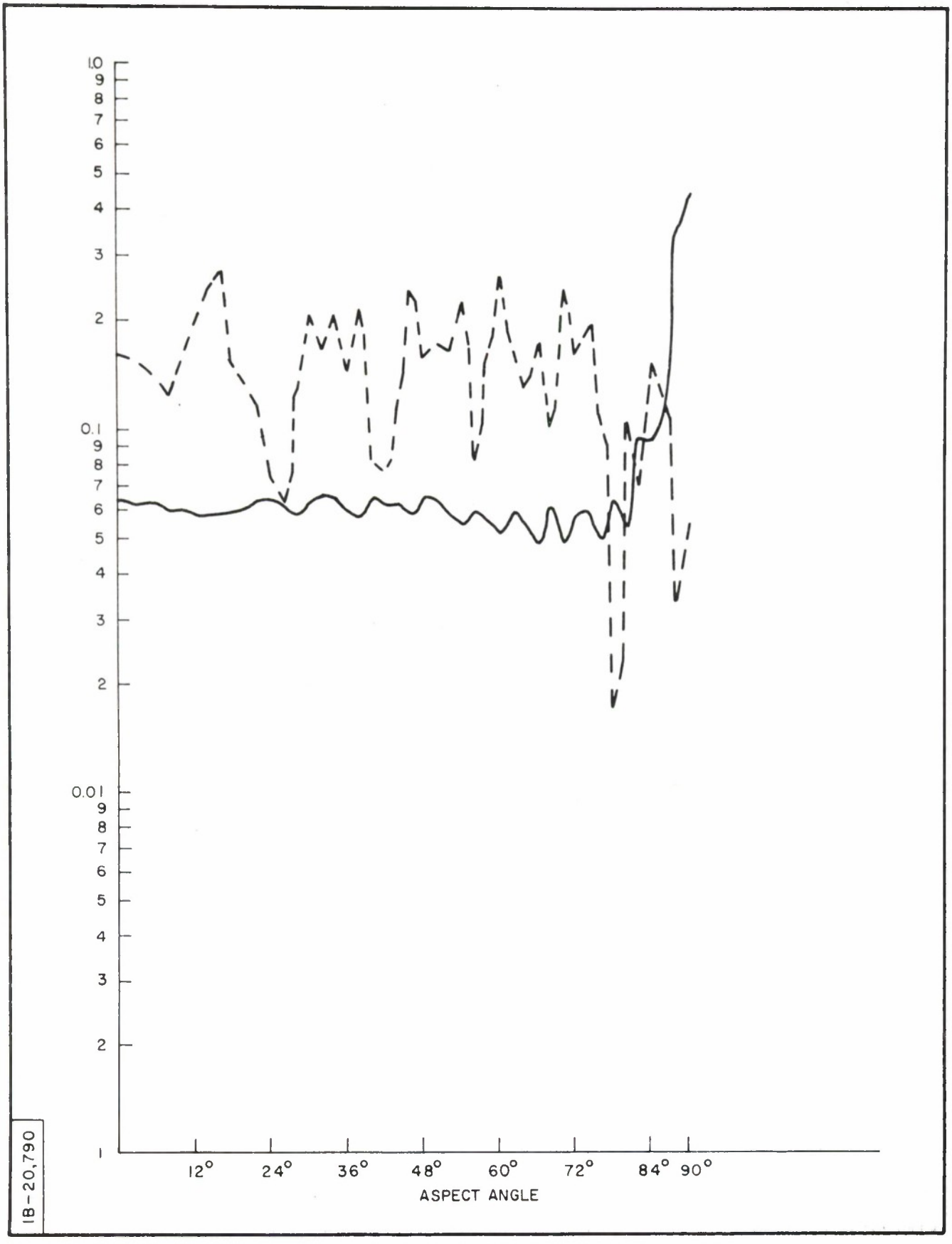

Figure 29. THE S-MATRIX ELEMENT s_{LR} (SOLID) AND $D = s_{LL}/s_{LR}$ (DOTTED) VERSUS ASPECT ANGLE FOR BODY NO. 2

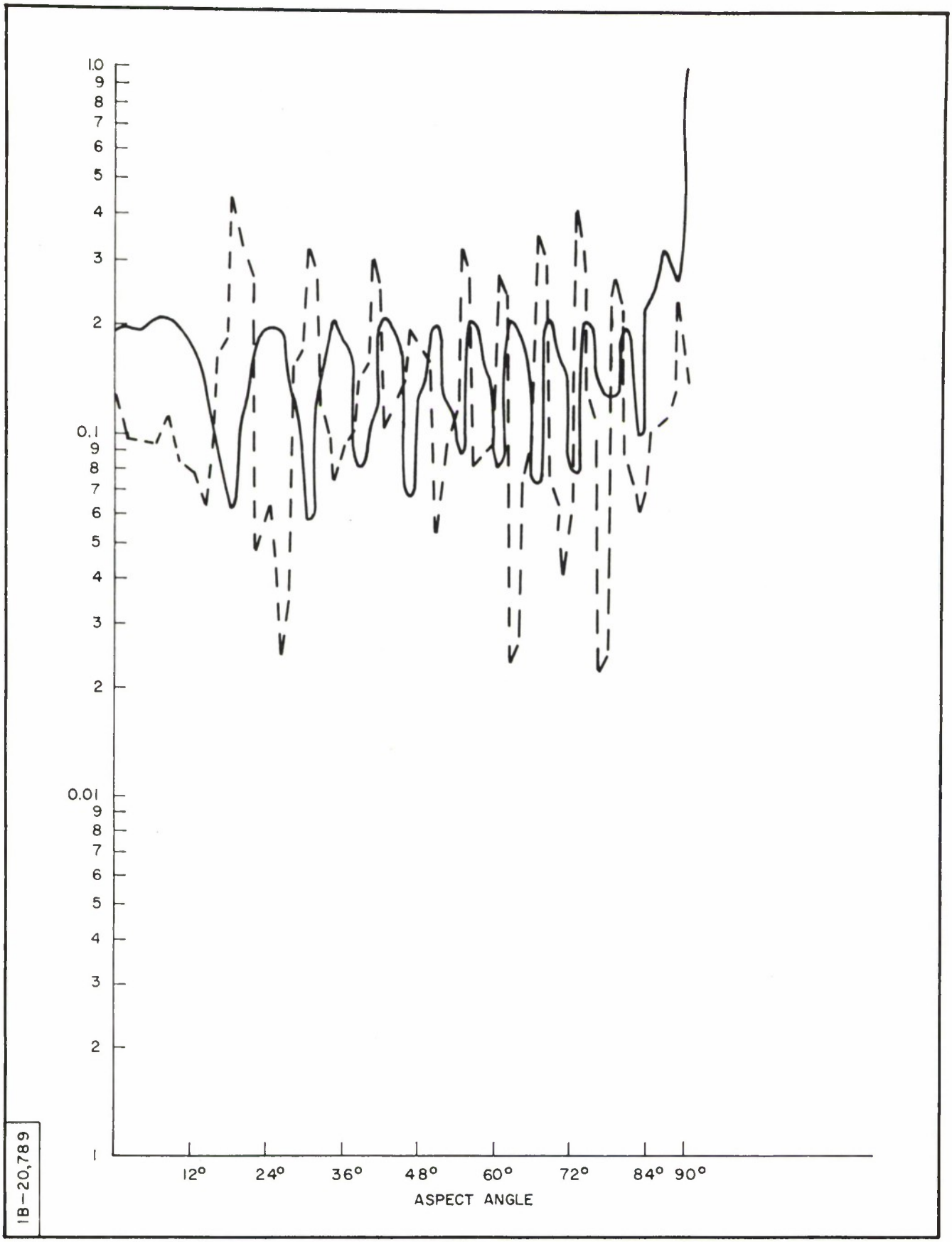

Figure 30. THE S-MATRIX ELEMENT s_{LR} (SOLID) AND $D=s_{LL}/s_{LR}$ (DOTTED) VERSUS ASPECT ANGLE FOR BODY NO. 3

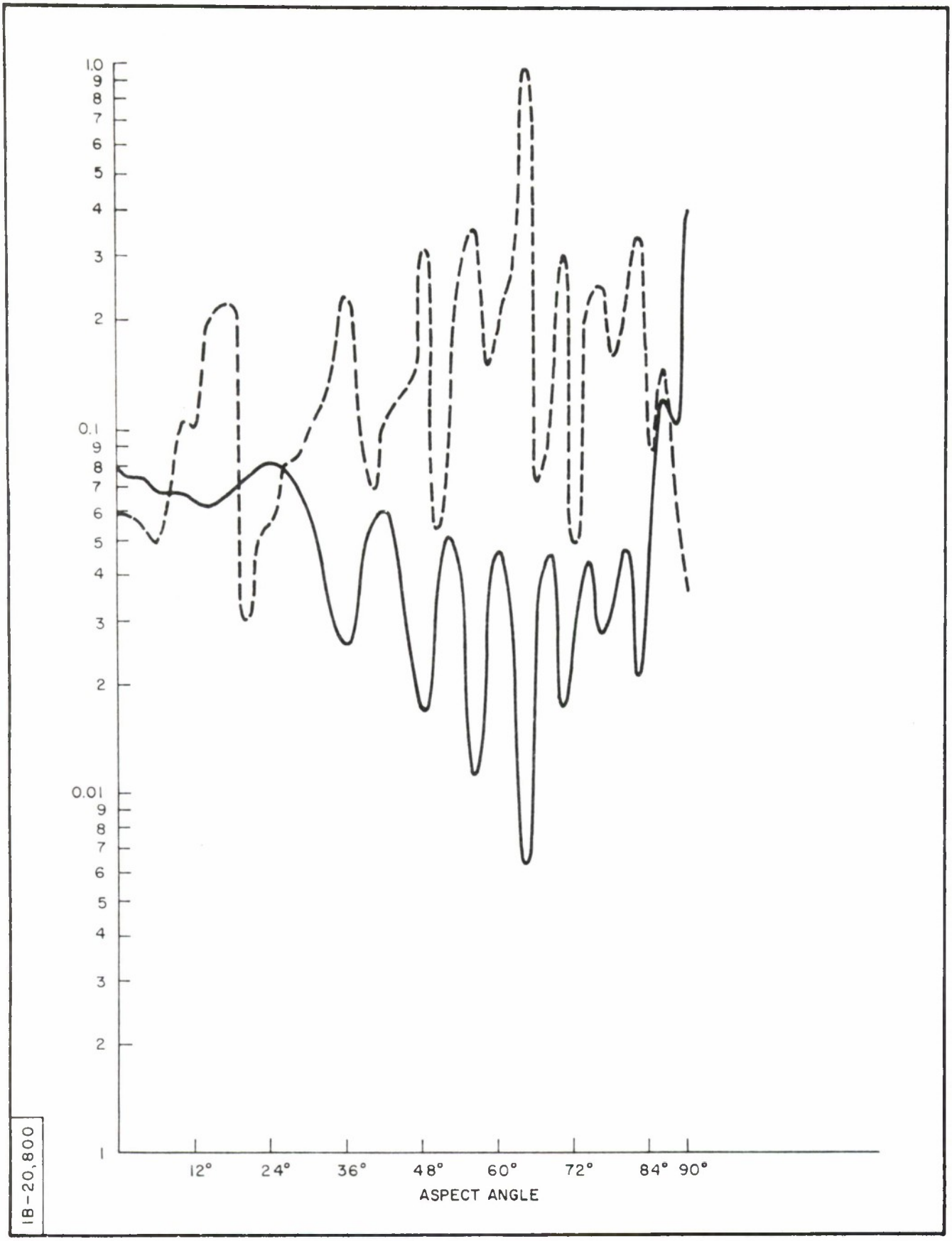

Figure 31. THE S-MATRIX ELEMENT s_{LR} (SOLID) AND $D = s_{LL}/s_{LR}$ (DOTTED) VERSUS ASPECT ANGLE FOR BODY NO. 4

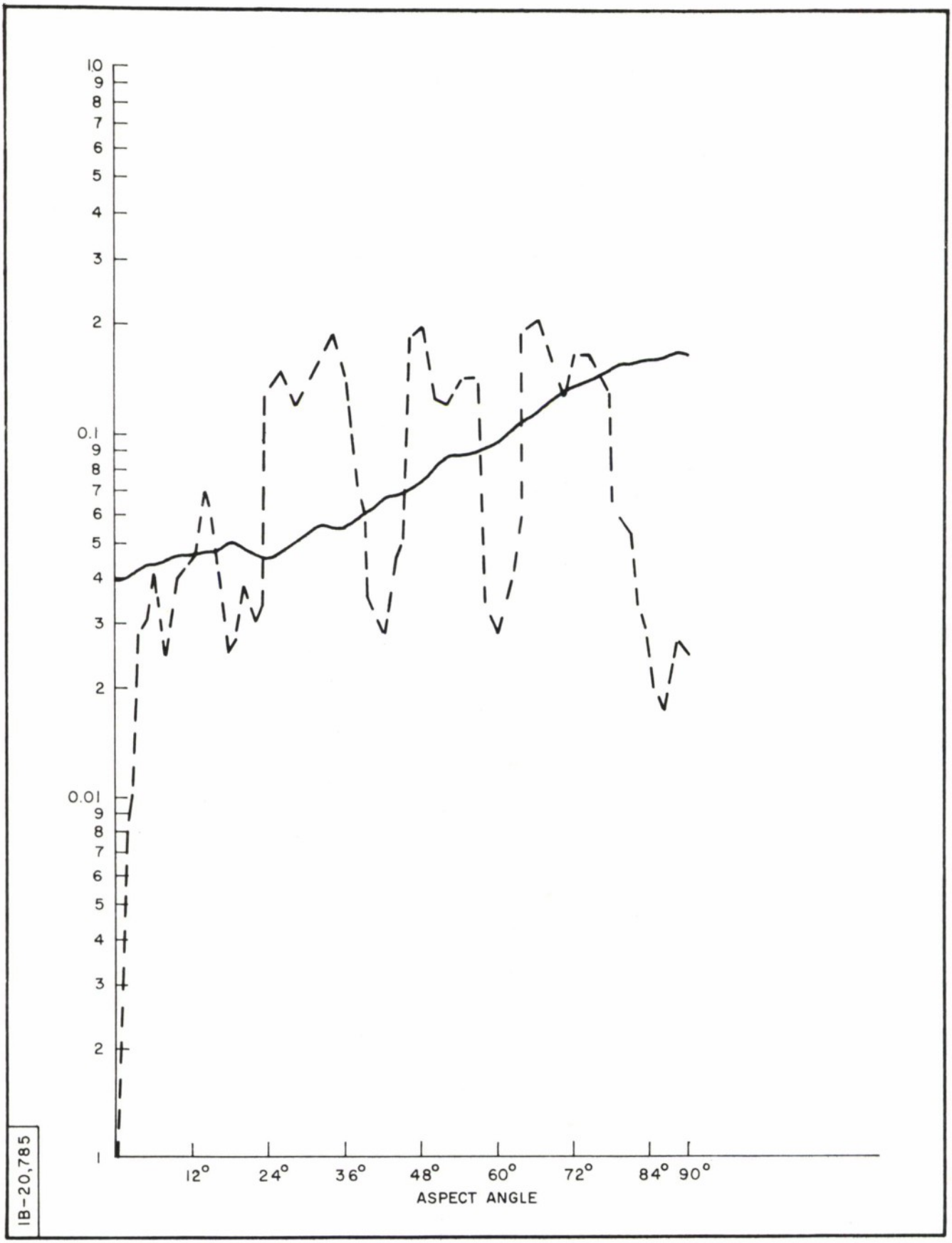

Figure 32. THE S-MATRIX ELEMENT s_{LR} (SOLID) AND $D = s_{LL}/s_{LR}$ (DOTTED) VERSUS ASPECT ANGLE FOR BODY NO. 5

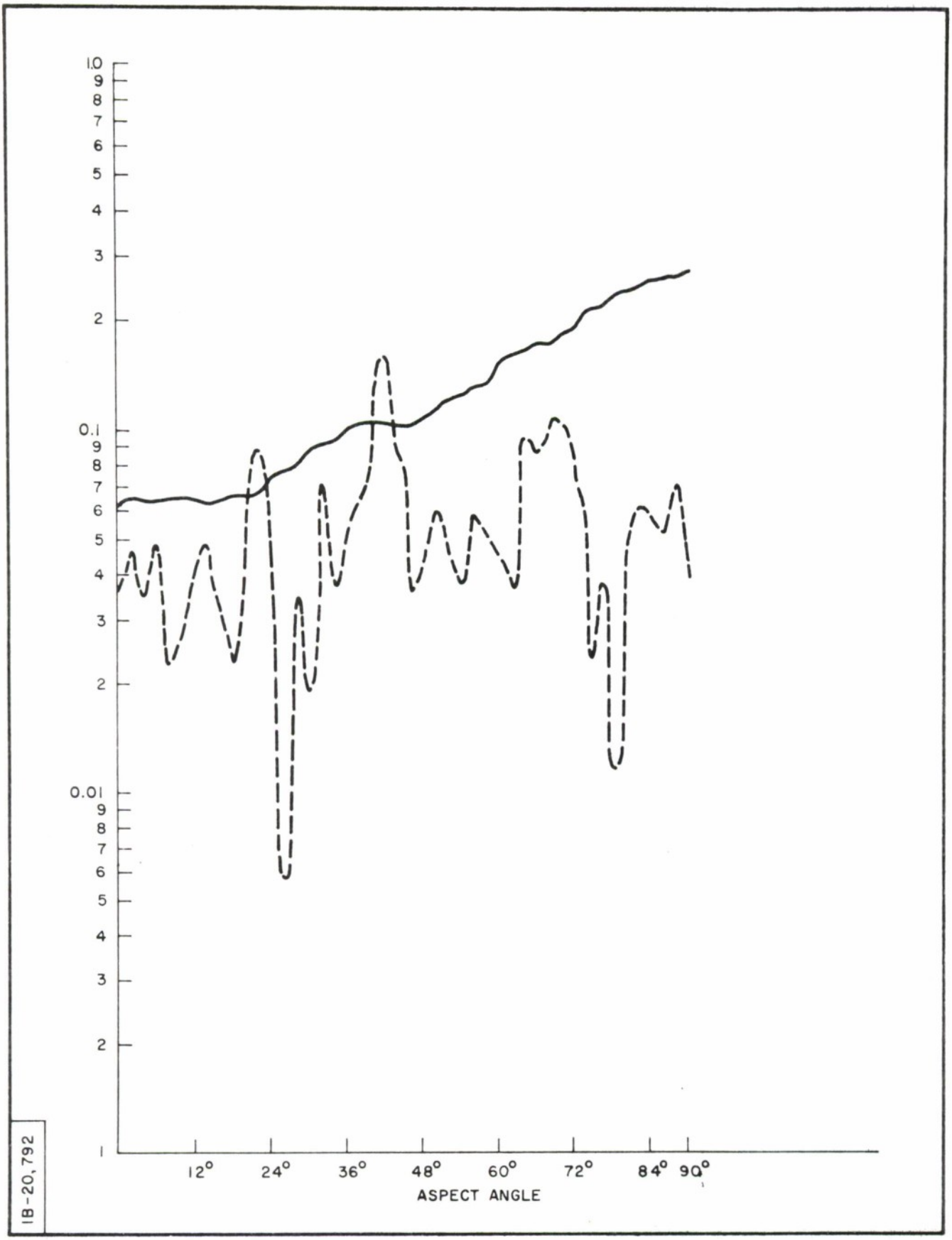

Figure 33. THE S-MATRIX ELEMENT s_{LR} (SOLID) AND $D = s_{LL}/s_{LR}$ (DOTTED) VERSUS ASPECT ANGLE FOR BODY NO. 6

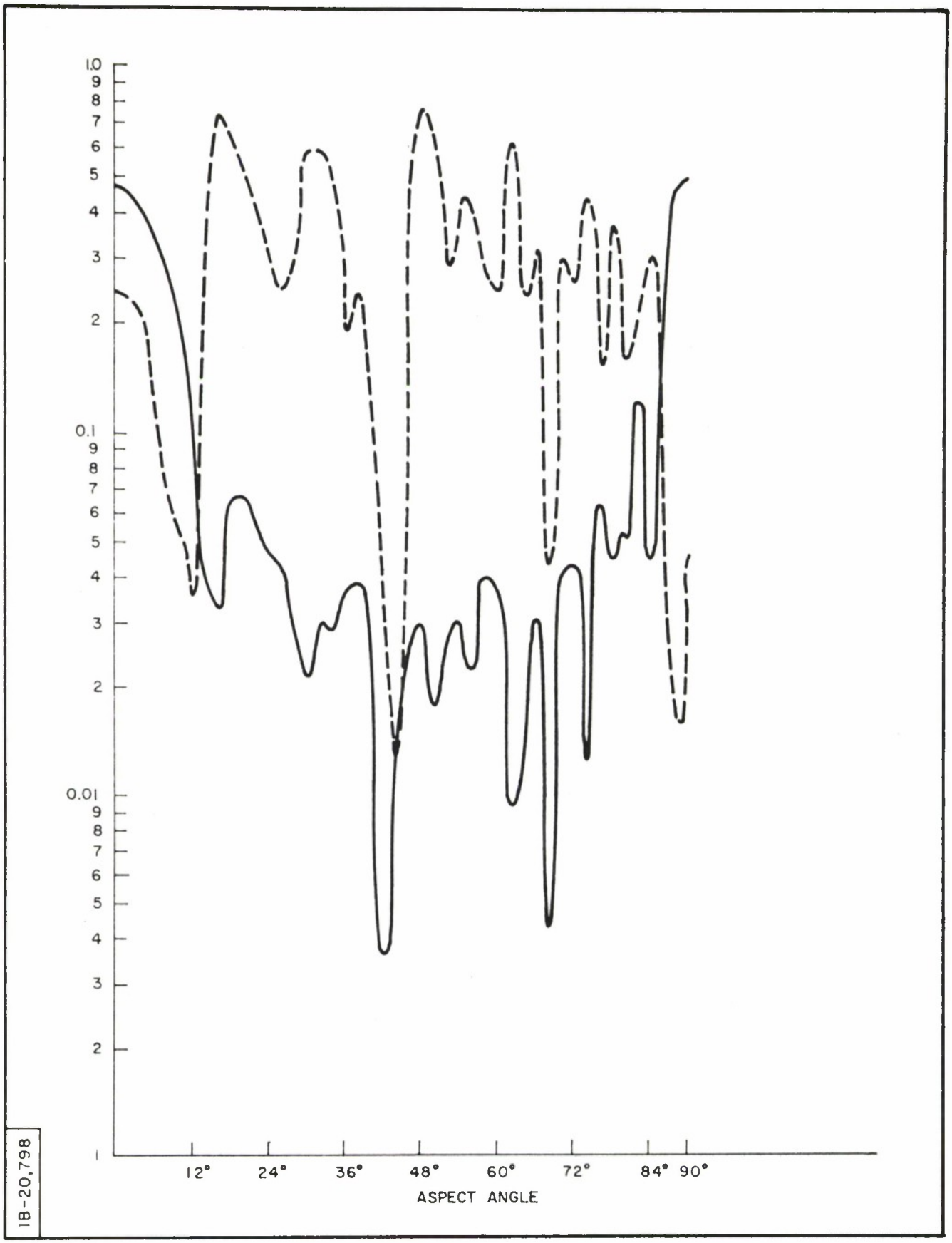

Figure 34. THE S-MATRIX ELEMENT s_{LR} (SOLID) AND $D=s_{LL}/s_{LR}$ (DOTTED) VERSUS ASPECT ANGLE FOR BODY NO. 7

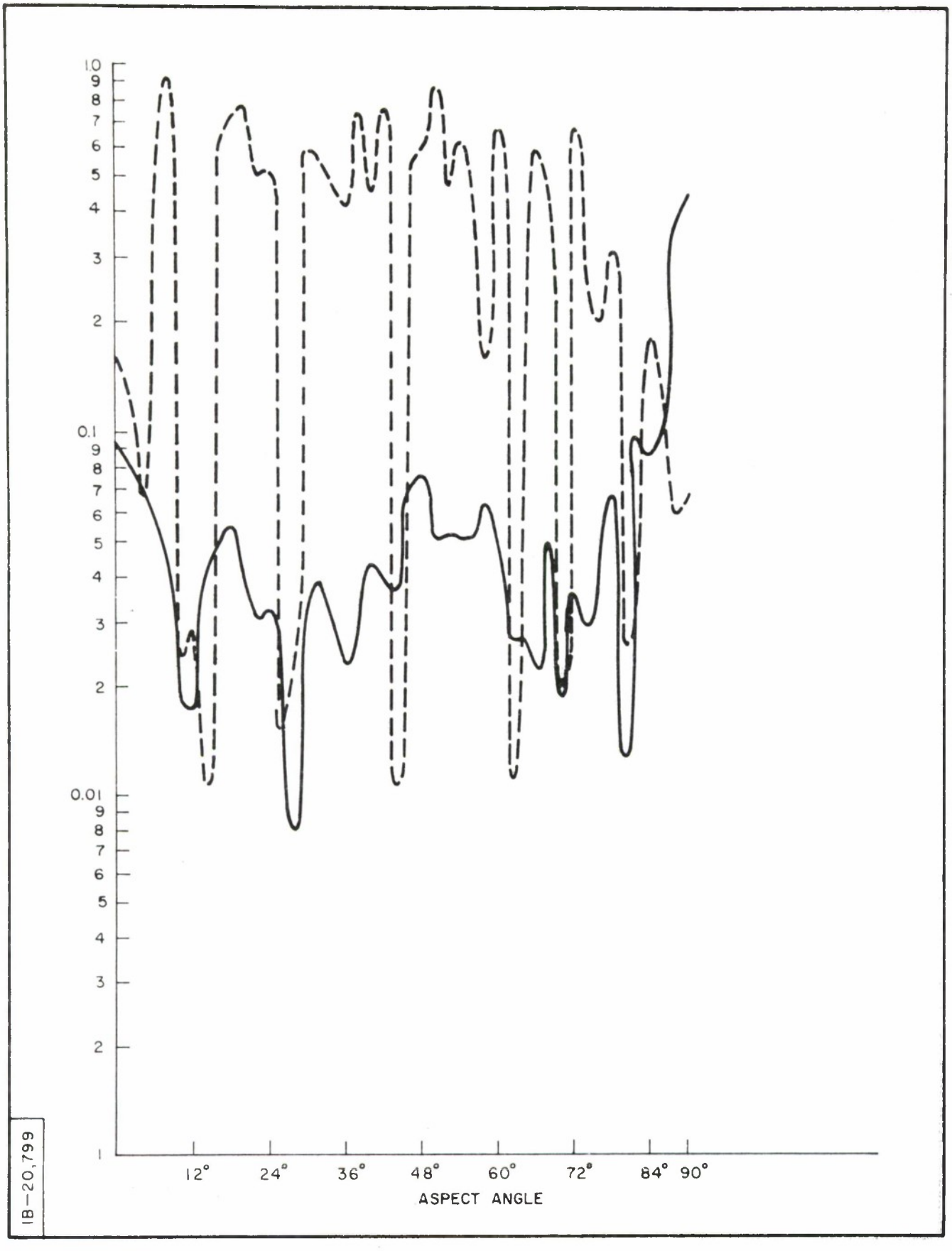

Figure 35. THE S-MATRIX ELEMENT s_{LR} (SOLID) AND $D = s_{LL}/s_{LR}$ (DOTTED) VERSUS ASPECT ANGLE FOR BODY NO. 8

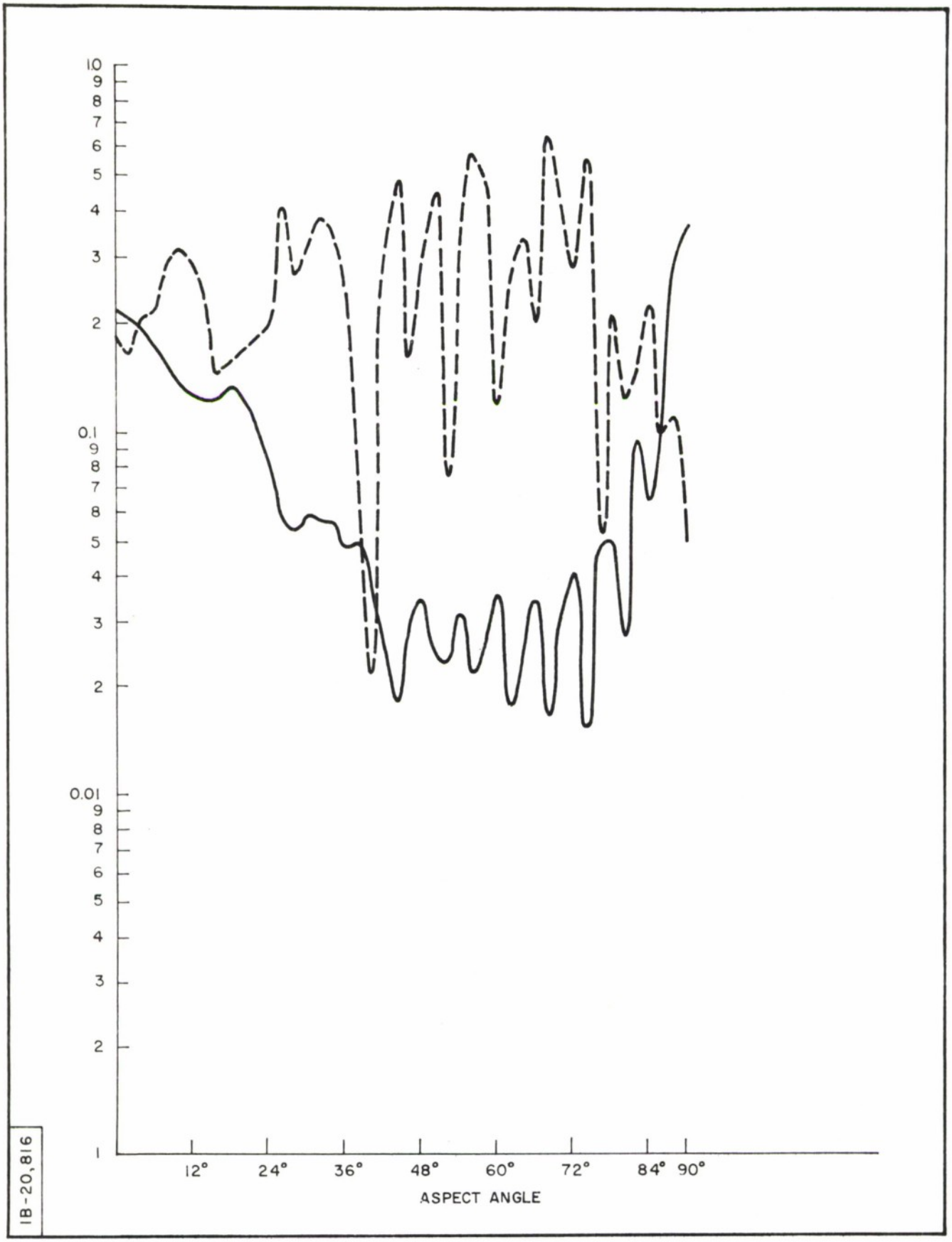

Figure 36. THE S-MATRIX ELEMENT s_{LR} (SOLID) AND $D=s_{LL}/s_{LR}$ (DOTTED) VERSUS ASPECT ANGLE FOR BODY NO. 9

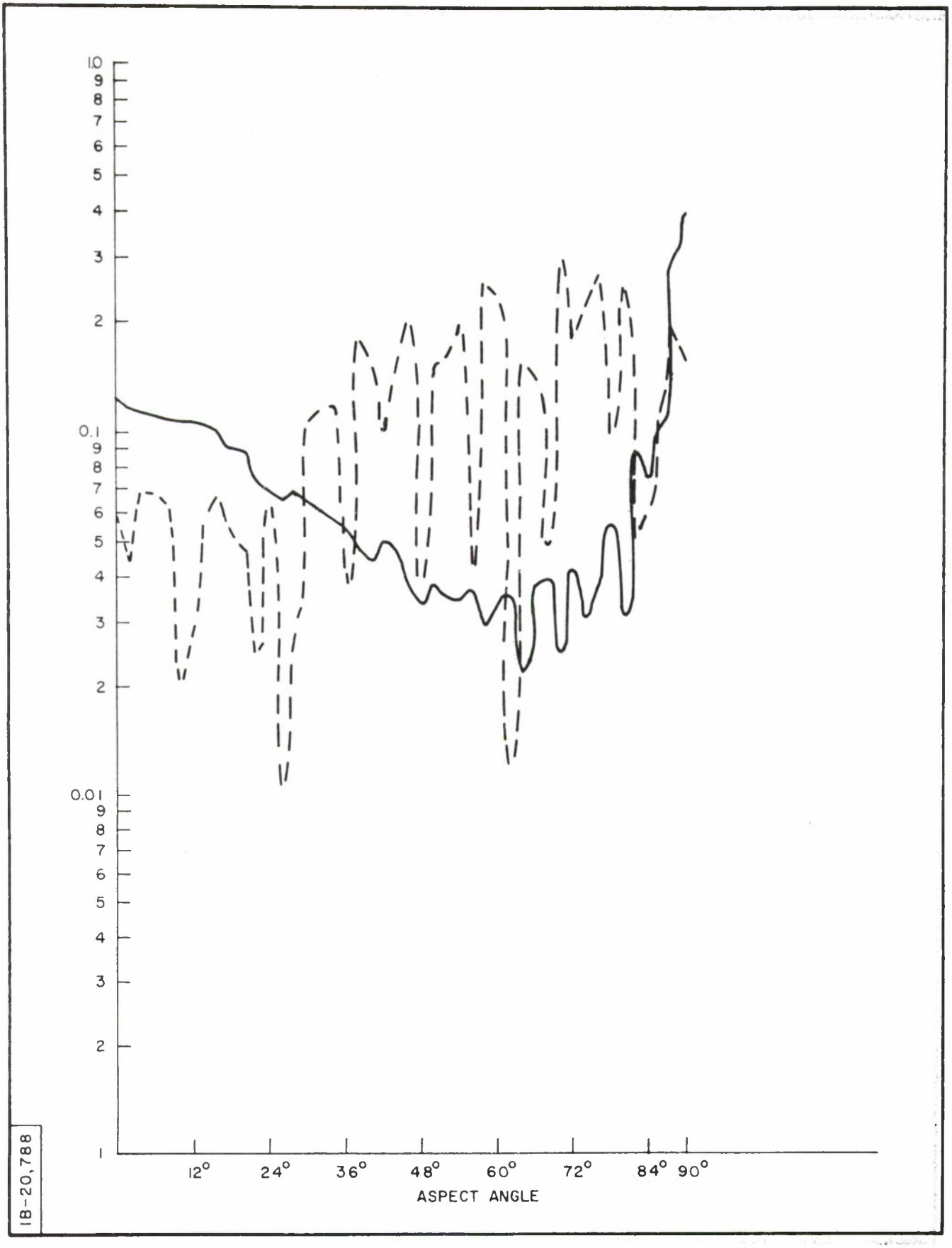

Figure 37. THE S-MATRIX ELEMENT s_{LR} (SOLID) AND $D = s_{LL}/s_{LR}$ (DOTTED) VERSUS ASPECT ANGLE FOR BODY NO. 10

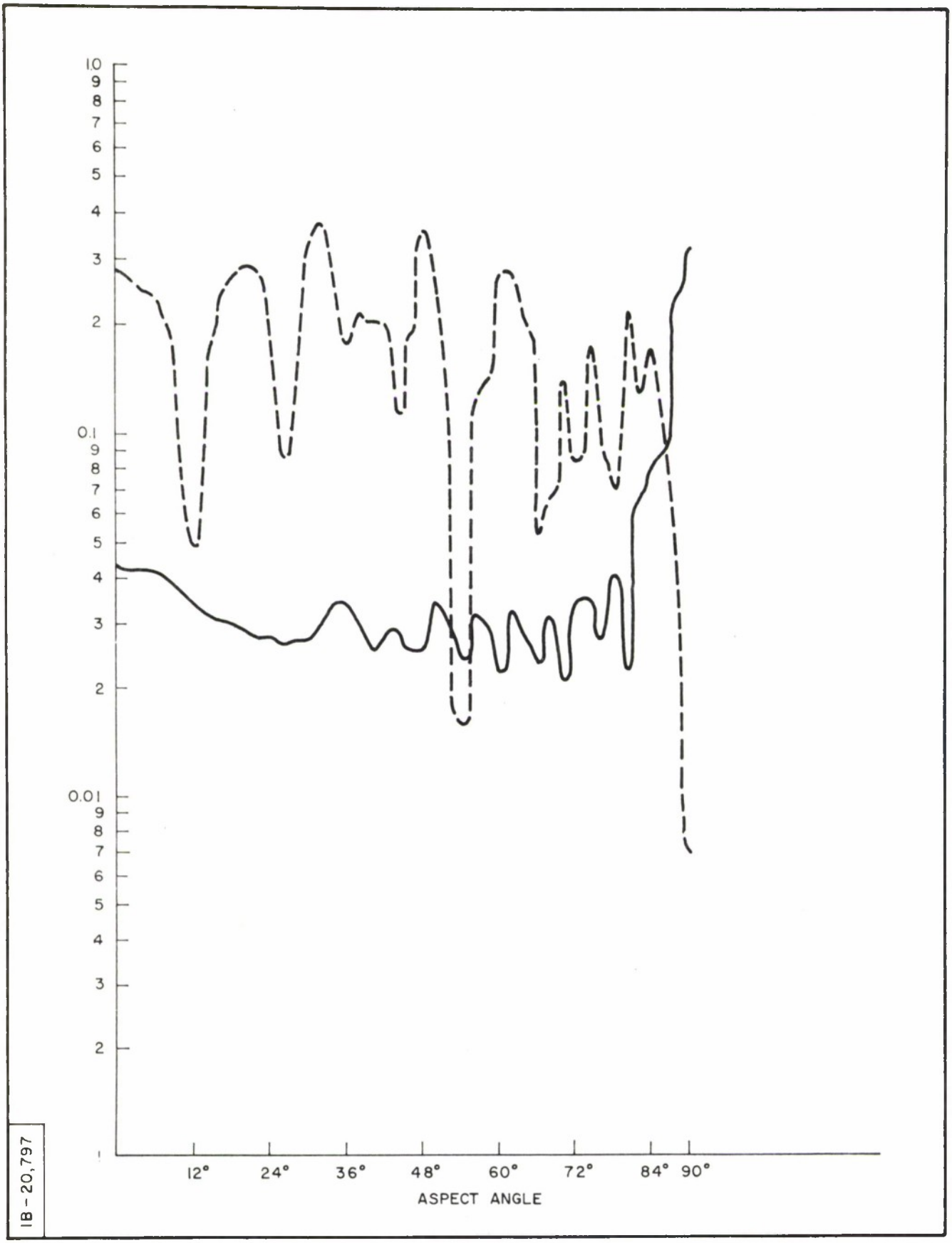

Figure 38. THE S-MATRIX ELEMENT s_{LR} (SOLID) AND $D = s_{LL}/s_{LR}$ (DOTTED) VERSUS ASPECT ANGLE FOR BODY NO. II

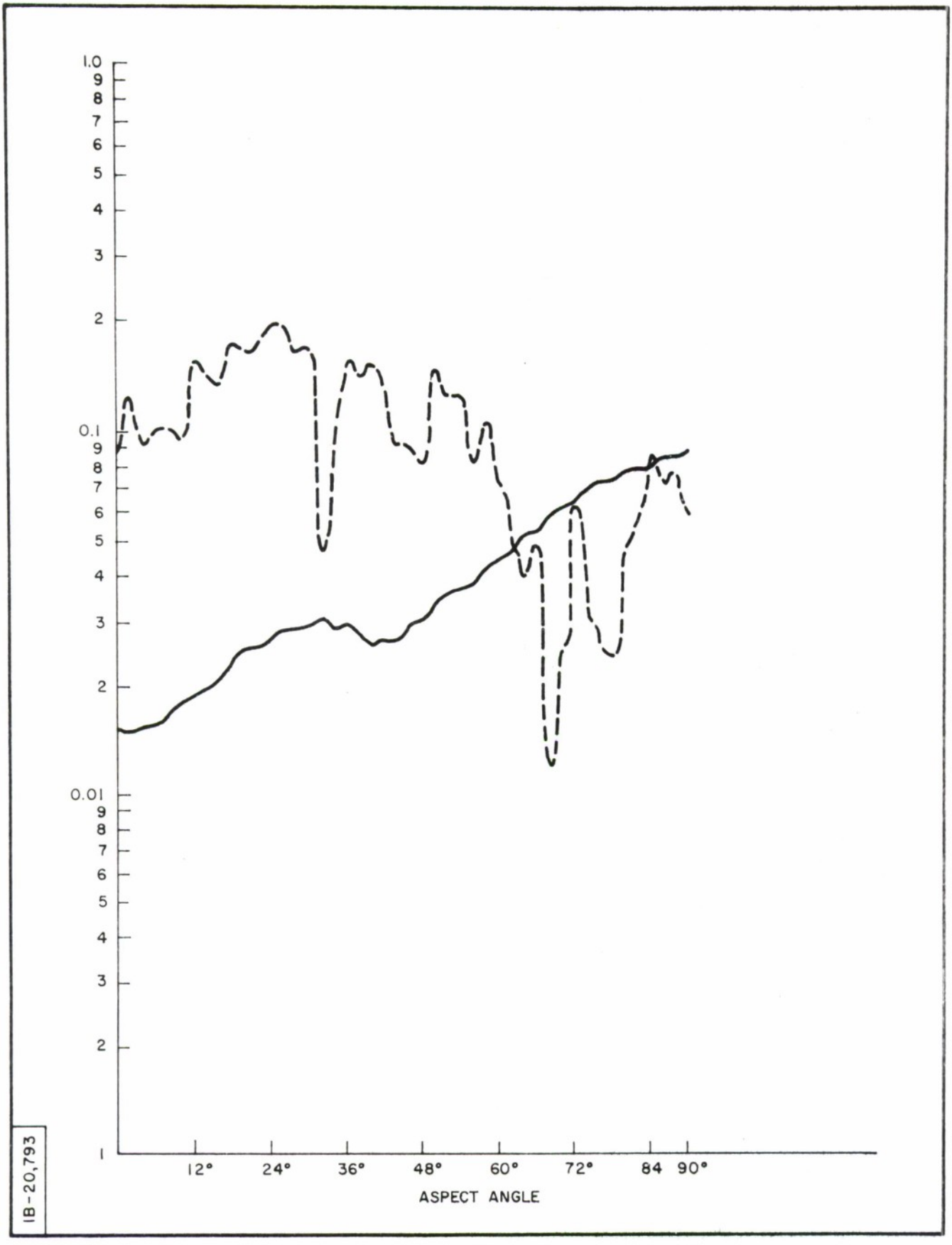

Figure 39. THE S-MATRIX ELEMENT s_{LR} (SOLID) AND $D=s_{LL}/s_{LR}$ (DOTTED) VERSUS ASPECT ANGLE FOR BODY NO. 12

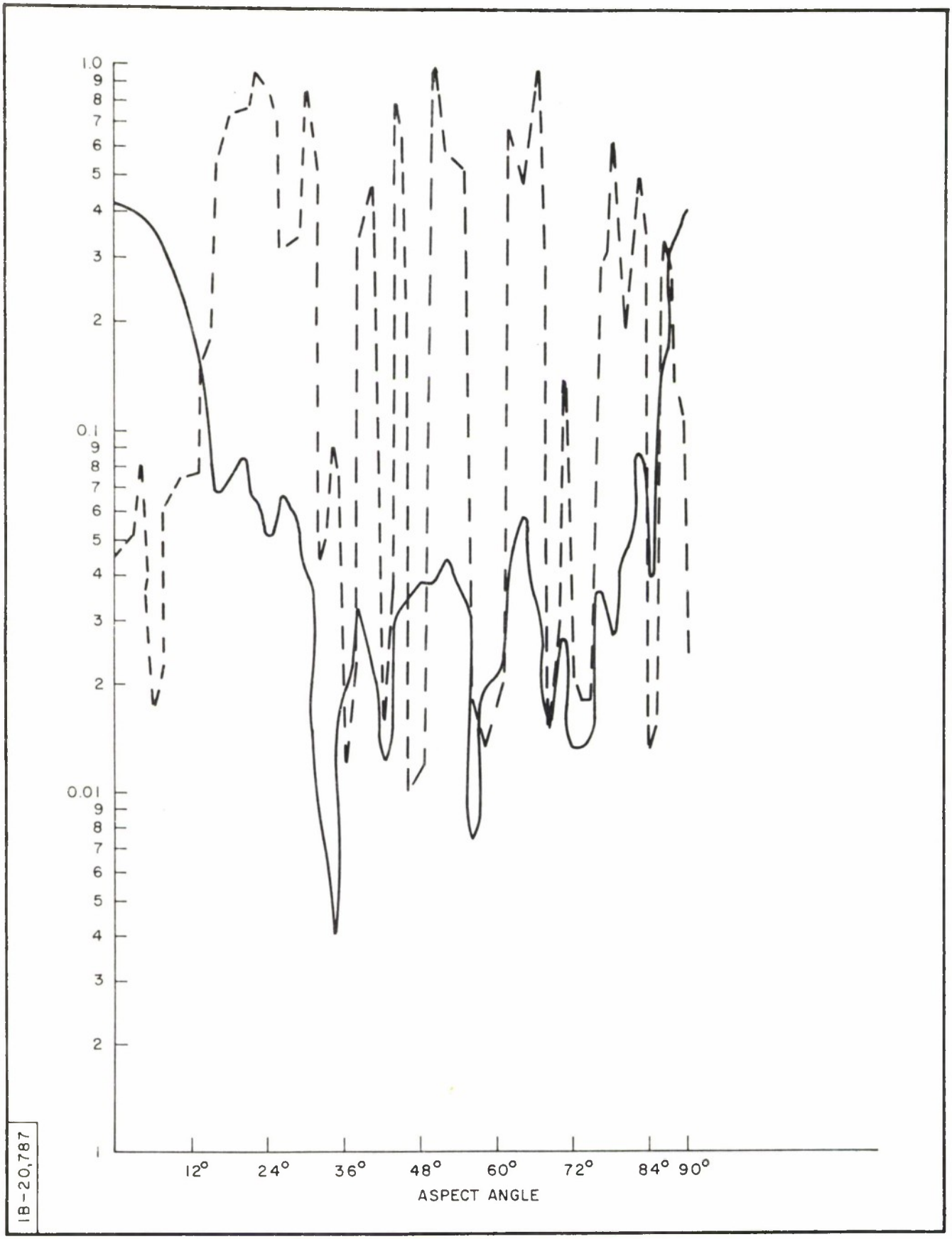

Figure 40. THE S-MATRIX ELEMENT s_{LR} (SOLID) AND $D=s_{LL}/s_{LR}$ (DOTTED) VERSUS ASPECT ANGLE FOR BODY NO. 13

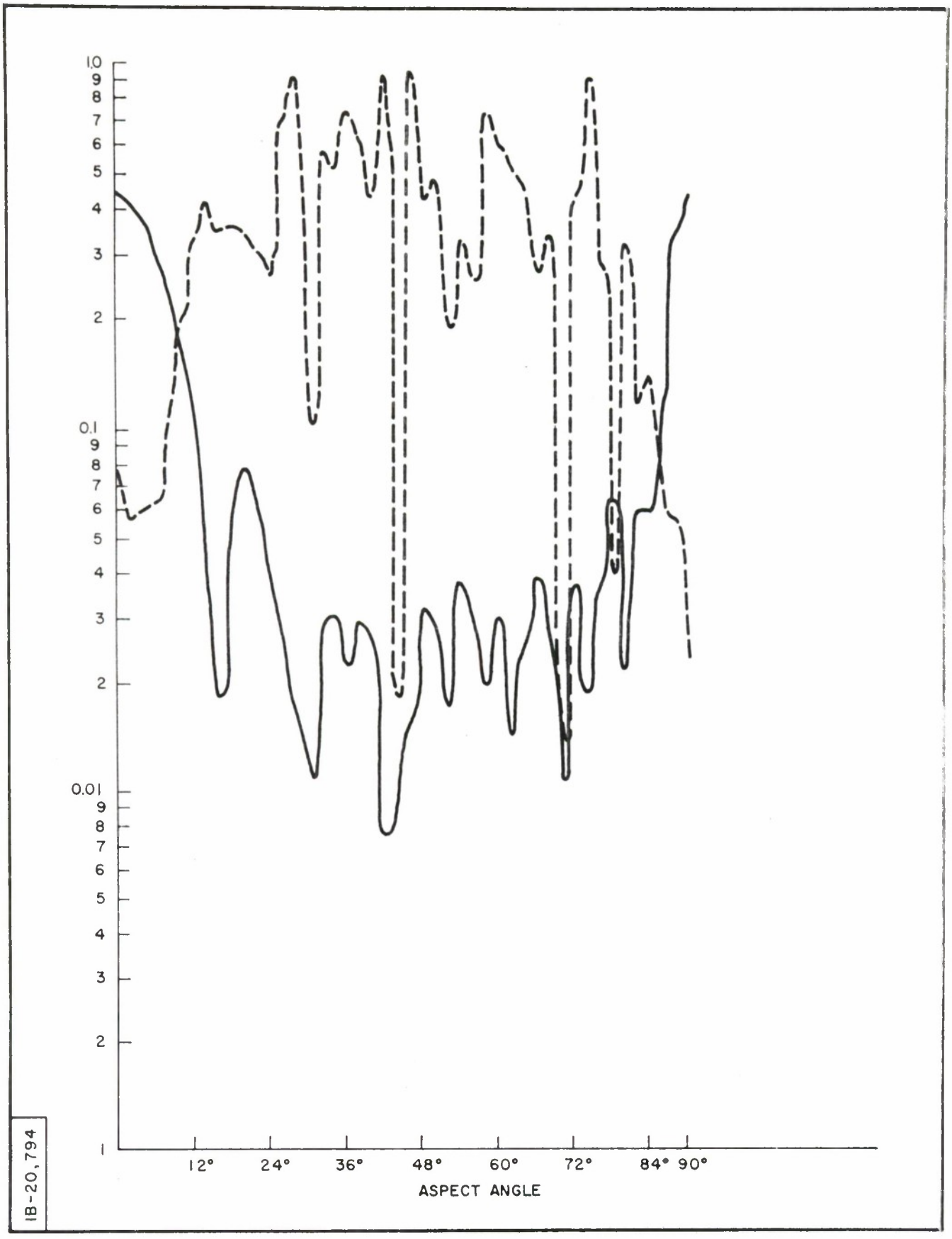

Figure 41. THE S-MATRIX ELEMENT s_{LR} (SOLID) AND $D = s_{LL}/s_{LR}$ (DOTTED) VERSUS ASPECT ANGLE FOR BODY NO. 14

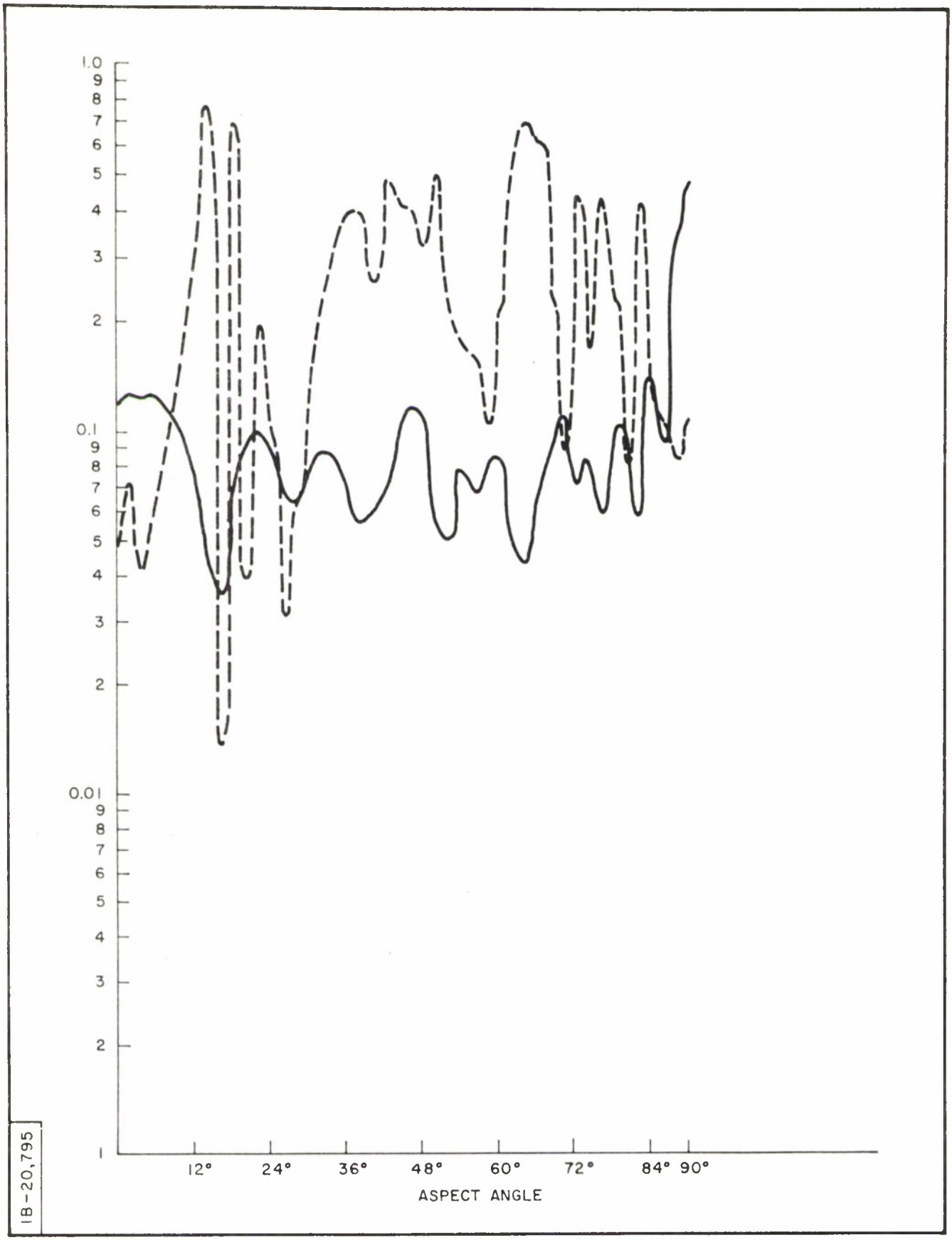

Figure 42. THE S-MATRIX ELEMENT s_{LR} (SOLID) AND $D = s_{LL}/s_{LR}$ (DOTTED) VERSUS ASPECT ANGLE FOR BODY NO. 15

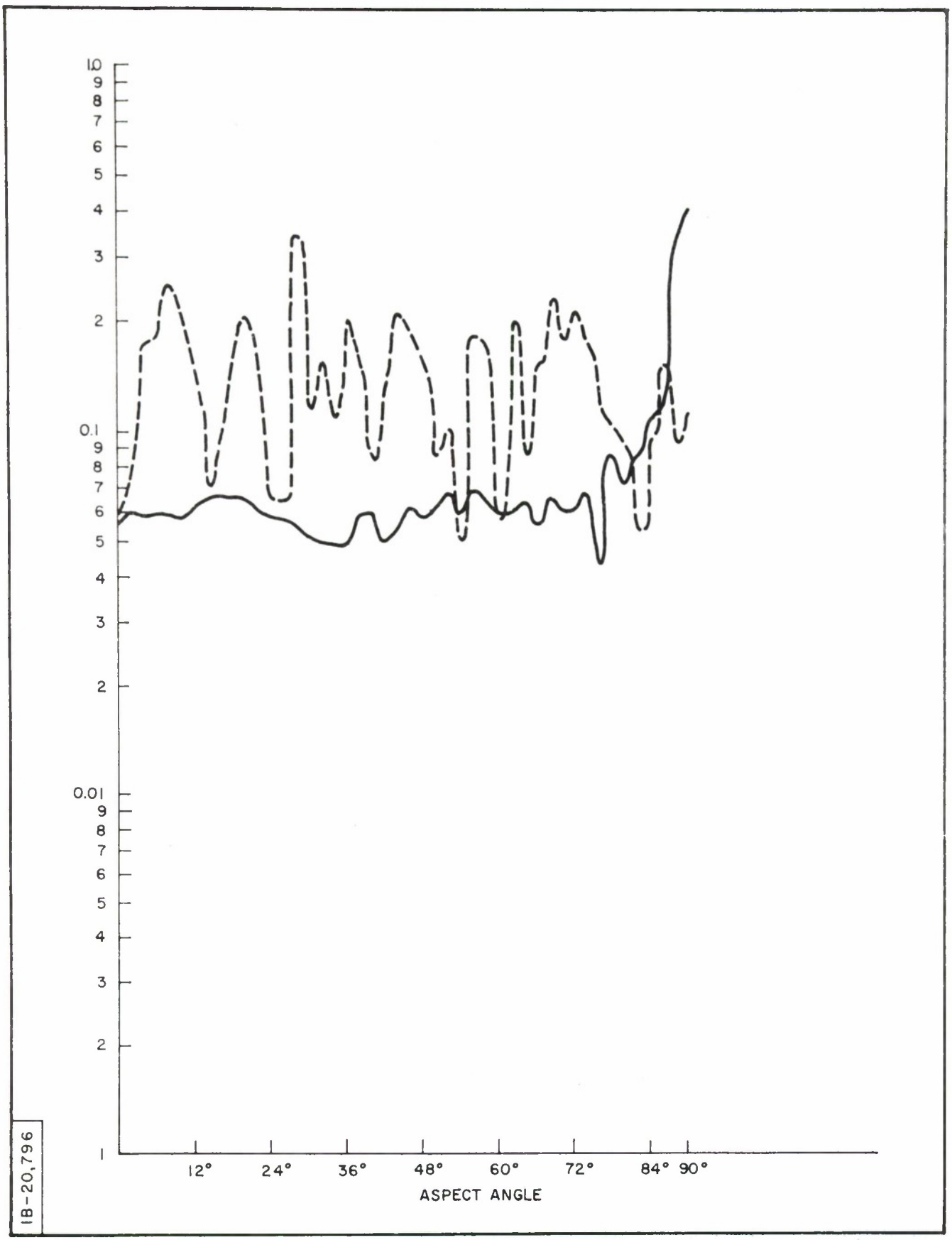

Figure 43. THE S-MATRIX ELEMENT s_{LR} (SOLID) AND $D = s_{LL}/s_{LR}$ (DOTTED) VERSUS ASPECT ANGLE FOR BODY NO. 16

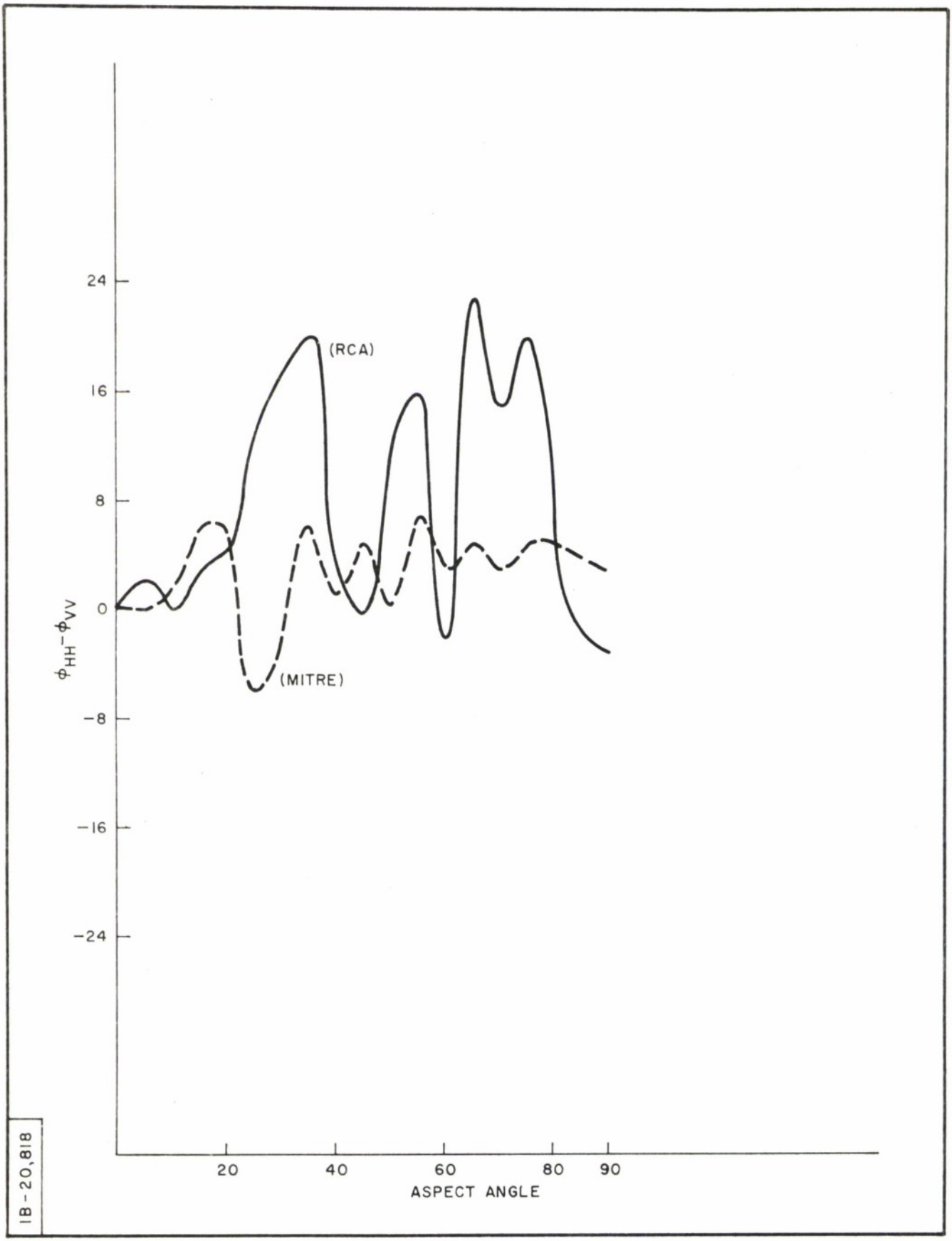

Figure 44. DIFFERENCE OF RELATIVE PHASE $\phi_{HH}-\phi_{VV}$ VERSUS ASPECT ANGLE FOR LARGE PROLATE SPHEROID. THEORETICAL (MITRE) & EXPERIMENTAL (RCA)

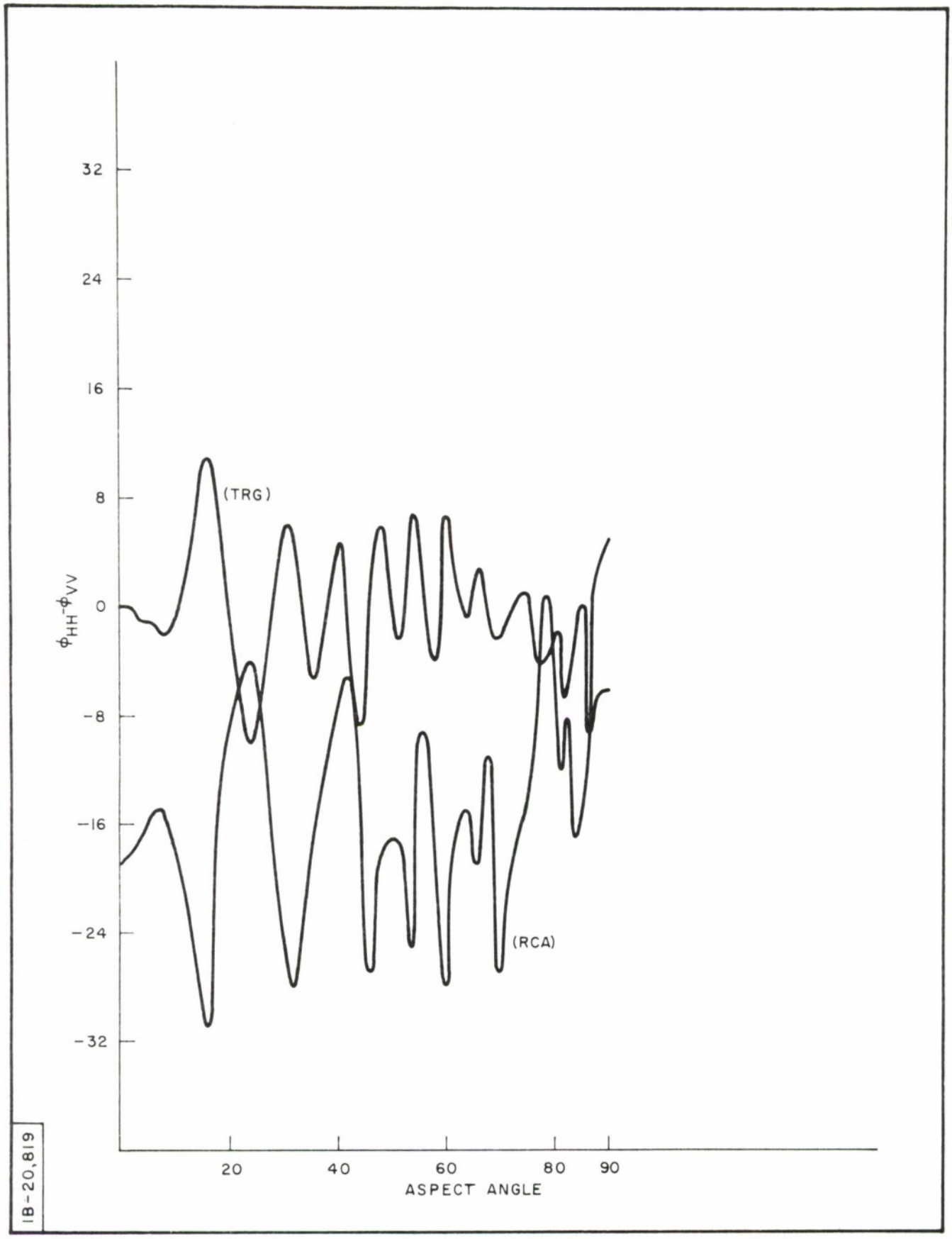

Figure 45. DIFFERENCE OF RELATIVE PHASE $\phi_{HH} - \phi_{VV}$ VERSUS ASPECT ANGLE FOR THE "TRG BODY" THEORETICAL (TRG) AND EXPERIMENTAL (RCA)

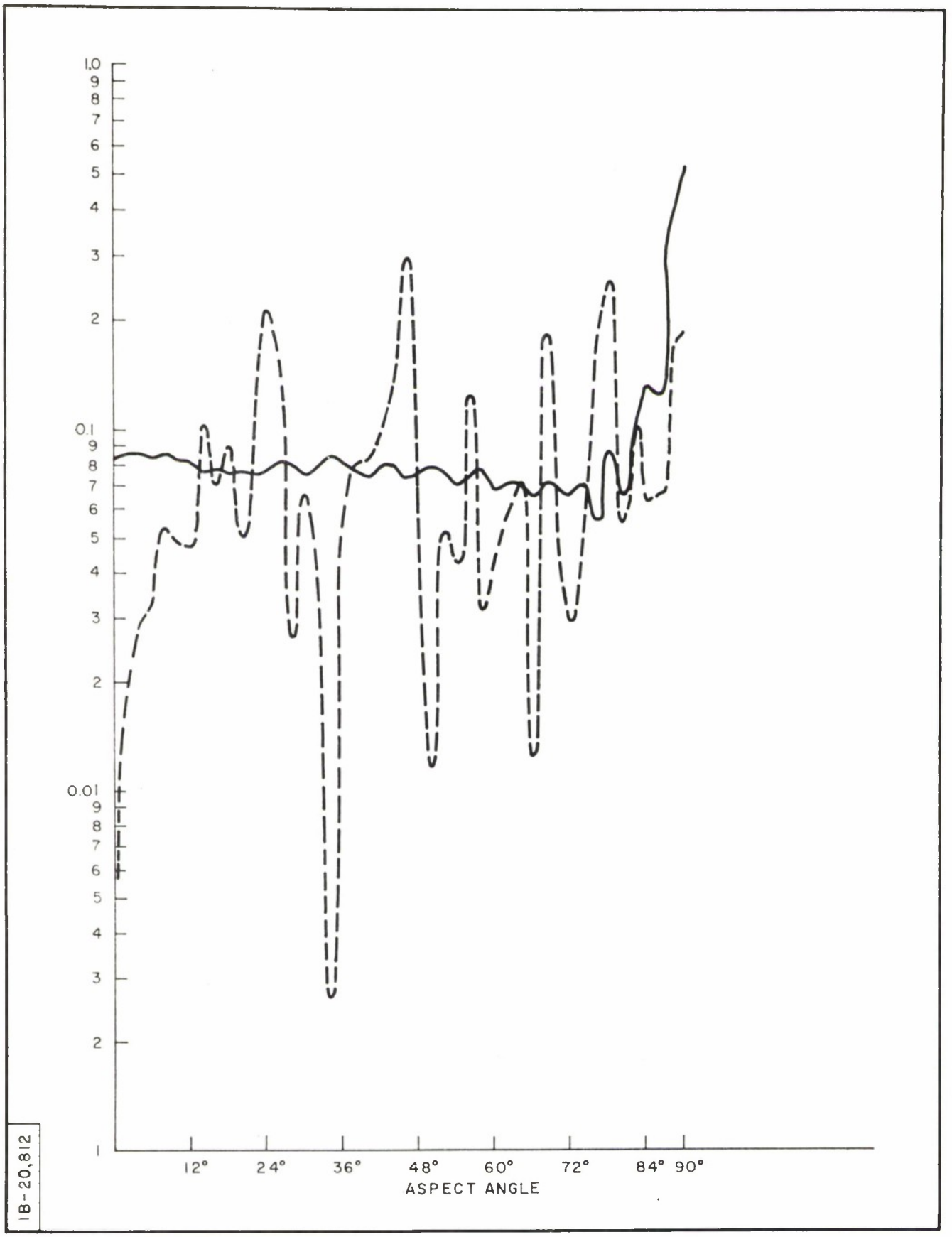

Figure 46. THE S-MATRIX ELEMENT s_{LR} (SOLID) AND $D=s_{LL}/s_{LR}$ (DOTTED) VERSUS ASPECT ANGLE FOR BODY NO. 1. (PHASE ADJUSTED TO $\phi_{HH}=\phi_{VV}$ AT NOSE-ON)

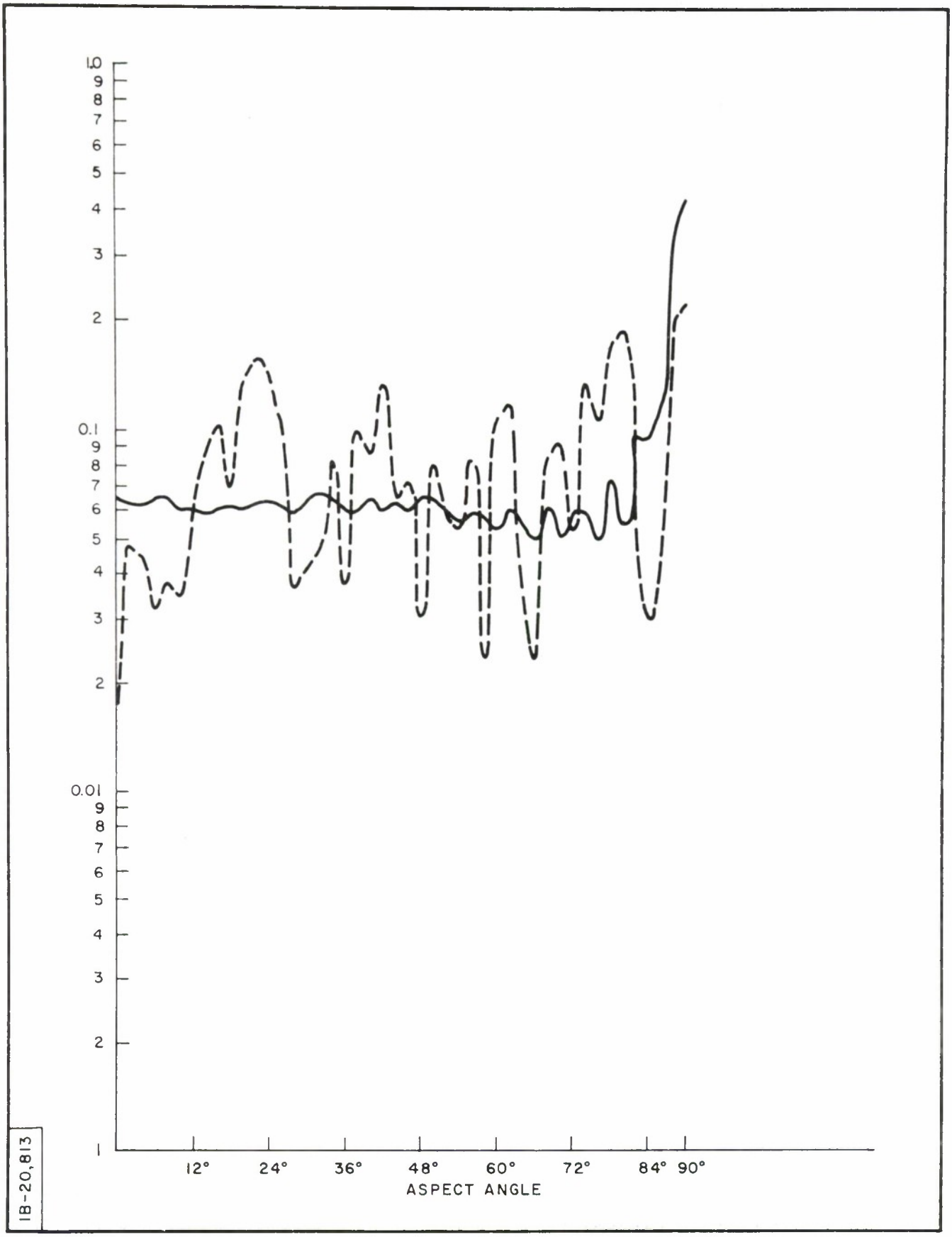

Figure 47. THE S-MATRIX ELEMENT s_{LR} (SOLID) AND $D=s_{LL}/s_{LR}$ (DOTTED) VERSUS ASPECT ANGLE FOR BODY NO. 2. (PHASE ADJUSTED TO $\phi_{HH}=\phi_{VV}$ AT NOSE-ON)

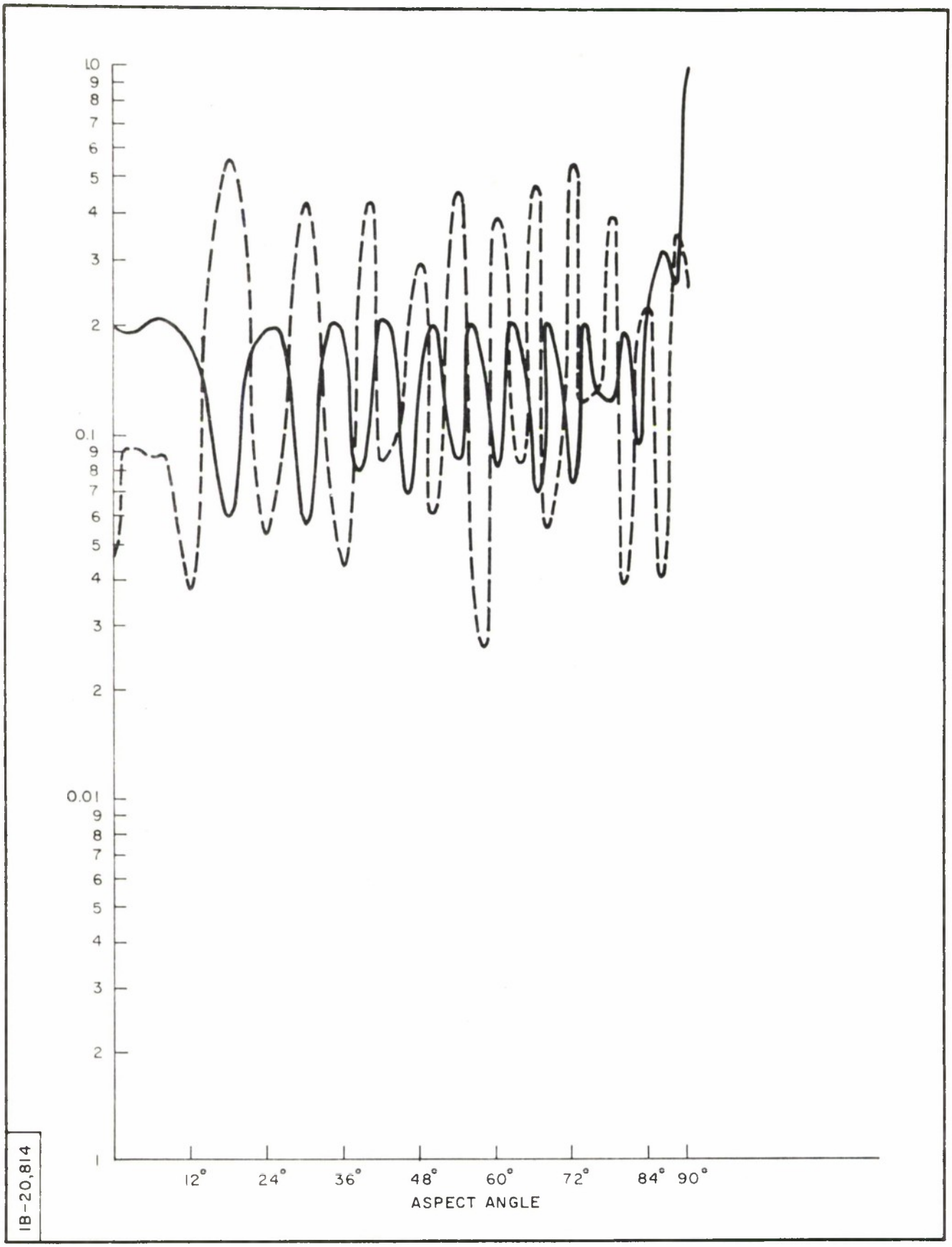

Figure 48. THE S-MATRIX ELEMENT s_{LR} (SOLID) AND $D=s_{LL}/s_{LR}$ (DOTTED) VERSUS ASPECT ANGLE FOR BODY NO. 3. (PHASE ADJUSTED TO $\phi_{HH}=\phi_{VV}$ AT NOSE-ON)

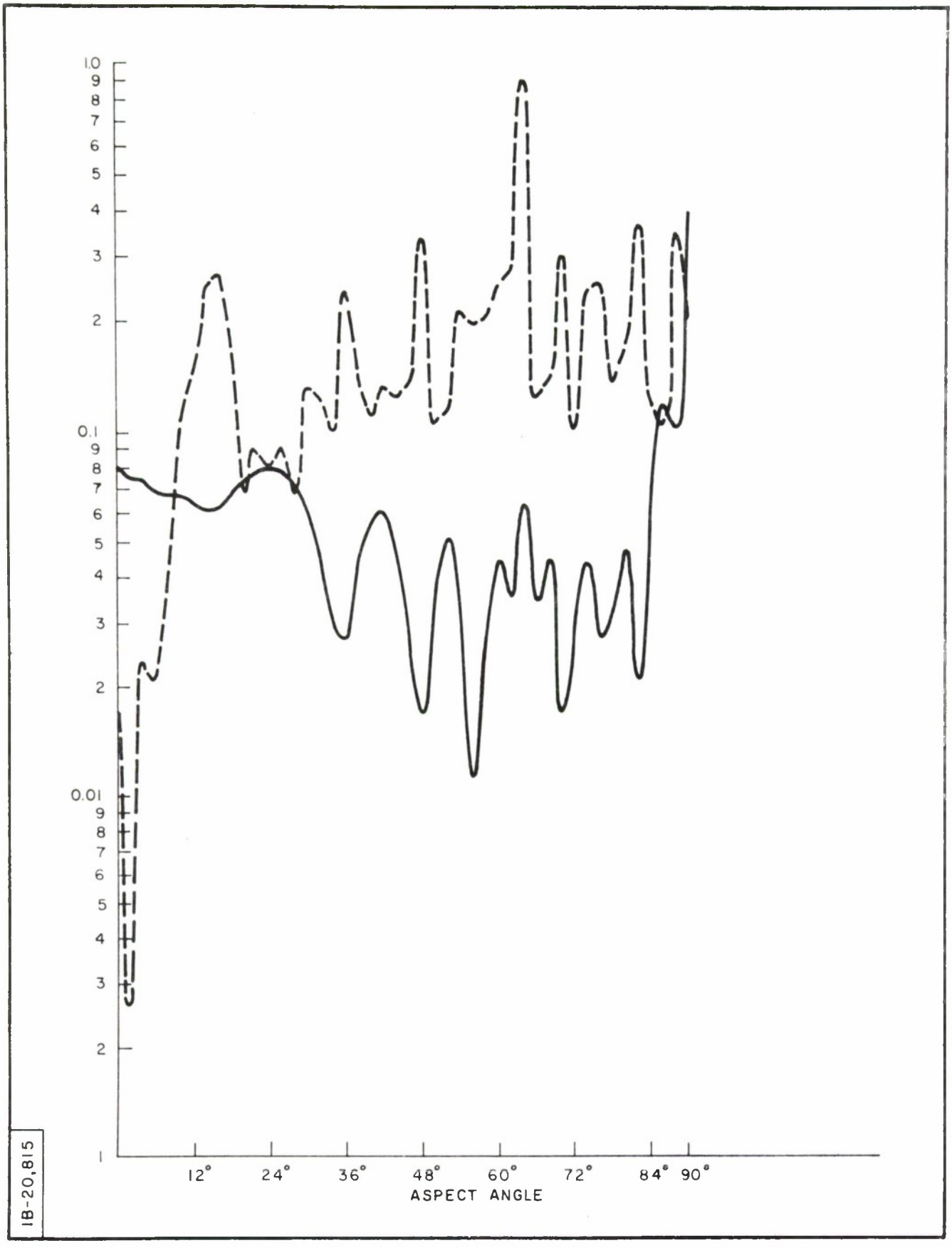

Figure 49. THE S-MATRIX ELEMENT s_{LR} (SOLID) AND $D=s_{LL}/s_{LR}$ (DOTTED) VERSUS ASPECT ANGLE FOR BODY NO. 4. (PHASE ADJUSTED TO $\phi_{HH}=\phi_{VV}$ AT NOSE-ON)

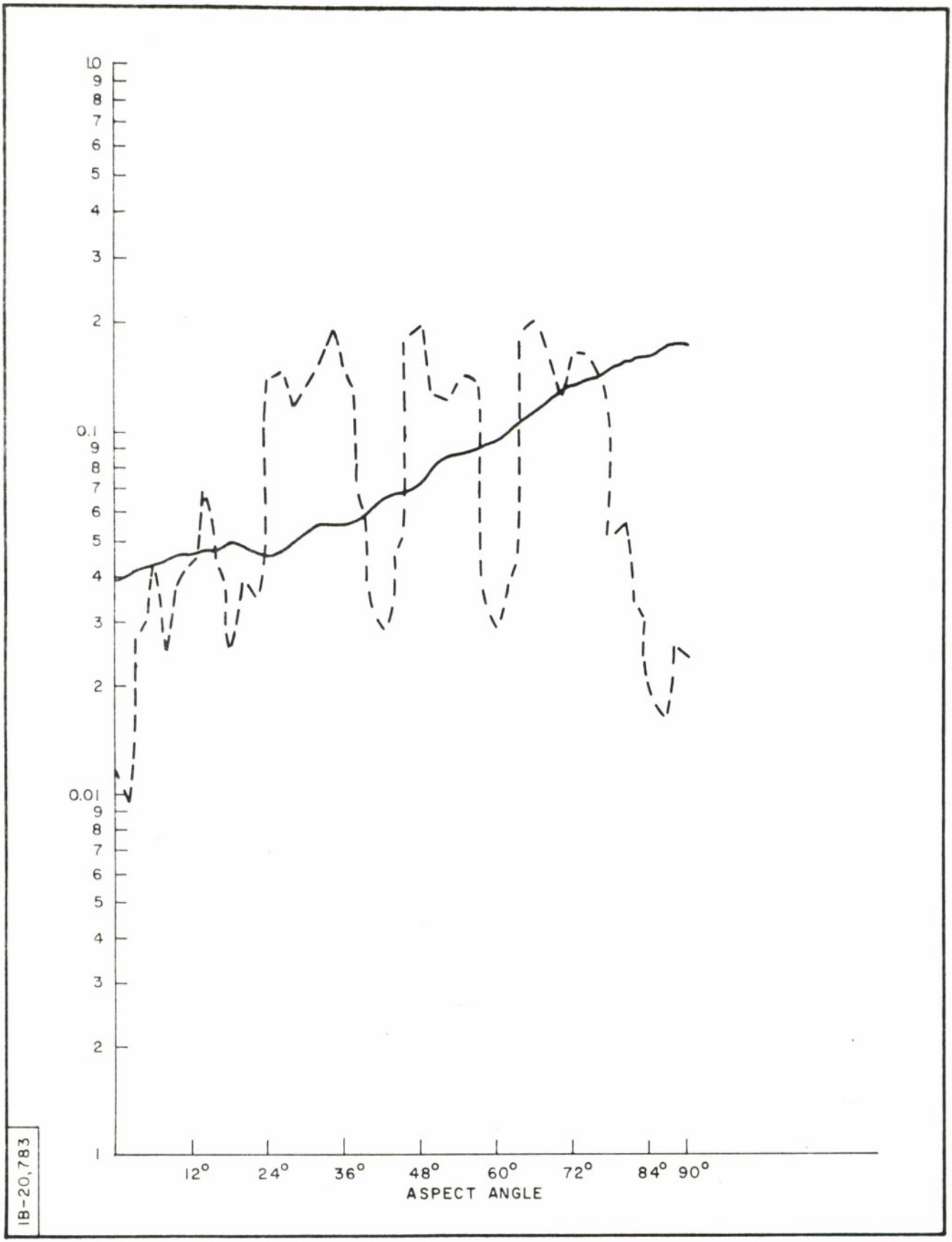

Figure 50. THE S-MATRIX ELEMENT s_{LR} (SOLID) AND $D=s_{LL}/s_{LR}$ (DOTTED) VERSUS ASPECT ANGLE FOR BODY NO. 5. (PHASE ADJUSTED TO $\phi_{HH}=\phi_{VV}$ AT NOSE-ON)

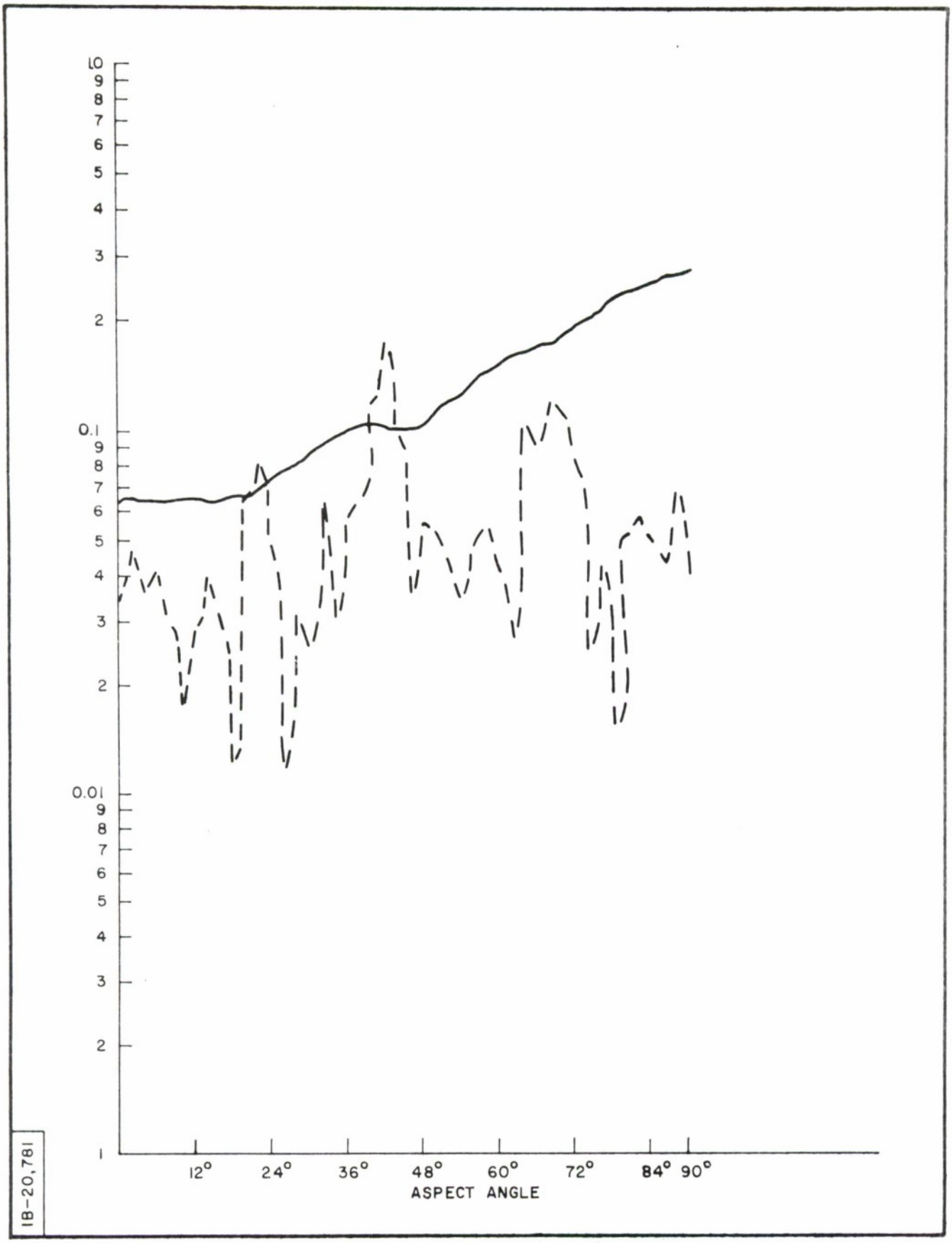

Figure 51. THE S-MATRIX ELEMENT s_{LR} (SOLID) AND $D = s_{LL}/s_{LR}$ (DOTTED) VERSUS ASPECT ANGLE FOR BODY NO. 6. (PHASE ADJUSTED TO $\phi_{HH} = \phi_{VV}$ AT NOSE-ON)

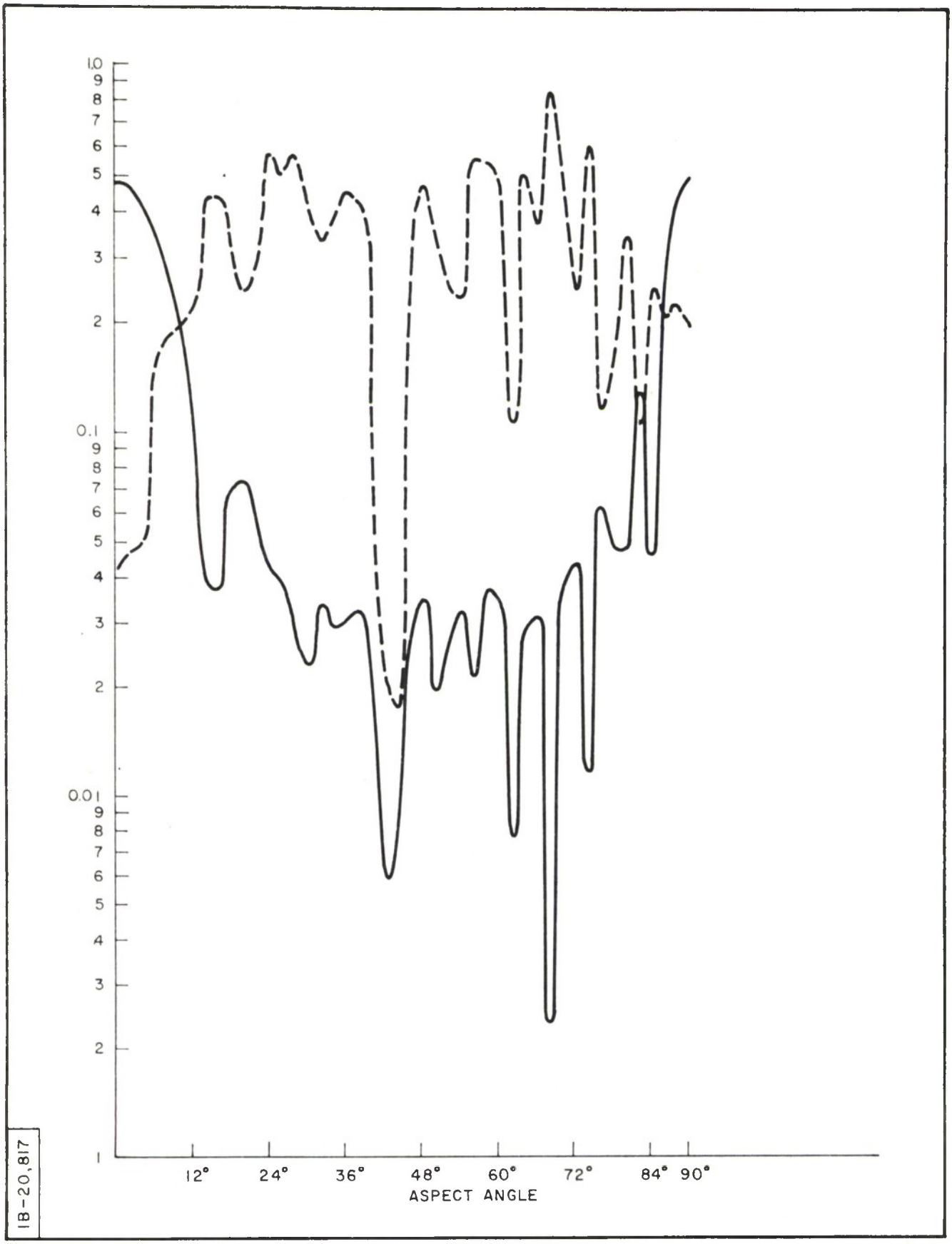

Figure 52. THE S-MATRIX ELEMENT s_{LR} (SOLID) AND $D=s_{LL}/s_{LR}$ (DOTTED) VERSUS ASPECT ANGLE FOR BODY NO. 7. (PHASE ADJUSTED TO $\phi_{HH}=\phi_{VV}$ AT NOSE-ON)

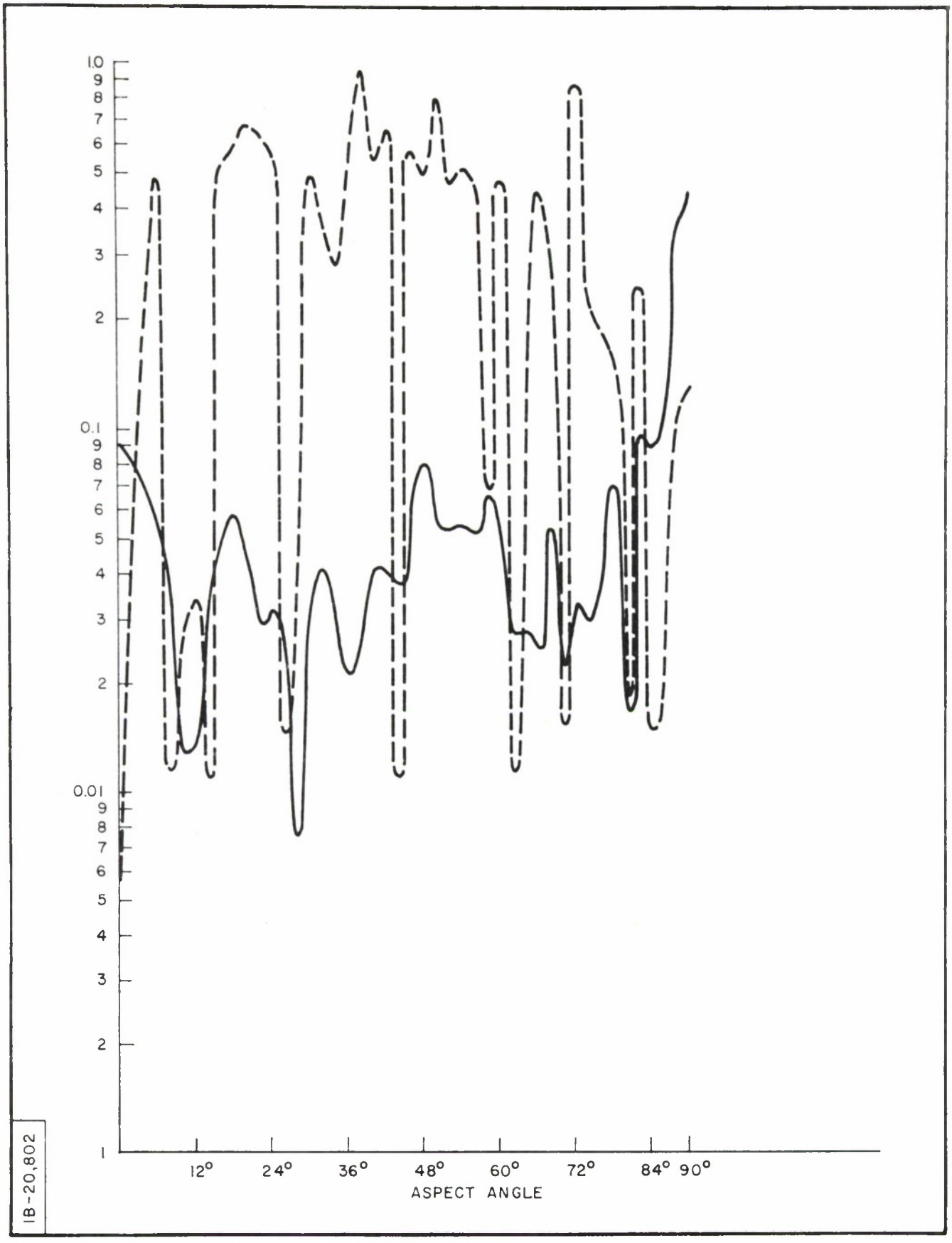

Figure 53. THE S-MATRIX ELEMENT s_{LR} (SOLID) AND $D=s_{LL}/s_{LR}$ (DOTTED) VERSUS ASPECT ANGLE FOR BODY NO. 8. (PHASE ADJUSTED TO $\phi_{HH}=\phi_{VV}$ AT NOSE-ON)

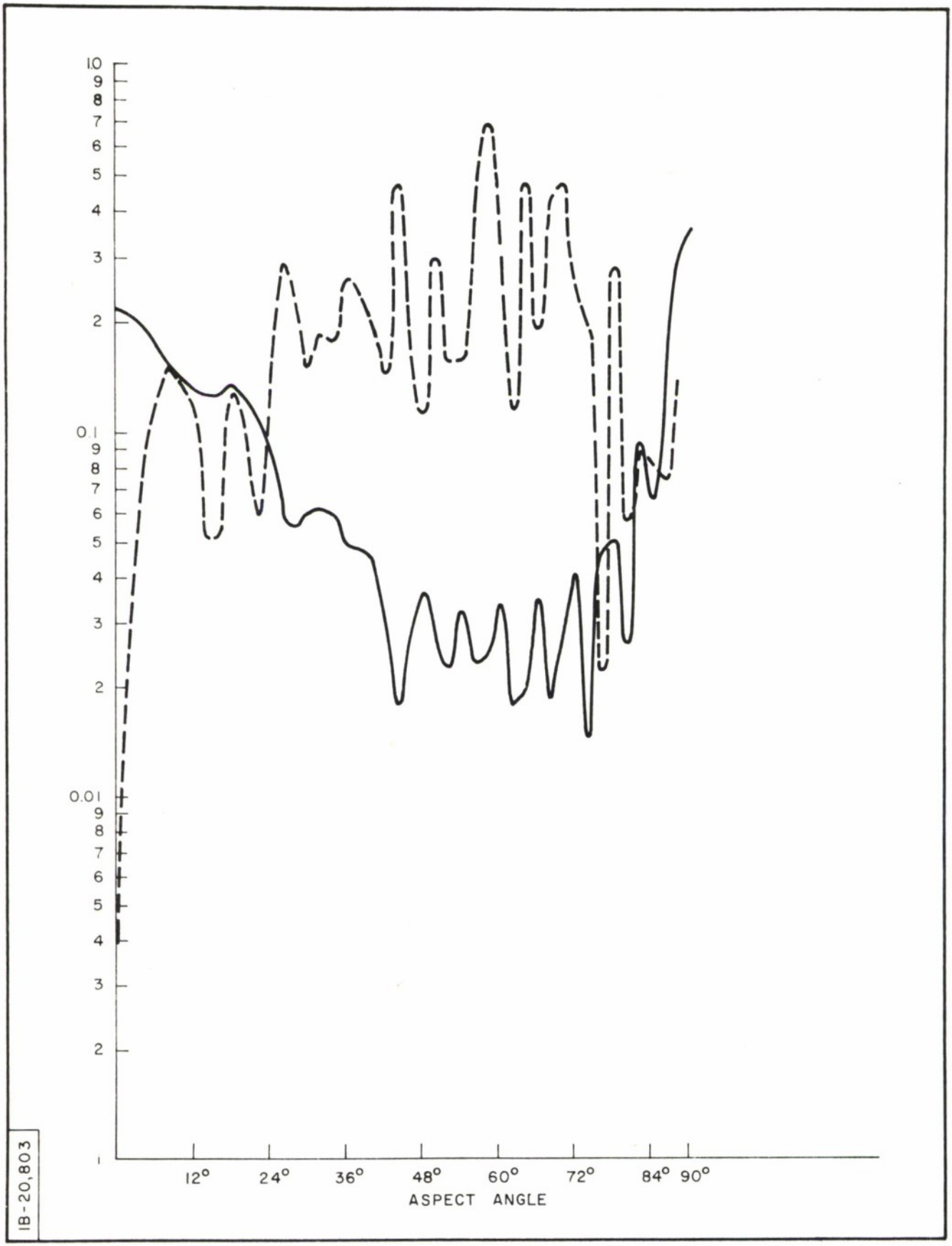

Figure 54. THE S-MATRIX ELEMENT s_{LR} (SOLID) AND $D = s_{LL}/s_{LR}$ (DOTTED) VERSUS ASPECT ANGLE FOR BODY NO. 9. (PHASE ADJUSTED TO $\phi_{HH} = \phi_{VV}$ AT NOSE-ON)

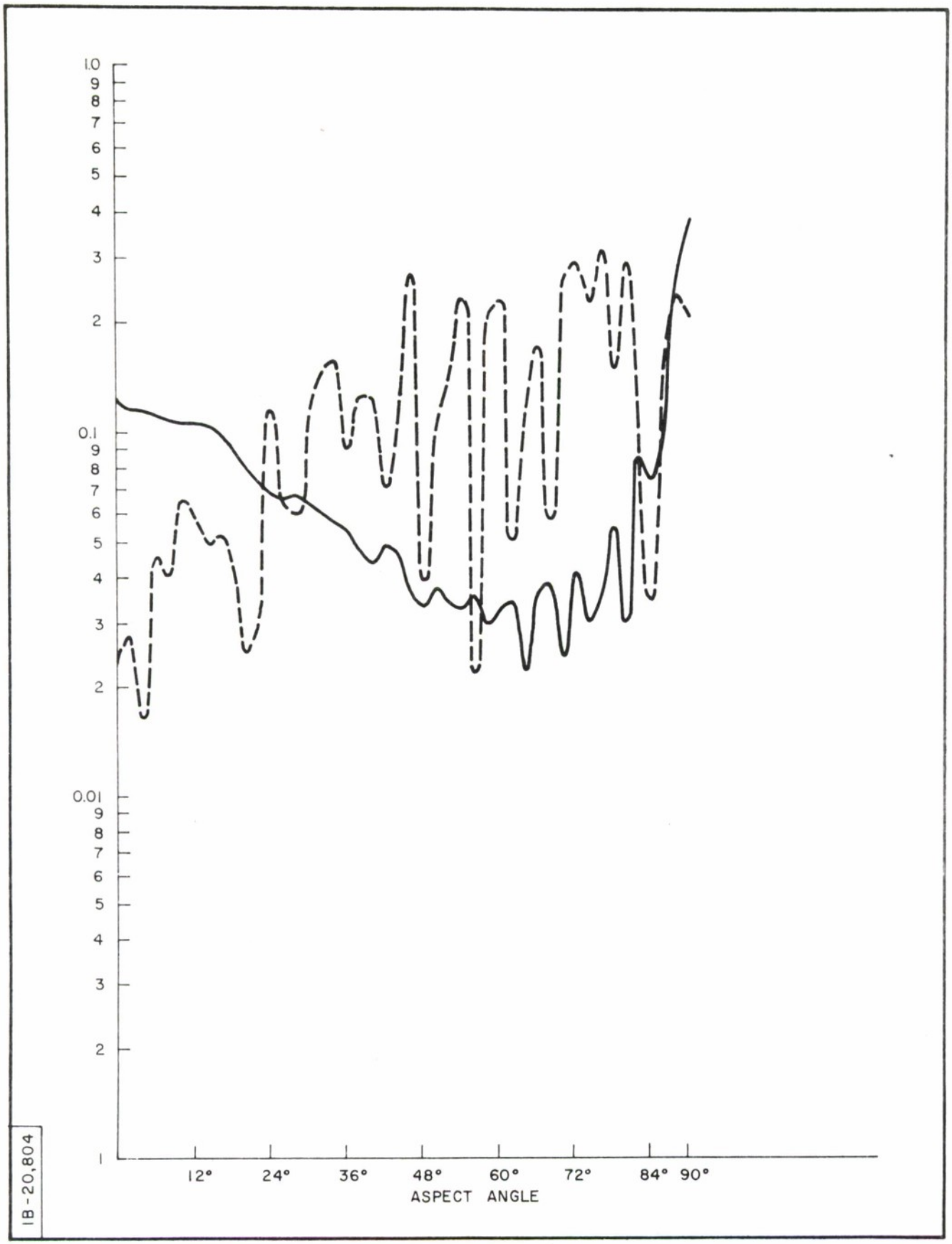

Figure 55. THE S-MATRIX ELEMENT s_{LR} (SOLID) AND $D=s_{LL}/s_{LR}$ (DOTTED) VERSUS ASPECT ANGLE FOR BODY NO. 10. (PHASE ADJUSTED TO $\phi_{HH}=\phi_{VV}$ AT NOSE-ON)

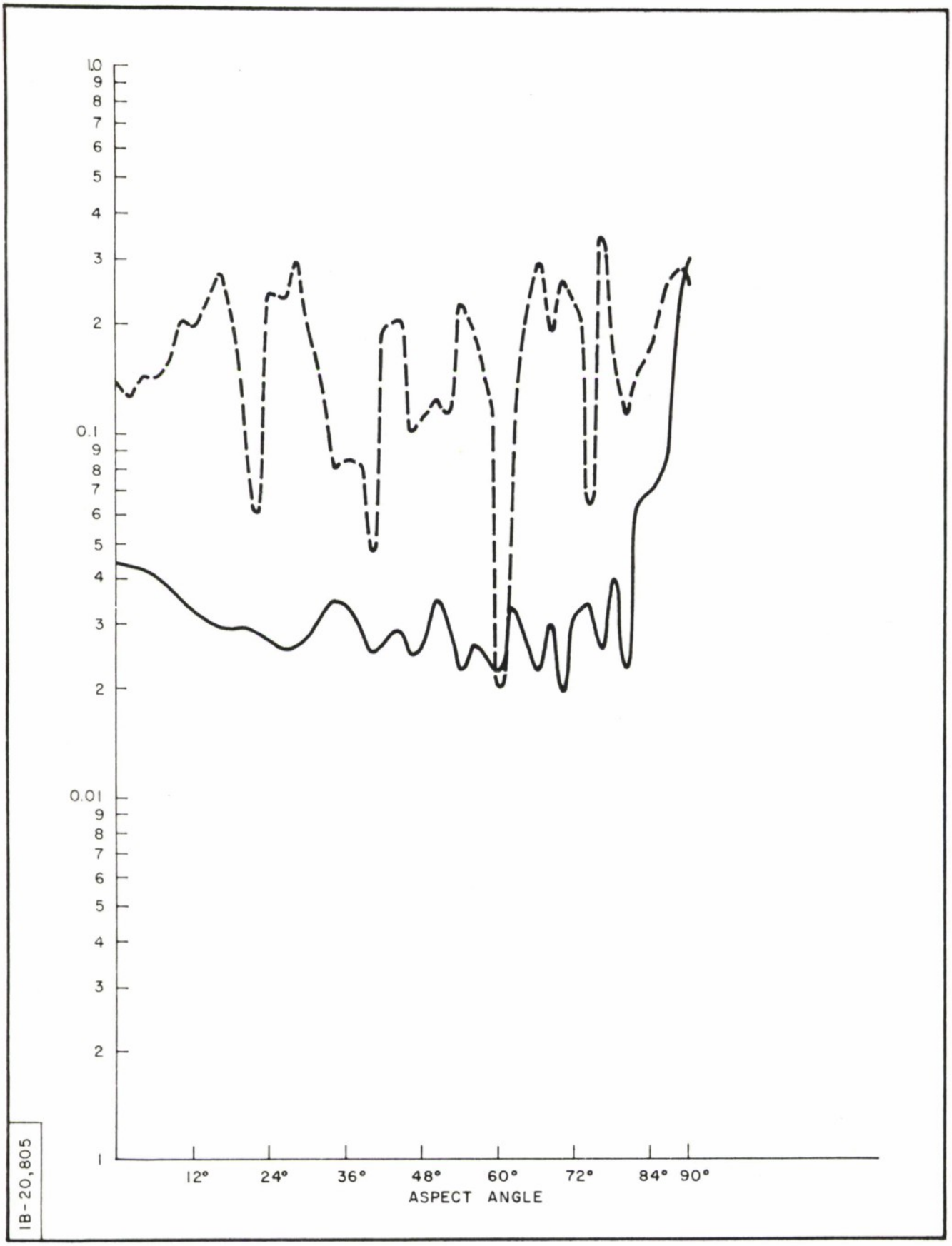

Figure 56. THE S-MATRIX ELEMENT s_{LR} (SOLID) AND $D=s_{LL}/s_{LR}$ (DOTTED) VERSUS ASPECT ANGLE FOR BODY NO. II. (PHASE ADJUSTED TO $\phi_{HH}=\phi_{VV}$ AT NOSE-ON)

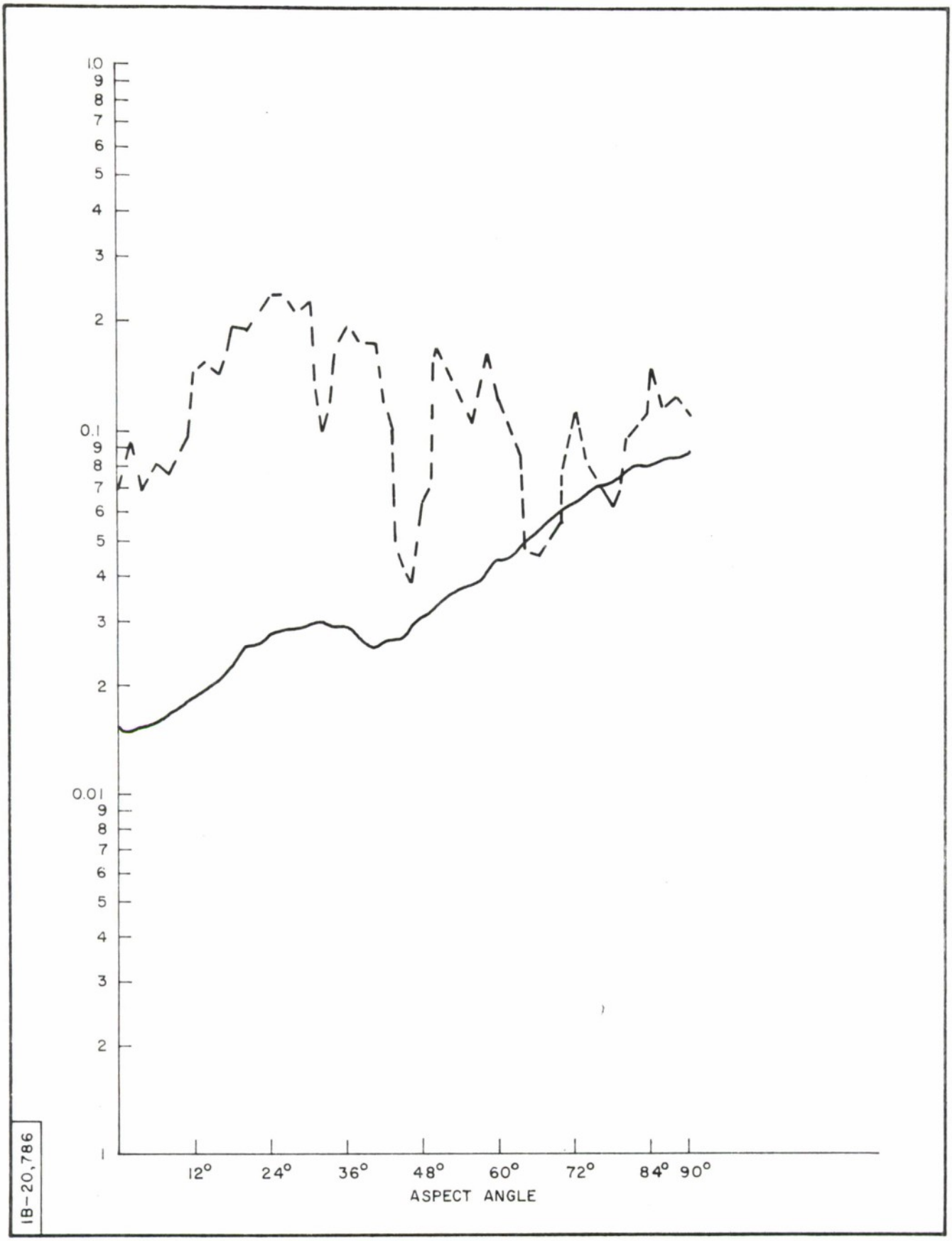

Figure 57. THE S-MATRIX ELEMENT s_{LR} (SOLID) AND $D=s_{LL}/s_{LR}$ (DOTTED) VERSUS ASPECT ANGLE FOR BODY NO. 12 (PHASE ADJUSTED TO $\phi_{HH}=\phi_{VV}$ AT NOSE-ON)

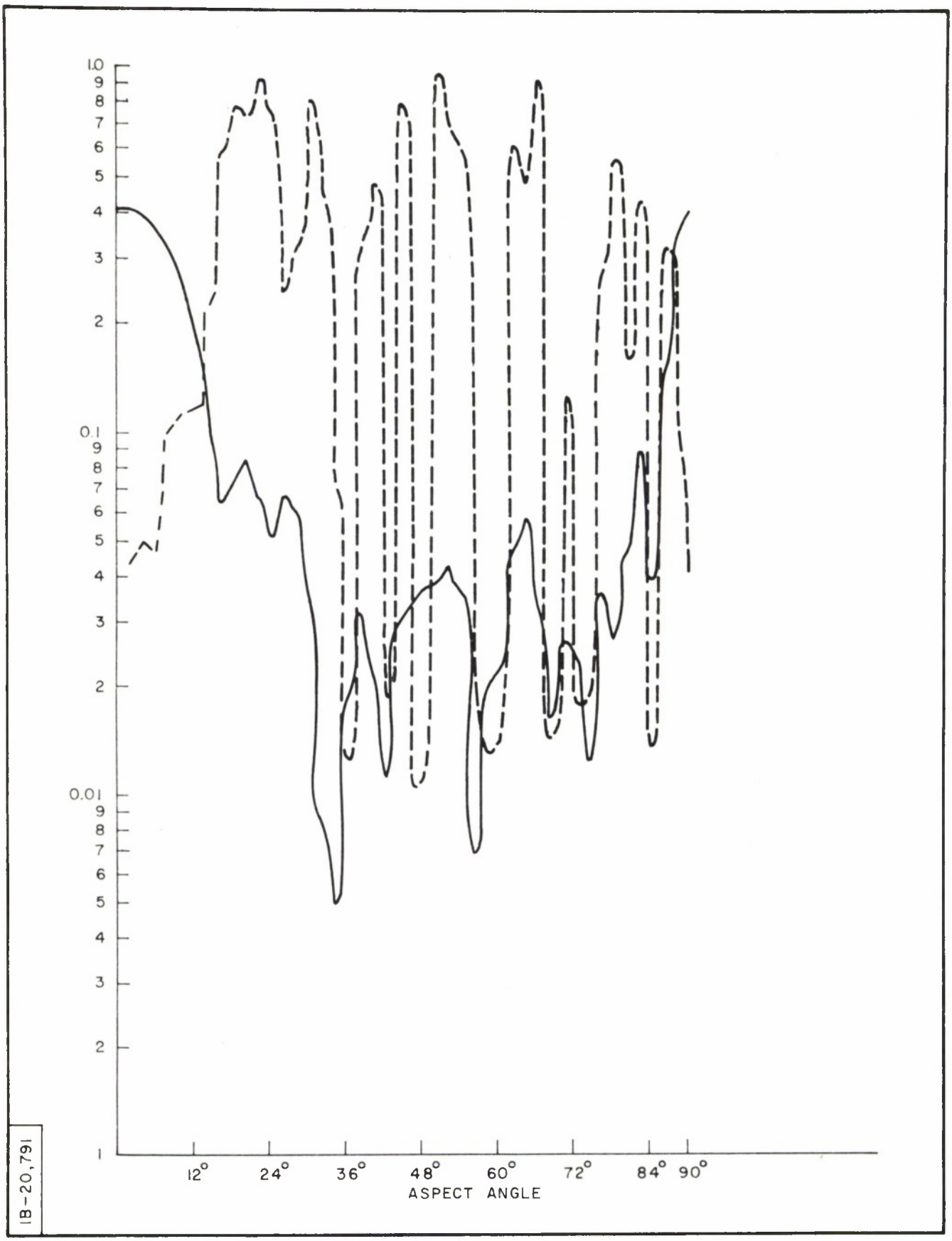

Figure 58. THE S-MATRIX ELEMENT s_{LR} (SOLID) AND $D=s_{LL}/s_{LR}$ (DOTTED) VERSUS ASPECT ANGLE FOR BODY NO. 13. (PHASE ADJUSTED TO $\phi_{HH}=\phi_{VV}$ AT NOSE-ON)

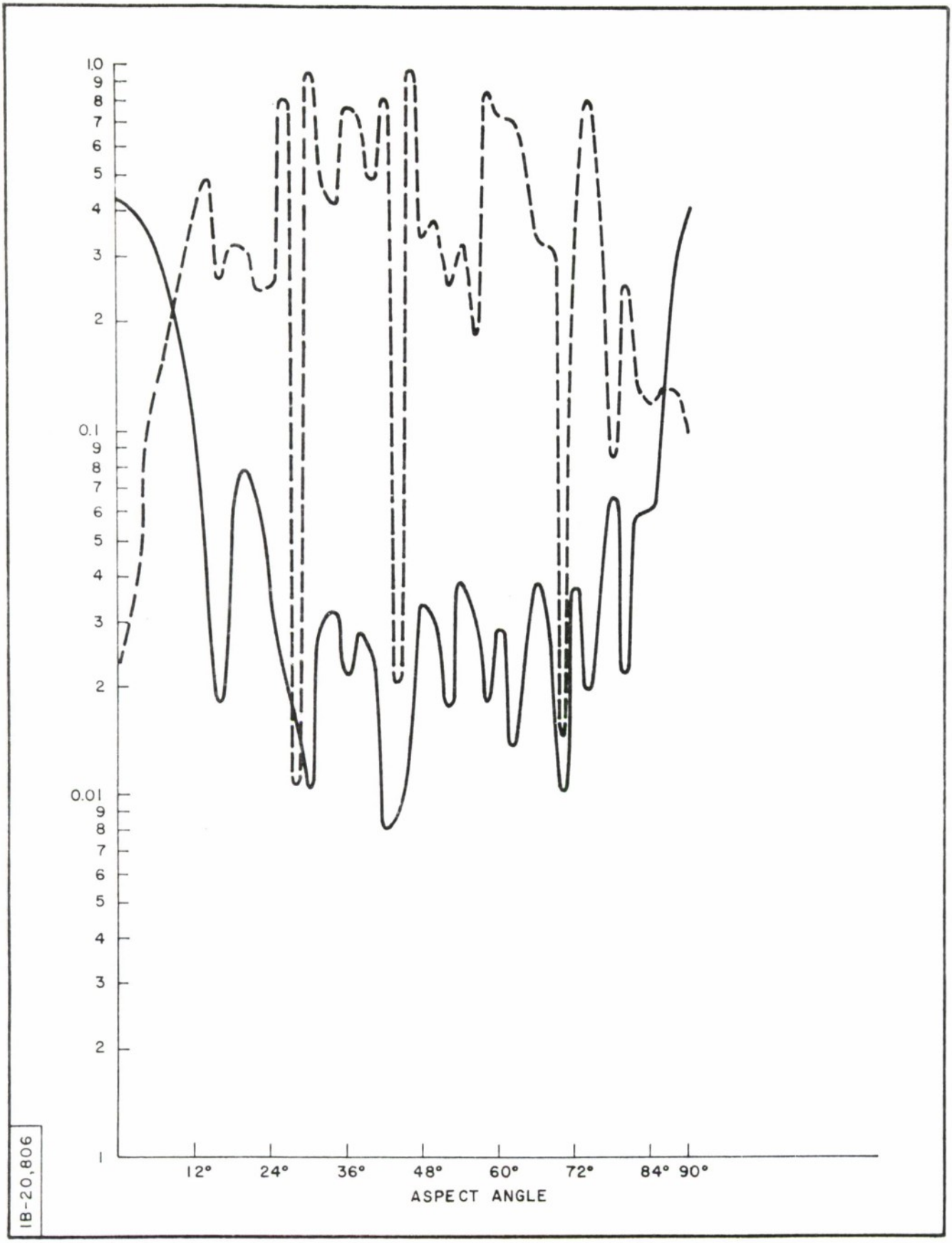

Figure 59. THE S-MATRIX ELEMENT s_{LR} (SOLID) AND $D=s_{LL}/s_{LR}$ (DOTTED) VERSUS ASPECT ANGLE FOR BODY NO. 14. (PHASE ADJUSTED TO $\phi_{HH}=\phi_{VV}$ AT NOSE-ON)

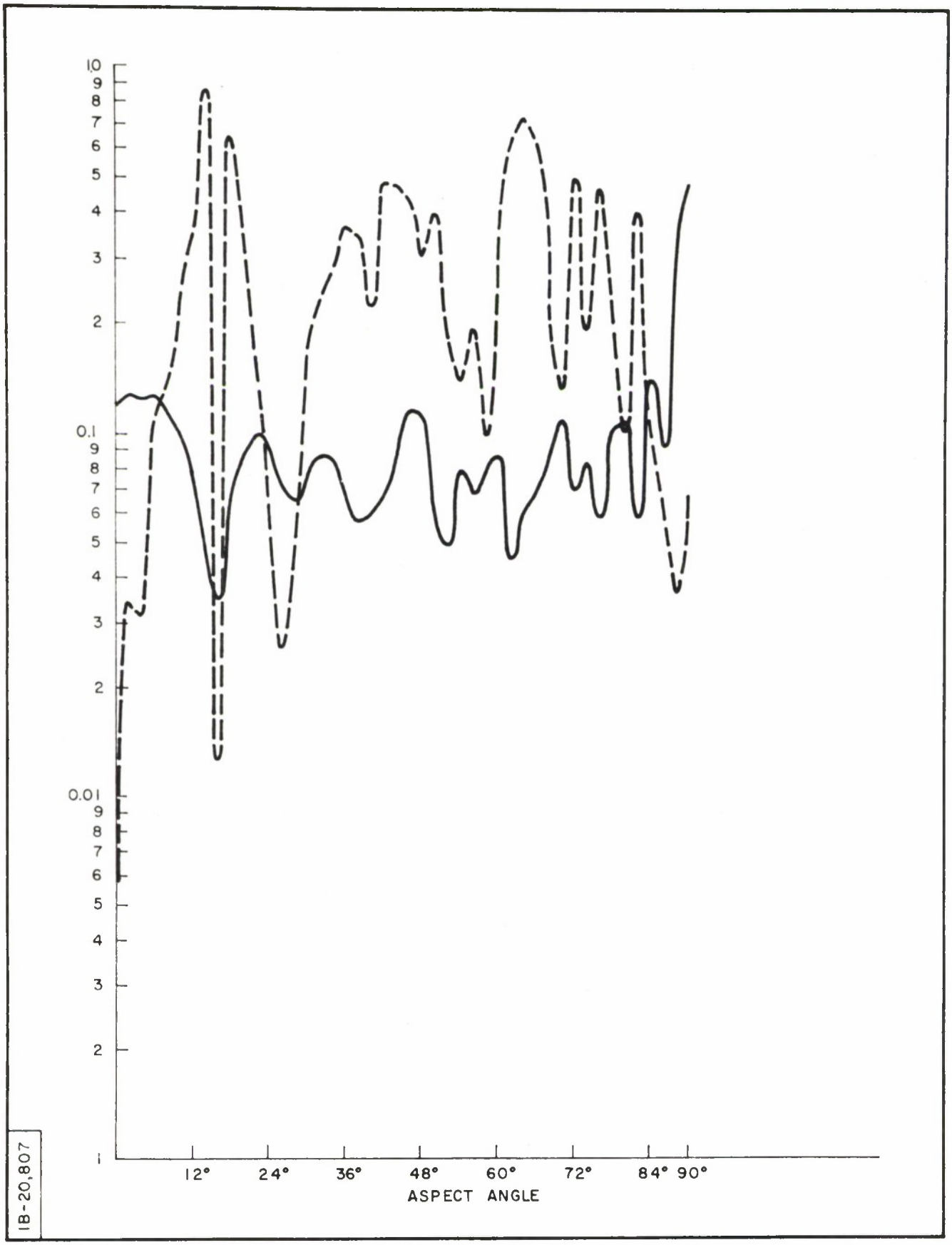

Figure 60. THE S-MATRIX ELEMENT s_{LR} (SOLID) AND $D=s_{LL}/s_{LR}$ (DOTTED) VERSUS ASPECT ANGLE FOR BODY NO. 15. (PHASE ADJUSTED TO $\phi_{HH}=\phi_{VV}$ AT NOSE-ON)

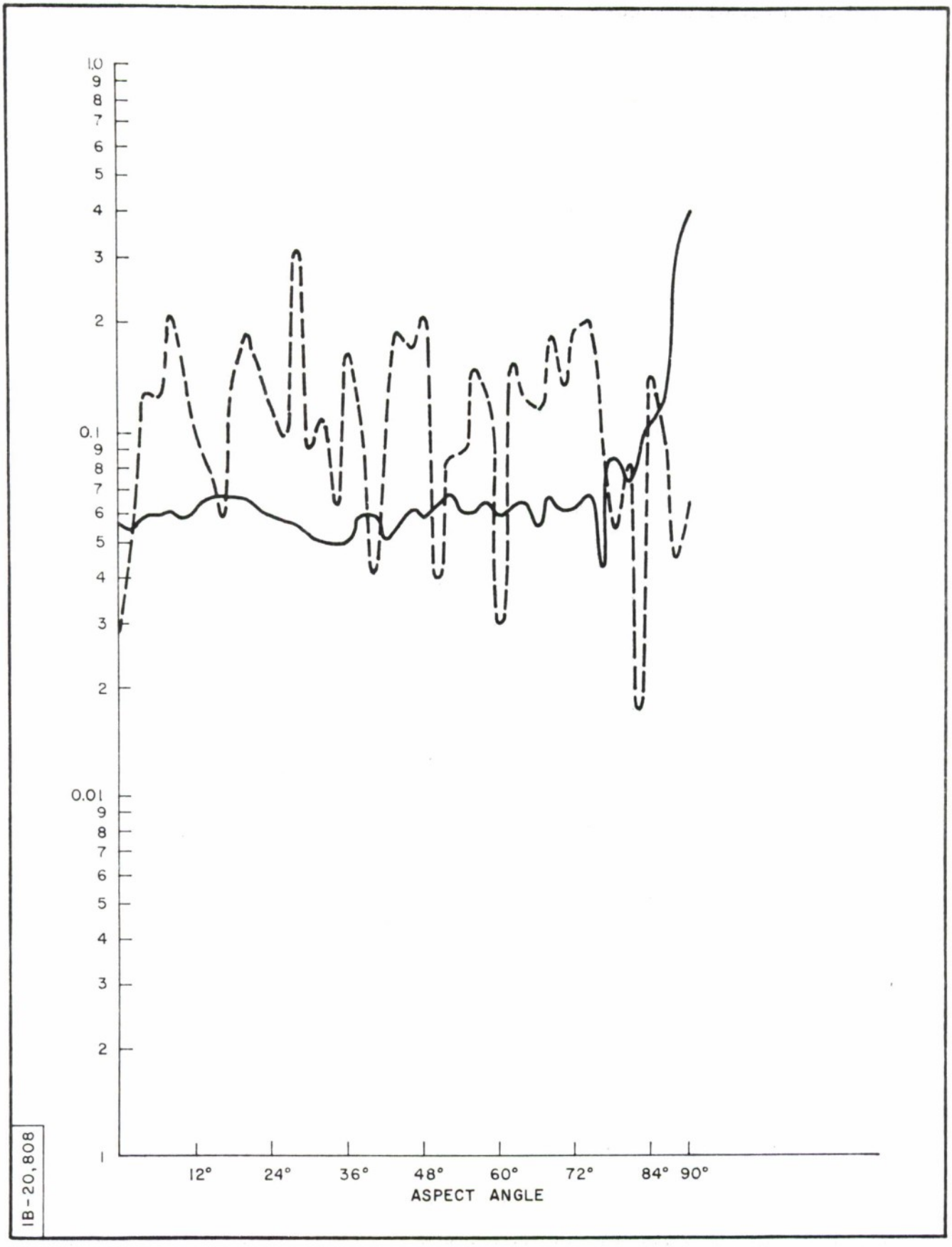

Figure 61. THE S-MATRIX ELEMENT s_{LR} (SOLID) AND $D = s_{LL}/s_{LR}$ (DOTTED) VERSUS ASPECT ANGLE FOR BODY NO. 16. (PHASE ADJUSTED TO $\phi_{HH} = \phi_{VV}$ AT NOSE-ON)

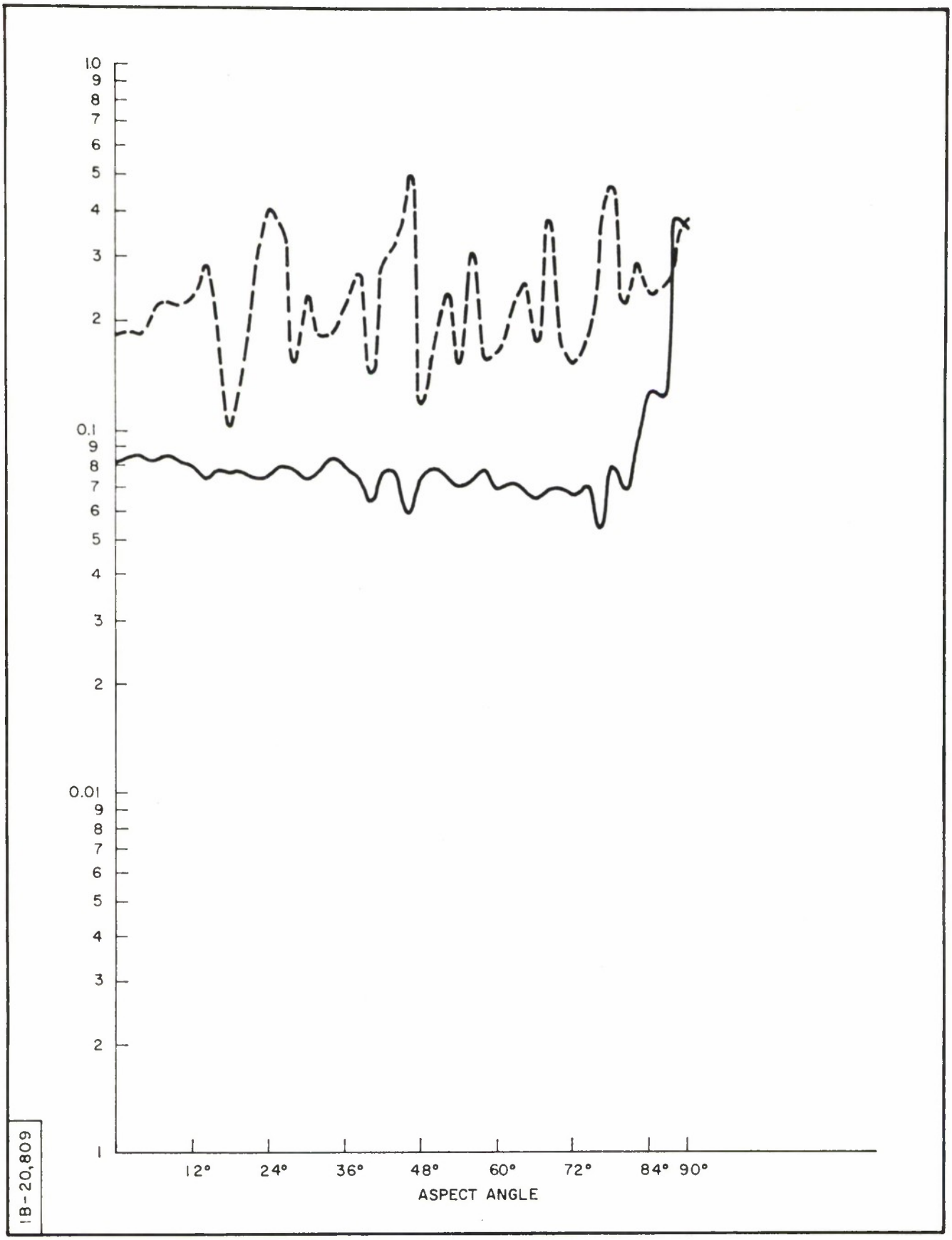

Figure 62. THE S-MATRIX ELEMENT s_{LR} (SOLID) AND $D = s_{LL}/s_{LR}$ (DOTTED) VERSUS ASPECT ANGLE FOR BODY NO. 1 (PHASE ADJUSTED BY -19°)

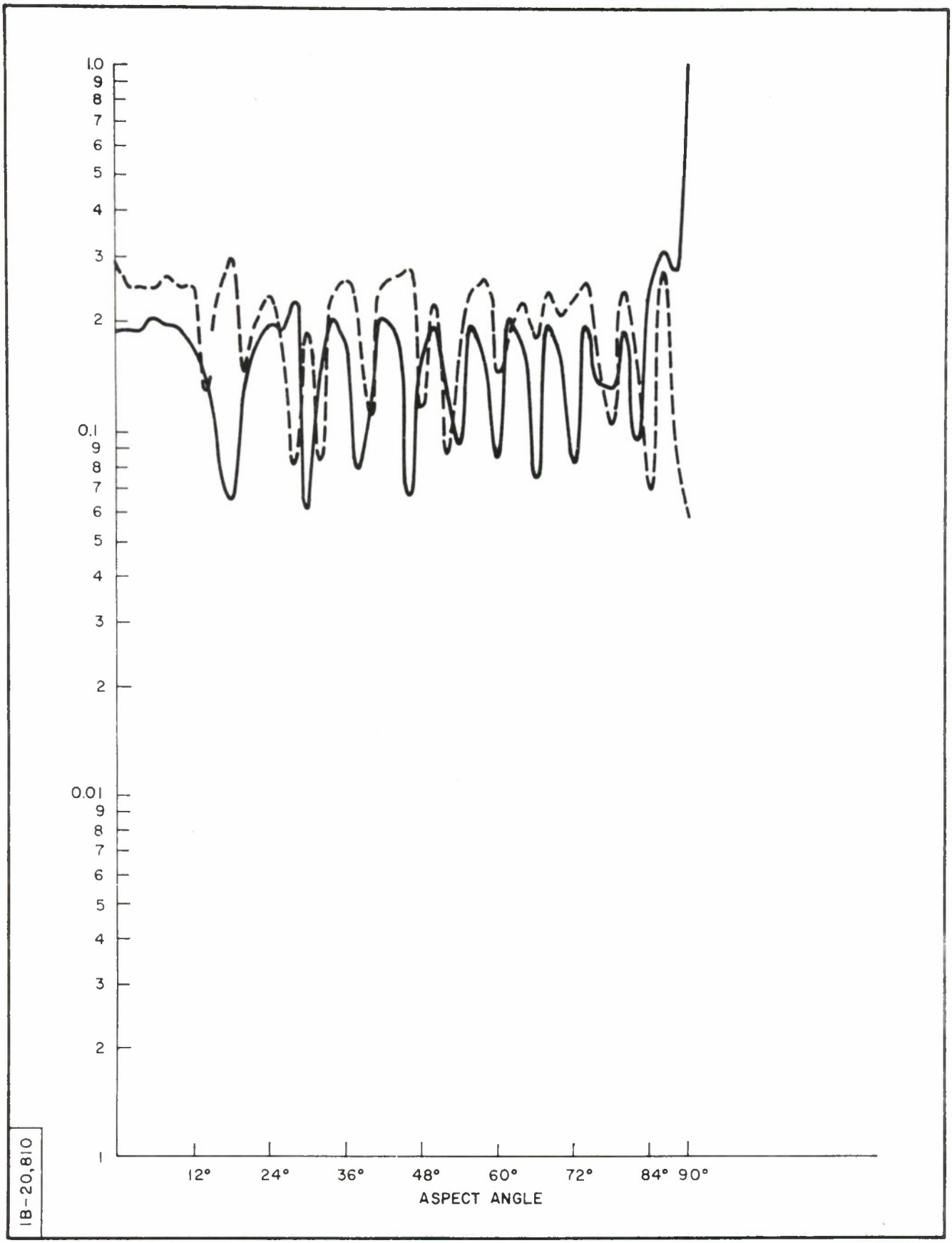

Figure 63. THE S-MATRIX ELEMENT s_{LR} (SOLID) AND $D=s_{LL}/s_{LR}$ (DOTTED) VERSUS ASPECT ANGLE FOR BODY NO. 3 (PHASE ADJUSTED BY −19°)

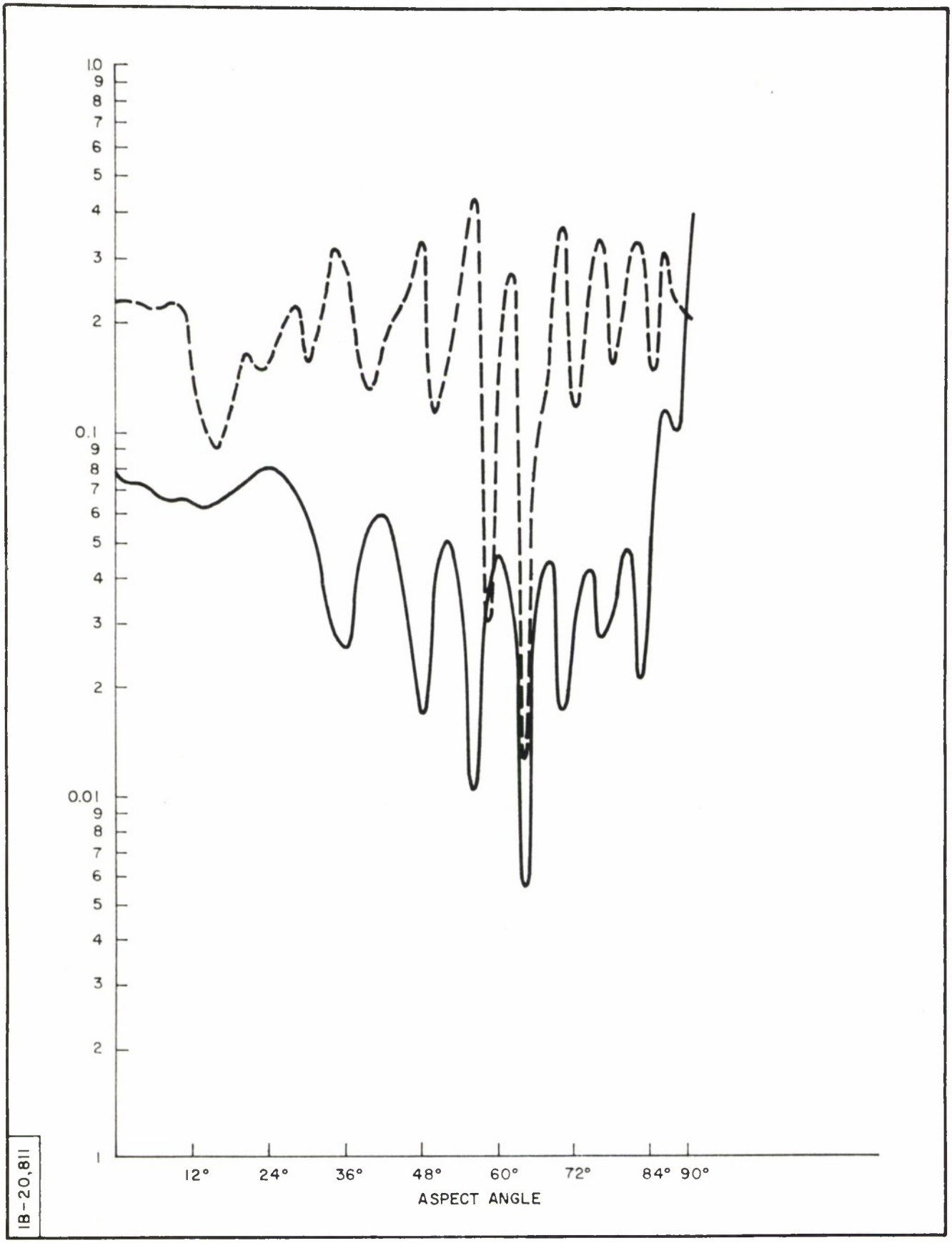

Figure 64. THE S-MATRIX ELEMENT s_{LR} (SOLID) AND $D=s_{LL}/s_{LR}$ (DOTTED) VERSUS ASPECT ANGLE FOR BODY NO. 4 (PHASE ADJUSTED BY -19°)

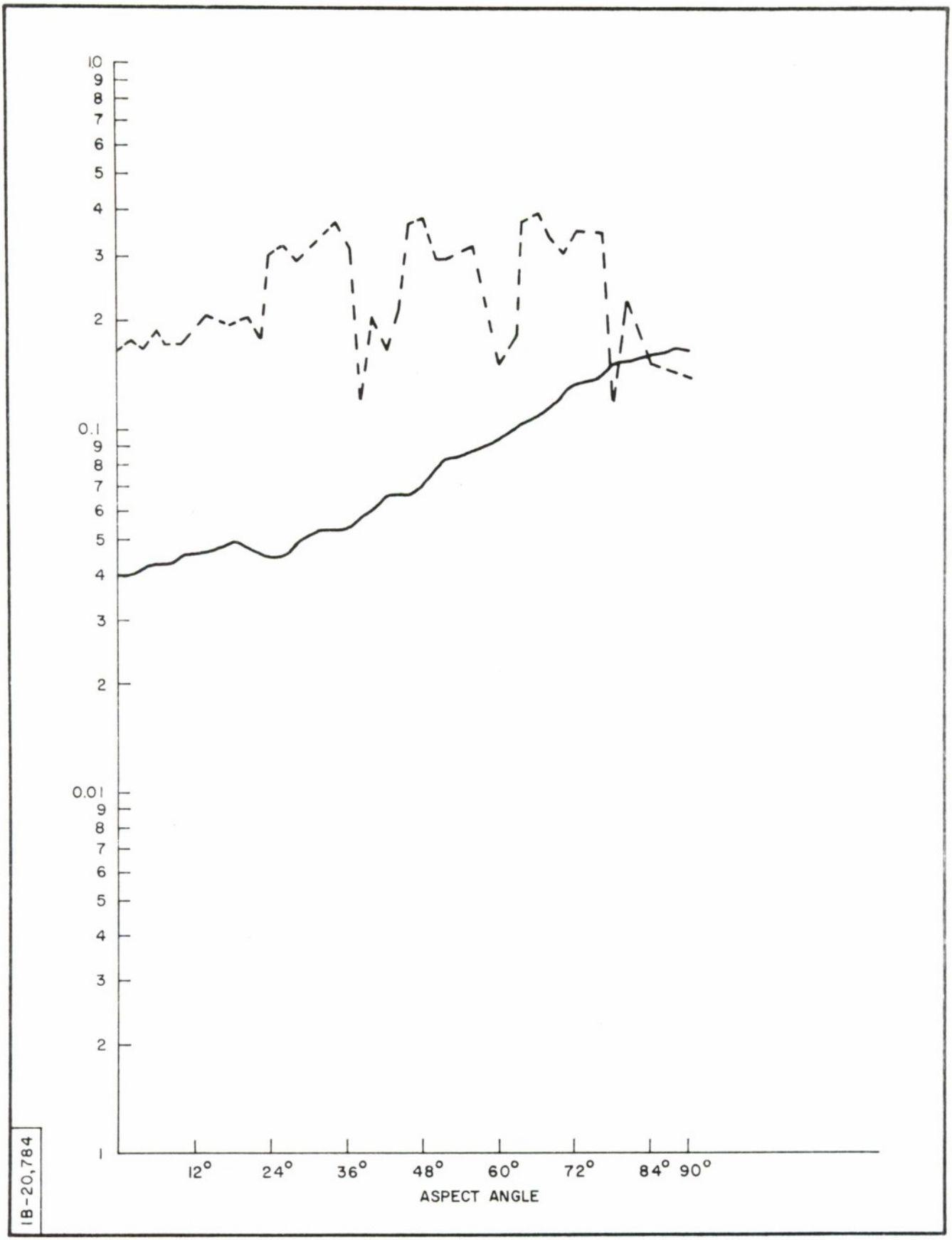

Figure 65. THE S-MATRIX ELEMENT s_{LR} (SOLID) AND $D = s_{LL}/s_{LR}$ (DOTTED) VERSUS ASPECT ANGLE FOR BODY NO. 5 (PHASE ADJUSTED BY -19°)

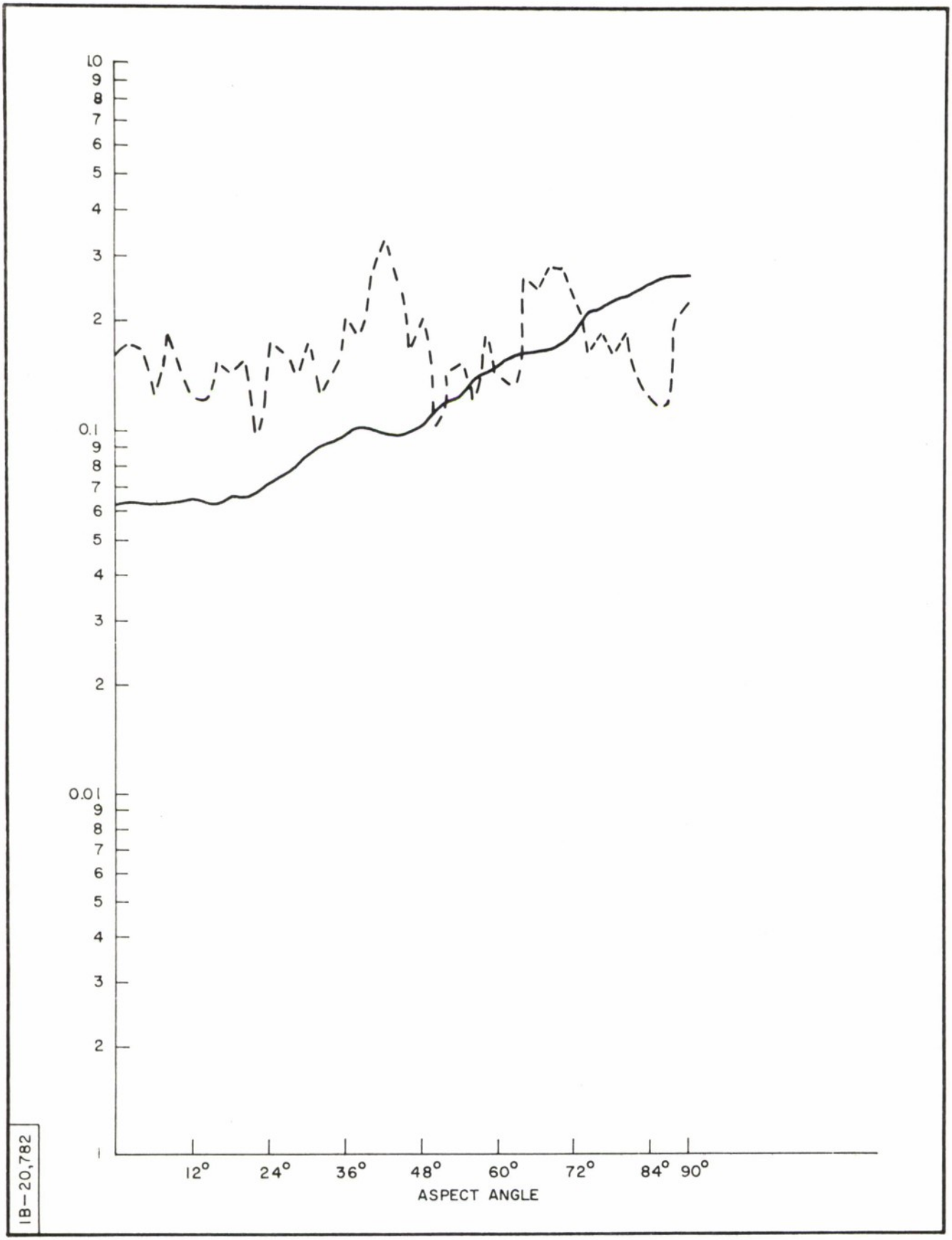

Figure 66. THE S-MATRIX ELEMENT s_{LR} (SOLID) AND $D = s_{LL}/s_{LR}$ (DOTTED) VERSUS ASPECT ANGLE FOR BODY NO. 6 (PHASE ADJUSTED BY -19°)

REFERENCES

1. Bickel, S.H., and Ormsby, J.F.A., Error Analysis, Calibration and the Polarization Scattering Matrix, Proc. IEEE, August 1965.

2. Long, M.W., Backscattering for Circular Polarization, Electronics, Letters, September 1966.

Security Classification

DOCUMENT CONTROL DATA - R & D

(Security classification of title, body of abstract and indexing annotation must be entered when the overall report is classified)

1. ORIGINATING ACTIVITY (Corporate author)

The MITRE Corporation
Bedford, Massachusetts

2a. REPORT SECURITY CLASSIFICATION

UNCLASSIFIED

2b. GROUP

N/A

3. REPORT TITLE

THE ARPA CALIBRATION SATELLITE – THEORETICAL AND EXPERIMENTAL ELECTROMAGNETIC SCATTERING CONSIDERATIONS

4. DESCRIPTIVE NOTES (Type of report and inclusive dates)

N/A

5. AUTHOR(S) (First name, middle initial, last name)

Leonard J. Kaplan

6. REPORT DATE	7a. TOTAL NO. OF PAGES	7b. NO. OF REFS
March 1968	97	2

8a. CONTRACT OR GRANT NO.	9a. ORIGINATOR'S REPORT NUMBER(S)
AF 19 (628)-5165	ESD-TR-67-358
b. PROJECT NO. 8051	
c.	9b. OTHER REPORT NO(S) (Any other numbers that may be assigned this report) MTR-424
d.	

10. DISTRIBUTION STATEMENT

This document has been approved for public release and sale; its distribution is unlimited.

11. SUPPLEMENTARY NOTES	12. SPONSORING MILITARY ACTIVITY
N/A	Development Engineering Division, Electronic Systems Division, L. G. Hanscom Field, Bedford, Mass.

13. ABSTRACT

This report contains a theoretical and experimental determination of the shape of the ARPA calibration satellite from the viewpoint of electromagnetic scattering. Theoretical and experimental scattering computations and measurements are discussed and presented in detail.

DD FORM 1 NOV 65 1473

Security Classification

14 KEY WORDS	LINK A		LINK B		LINK C	
	ROLE	WT	ROLE	WT	ROLE	WT
ELECTROMAGNETIC SCATTERINGS						
BACK-SCATTER MEASUREMENT						
CALIBRATION SATELLITE						

ADVANCED RESEARCH PROJECTS AGENCY
WASHINGTON, D. C. 20301

14 August 1969

Mr. Edward M. Doherty
Chief, Scientific and Technical
Information
Hq(ESD)AFSC
L. G. Hanscom Field
Bedford, Massachusetts 01730

Dear Mr. Doherty:

Report ESD-TR-67-358 was cleared for Open Publication by the Directorate for Security Review, OASD-Public Affairs on 7 Aug 69.

Sincerely,

Clifton A. Mann Jr.

Fred A. Koether
Director,
Technical Information

Incls:
ESD - TR-67-358(U)

ESTI

20 August 1969

ESD-TR-67-358

DDC

As per instructions of the Advanced Research Projects Agency the distribution statement on ESD-TR-67-358 should be changed to:

"This document has been approved for public release and sale; its distribution is unlimited."

FOR THE COMMANDER

Original Signed By
EDWARD M. DOHERTY

EDWARD M. DOHERTY
Chief, Scientific & Technical
Information Division

1 Atch
ARPA Ltr, 14 Aug 69